
Visualizing T cell activation around the blood-brain barrier

Dissertation
zur Erlangung des Doktorgrades der Naturwissenschaften
Fakultät für Biologie
Ludwig-Maximilians-Universität München

Marija Pesic
München 2013

1. Gutachter: Prof. Mark Hübener

Max-Planck-Institut für Neurobiologie, Martinsried;
Abteilung Synapsen – Schaltkreise – Plastizität

2. Gutachter: Prof. Elisabeth Weiß

Ludwig-Maximilians-Universität, München;
Fachbereich Biologie

Doktorarbeit eingereicht am: 11.06.2013

Tag der mündlichen Prüfung: 23.07.2013

TABLE OF CONTENTS

SUMMARY	1
ZUSAMMENFASSUNG	3
1 INTRODUCTION.....	5
1.1 Multiple Sclerosis	5
1.2 Experimental Autoimmune Encephalomyelitis (EAE).....	7
1.3 <i>t</i> EAE in rat.....	8
1.4 Breakage of the BBB.....	10
1.5 T cell activation	12
1.5.1 T cell – APC contacts	12
1.5.2 Immunological synapse	14
1.5.3 Signal transduction in lymphocyte activation	15
1.6 NFAT proteins.....	17
OBJECTIVES	21
2 MATERIAL AND METHODS.....	23
2.1 Material	23
2.1.1 Reagents and Buffers.....	23
2.1.2 Antibodies.....	25
2.1.3 Antigens.....	26
2.1.4 Animals.....	26
2.2 Methods	27
2.2.1 Cell culture.....	27
2.2.2 Flow cytometric analysis (FACS).....	28
2.2.3 Histology.....	29
2.2.4 Animal experiments	30
2.2.5 Fluorescent video-microscopy	31
2.2.6 <i>In vivo</i> two-photon microscopy	31
2.2.7 Statistical analysis	33
3 RESULTS	35
3.1 Infiltration of leptomeninges and parenchyma.....	35
3.2 Intraluminal crawling is unaffected by pathogenic potential.....	37
3.3 Perivascular detachment is impaired in EAE ^{lo} T cells	38
3.4 After extravasation, EAE ^{hi} T cells have lower motility compared to EAE ^{lo} T cells	40

3.5	EAE ^{hi} T cells stay longer in contact with perivascular APCs compared to EAE ^{lo} T cells.	41
3.6	Exogenous myelin antigen	44
3.7	Transfer into F1 recipients.....	51
3.8	The effect of a pro-inflammatory milieu	52
3.9	Δ NFAT-GFP as fluorescent marker of T cell activation <i>in vivo</i>	53
3.10	Activation status of intraluminal T cells	56
3.11	Δ NFAT-GFP translocation in perivascular T cells	57
3.12	Contacts with local APCs are crucial for T cell activation.....	60
3.13	Antigen availability and T cell activation in the CNS meninges.....	64
3.14	T cell activation state in peripheral lymphoid organs and CNS parenchyma	67
3.15	Modeling of T cell/APC interactions in the leptomeningeal area	69
3.15.1	Basic model assumptions.....	69
3.15.2	T cell in search of an activating APC.....	70
3.15.3	Correlation between <i>Tfind</i> and <i>Tact</i>	74
3.15.4	Modeling T cell activation during antigen recognition and signal transduction.....	76
4	DISCUSSION.....	79
	REFERENCES.....	87
	ABBREVIATIONS	99
	RESOURCES	103
	PUBLICATIONS.....	105
	CURRICULUM VITAE.....	107
	ACKNOWLEDGEMENTS	109

SUMMARY

T cells recognizing myelin auto-antigens penetrate into the CNS to induce inflammatory autoimmune disease following complex sequential interactions with individual components of the vascular blood-brain barrier (BBB), particularly endothelial cells, and perivascular phagocytes. To determine the functional consequences of these processes, two-photon intravital imaging was performed to compare the behavior of three myelin-specific GFP-expressing T cell lines with different potentials for transferring Experimental Autoimmune Encephalomyelitis. Imaging documented that, irrespective of their pathogenic potential, all T cell lines reached the CNS and interacted with vascular endothelial cells indistinguishably, crawling on the luminal surface, preferably against blood flow, before crossing the vessel wall. In striking contrast, after extravasation the T cell motility and their interactions with perivascular antigen presenting cells (APCs) varied dramatically. While highly encephalitogenic T cells showed a low motility, made stable contacts with local APCs and became activated, the corresponding contacts of weakly encephalitogenic T cells remained short, their motility high and their activation marginal. Supplying auto-antigen, via either local injection or by transfer of antigen-pulsed meningeal APCs, lowered their motility and prolonged the contact duration of weakly encephalitogenic T cells to values characteristic for highly pathogenic ones. Only after exogenous antigen supply, the weakly encephalitogenic T cells became activated, infiltrated the CNS parenchyma, and triggered clinical EAE, suggesting that the strength of the antigen-dependent signals received by immigrating effector T cells from leptomeningeal APCs is crucial for their pathogenic effect within the target tissue.

To directly correlate the activation of encephalitogenic T cells with their dynamic behavior in the CNS, a truncated fluorescent derivative of nuclear factor of activated T cells (NFAT) was introduced as a real-time activation indicator. Two-photon imaging documented the activation of the auto-reactive T cells extravasated into the perivascular space, but not within the vascular lumen. Activation correlated with reduced T cell motility, and it was related to contacts with the local APCs. However, it did not necessarily lead to a long-lasting arrest, as individual, activated T cells

were able to sequentially contact other APCs. A spontaneous cytosol-nuclear translocation of the marker was noted only in T cells with a high pathogenic potential. The translocation implied the presentation of an auto-antigen, as the weakly pathogenic T cells, which remained silent in the untreated hosts, were activated upon the instillation of exogenous auto-antigen. It is proposed here that the presentation of local auto-antigen by BBB-associated APCs provides stimuli that guide autoimmune T cells to the CNS destination and enable them to attack the target tissue.

In addition, a theoretical, physicist approach was used for modeling T cell activation in the leptomeningeal space. Assuming that T cells have evolved to gain their activation signal in a way that is energetically optimal for them, two possible scenarios for T cell activation were compared. The first one assumes that, after finding an APC presenting the epitope of interest, the T cell will stop and interact with the APC until it becomes fully activated. The second model considers the possibility that a T cell can accumulate activation signals from different APCs while scanning them without stopping, until a certain threshold is exceeded and the T cell becomes activated. Using this approach, it is proposed that the T cells in EAE are more likely to become activated following the first scenario. However, in a more natural environment such as a lymph node, the second scenario could give them some advantages.

ZUSAMMENFASSUNG

Entzündliche Autoimmunerkrankungen des zentralen Nervensystems (ZNS) können durch T-Zellen ausgelöst werden, welche in das Gewebe einwandern und dort vielfältige Wechselwirkungen mit Komponenten der Blut-Hirn-Schranke (BBB), insbesondere Endothelzellen und perivaskulären Makrophagen, eingehen. Zur Aufklärung der genauen funktionellen Abläufe wurde in dieser Arbeit die Methode der intravitalen 2-Photonen-Mikroskopie eingesetzt. Hiermit konnten drei verschiedene Myelin-spezifische GFP-exprimierende T-Zelllinien untersucht werden, welche ein unterschiedliches Potential bei der Auslösung der Experimentellen Autoimmunen Enzephalomyelitis (EAE) besitzen. Die Mikroskopie konnte zeigen, dass alle T-Zelllinien unabhängig von ihrer Pathogenität in die Meningen einwandern konnten und dort gleichermaßen mit dem Endothel interagierten. Dabei war insbesondere die Migration der T-Zellen auf der interluminalen Seite der Blutgefäße, welche überwiegend gegen den Blutstrom verläuft, bei allen Zelllinien identisch. Nach der Extravasation unterschieden sich die Motilität der T-Zellen und ihre Interaktion mit perivaskulären Antigen-präsentierenden Zellen (APCs) jedoch grundlegend zwischen den T-Zelllinien. Während die hoch enzephalitogenen Zellen bei einer stark reduzierten Motilität stabile Kontakte mit APCs ausbildeten, waren die Wechselwirkungen zwischen APCs und den gering pathogenen Zellen kürzer. Zudem bewegten sich Letztere mit höherer Geschwindigkeit und waren nur geringfügig aktiviert. Die Applikation von Autoantigenen durch lokale Injektion in die Meningen oder mittels Transfer von *in vitro* beladenen meningealen APCs führte zu einer Verlangsamung der gering enzephalitogenen T-Zellen. Die Dauer der Kontakte mit den APCs glich sich der von hoch pathogenen Zellen an. Nur durch exogenes Antigen konnten die gering enzephalitogenen Zellen aktiviert werden, welche daraufhin in das ZNS-Parenchym einwanderten und dort die klinischen Symptome der EAE auslösen konnten. Daraus kann geschlossen werden, dass die Stärke der Antigen-abhängigen Signale, welche die T-Zellen von den leptomeningealen APCs erhalten, für die Induktion der pathogenen Effektorfunktionen maßgeblich ist.

Um die Motilität der enzephalitogenen T-Zellen und ihre Interaktionen mit APCs direkt miteinander korrelieren zu können, wurde eine verkürzte GFP-markierte

Version des nukleären Faktors aktivierter T-Zellen (NFAT-GFP) verwendet. Hiermit war es möglich die Aktivierung der Zellen direkt visuell darzustellen. Mittels 2-Photonen-Mikroskopie konnte so gezeigt werden, dass die Zellen erst in den Leptomeningen aktiviert werden, jedoch noch nicht während der intraluminale Migration. Darüber hinaus korrelierte die Aktivierung der Zellen mit reduzierter Motilität und intensivierten Kontakten mit den perivaskulären APCs, führte aber nicht notwendigerweise zu einem lang andauernden Arrest der T-Zellen. Der Import von NFAT in den Nukleus trat nur in hoch enzephalitogenen Zellen spontan auf, konnte jedoch bei den gering pathogenen T-Zellen durch die Zuführung von exogenem Autoantigen gezielt induziert werden.

Aus diesen Beobachtungen kann geschlossen werden, dass die perivaskulären APCs in den Leptomeningen durch die Präsentation von Autoantigen selbst-reaktive T-Zellen aktivieren können und sie so zur weiteren Einwanderung in das ZNS und letztlich zur Schädigung des Nervengewebes befähigen.

In einem weiteren Teil der Arbeit wurde ein theoretischer Ansatz entwickelt, um die T-Zell-Aktivierung in den Meningen mathematisch zu beschreiben. Hierbei wurde die Grundannahme gemacht, dass T-Zellen sich evolutionär so entwickelt haben, dass sie mit einem minimalen energetischen Aufwand aktiviert werden können. Es wurden in dem hier erarbeiteten Modell zwei Szenarien verglichen: Das erste Szenario nimmt an, dass die T-Zellen bereits durch eine einzelne APC bei einer längeren produktiven Interaktion aktiviert werden können. Im zweiten Fall wird postuliert, dass die T-Zellen für eine erfolgreiche Aktivierung die Signale von mehreren APCs akkumulieren müssen. Unter Verwendung dieses Modells konnte gezeigt werden, dass im ZNS die T-Zell-Aktivierung unter energetischen Aspekten idealerweise nach dem ersten Szenario ablaufen wird. In anderen anatomischen Umgebungen, wie etwa einem Lymphknoten, könnte die Aktivierung nach dem zweiten Szenario energetisch bevorzugt sein.

1 INTRODUCTION

1.1 Multiple Sclerosis

Multiple Sclerosis (MS) is a chronic autoimmune inflammatory disease in which myelin sheaths around axons of the brain and the spinal cord are damaged, ultimately resulting in neuronal death. Depending on the region in the Central Nervous System (CNS) where demyelination occurs, the disease symptoms are manifold, with patients having individual patterns of defects and a highly unpredictable disease course. For this reason responsiveness to available therapies is often uncertain (Compston and Coles, 2008; Gold et al., 2006). The disease affects 2.5 million people worldwide, mostly young adults (20–40 years of age), and is twice more frequent in women than in men (Flachenecker and Stuke, 2008).

MS can be classified in subtypes based on two criteria: 1) clinical course and 2) morphology of the CNS lesions. According to the heterogeneity of the clinical course, four different types of MS were described (Kieseier and Hartung, 2003). The most common type is a relapsing-remitting (RRMS) disease course, which is present in 85% of MS patients, and is characterized by alternating periods of acute disease and recovery. In secondary-progressive MS (SPMS), disease symptoms are constantly worsening without occasional relapses, and 50% of patients with RRMS will eventually develop SPMS. A minority of patients develops primary-progressive MS (PPMS), where the disease is gradually progressing from the beginning, or progressive-relapsing MS (PRMS), where a progressive disease course is interrupted by acute relapses that may or may not include recovery. Four different MS subtypes were also defined on the basis of myelin protein loss, the geography of lesions, patterns of oligodendrocyte destruction, and the immunopathological evidence of complement activation (Lassmann et al., 2007).

By current hypothesis on MS pathology, the immune system produces an inflammatory response against a tissue-specific self-antigen, which identity to-date remains unknown. In consequence, cells of the immune system attack the myelin sheaths, leading to axonal damage and ultimately neuronal death (Engelhardt and

Coisne, 2011). This view on MS pathogenesis is mostly established from animal models for MS. It is considered that self-reactive T cells, which exist in the healthy immune system, get primed e.g. via bystander activation or antigenic mimicry, become auto-aggressive and acquire the capacity to traverse the blood–brain barrier (BBB). Once in the CNS, they encounter locally presented CNS-antigen(s), and are reactivated. Subsequently, these T cells orchestrate a complex cascade involving recruitment of antibody producing plasma cells and peripheral macrophages, culminating in myelin and axon damage (Hohlfeld, 2009). Supporting this, cytotoxic and helper T lymphocytes targeted against CNS-specific antigen have been found in MS patients, and the presence of oligoclonal bands (OCB) has been used as diagnostic marker for MS. This underlines the unambiguous role of B-cells and secreted antibodies in disease development. However, even 50 years after discovery of OCB in MS, their specificity is still not identified.

Etiology of MS remains unknown to this day; however many observations have been made, suggesting that both genetic susceptibility and environmental factors play a role. Twin studies showing that disease concordance in monozygotic twins is much higher than in dizygotic (25% vs. 2%) (Dyment et al., 1997), provide clear evidence for a genetic contribution to MS etiology. Recent Genome-wide association study (GNAS) showed a correlation between human leukocyte antigen (HLA) type I and II genes and susceptibility to MS, where some of them (HLA-DR15, type II; HLA-A*03, type I) (De Jager et al., 2008) are shown to increase probability for disease, and others (HLA-C554 and DRB11*1, type II; HLA-A*02, type I) (Compston and Coles, 2008; Fogdell-Hahn et al., 2000) appear to have a protective effect. GNAS also revealed associations outside of the HLA, in particular the genes for the IL-2 and IL-17 receptor (Sawcer, 2008). The fact that most of the risk alleles are linked to the immune system, stresses its importance in disease development.

MS risk differs between geographical regions, with disease being rare in tropical areas (Africa and South America), but common in temperate regions (Northern Europe and Northern America) (McAlpine, 1956), an evidence that the environment plays an important role in the disease etiology. Multiple migration studies also contribute to proof of an environmental component. The results suggest, that people who migrate before adolescence acquire the incidence rates of the region to which

they have migrated (Alter et al., 1978; Alter et al., 1966; Alter et al., 1970; Dean and Elian, 1997; Detels et al., 1978; Hammond et al., 2000), while people migrating to a region after adolescence retain the incidence rate of the region from which they grew up (Gale and Martyn, 1995). A possible explanation for the geographic discrepancy can be a lack of vitamin D in Northern countries due to a reduced exposure to sunlight (Smolders et al., 2008), as well as alterations in nutrition between different regions (Schwarz and Leweling, 2005). It has also been suggested that exposure to viruses such as EBV (Serafini et al., 2007), can trigger the disease through mechanisms of molecular mimicry (Lünemann et al., 2007). However, direct evidence for this has been lacking to date.

1.2 Experimental Autoimmune Encephalomyelitis (EAE)

The Experimental Autoimmune Encephalomyelitis (EAE) is the most intensively studied animal model of human MS. It was first described in 1925 by Koritschoner and Schweinburg (Koritschoner and Schweinburg, 1925) when they demonstrated that immunization with human brain homogenate, leads to the development of MS-like symptoms in rabbits. Today there are many EAE models available with diverse clinical outcome and pathology, determined by the strain and species used, sex, auto-antigen, its dose and route of administration (Krishnamoorthy and Wekerle, 2009). None of these EAE models represents the entire variability of the human disease, but each of them rather reflects certain aspects of MS (Wekerle et al., 1994). Studies on EAE models have provided great insight into the disease mechanisms, and enabled immense progress in developing new drug treatments for human MS.

There are three common ways to induce EAE (Gold et al., 2006). Active immunization with CNS auto-antigen, emulsified with Complete Freund's Adjuvant (CFA) is known as active EAE (*a*EAE). Alternatively EAE can be induced by the passive transfer of CNS auto-antigen-specific CD4⁺ T cells that have been *in vitro* cultured and selected for antigen of interest, and is referred to as - transfer EAE (*t*EAE). Both approaches result in a neurological disease that starts with the loss of tail tonus and is followed, from caudal to rostral, by limb weakness and paralysis.

These symptoms are associated with a strong inflammation in the CNS. The main difference between active and transfer EAE is in their kinetics, as the onset of *t*EAE is earlier compared to *a*EAE. The reason is that in *a*EAE, the T cells first need to get primed in lymph nodes, while in *t*EAE already primed T cells are injected. CNS auto-antigens used for induction of both active and transfer EAE include myelin antigens such as oligodendrocyte glycoprotein (MOG), myelin basic protein (MBP), and proteolipid protein (PLP), but also some non-myelin CNS antigens such as S100 β , which is expressed primarily on astrocytes (Kojima et al., 1994).

Over the past years spontaneous EAE models have been developed. They include single transgenic mouse models based on a MBP-specific TCR (Goverman et al., 1993; Lafaille et al., 1994) developing classical EAE, as well as a MOG-specific TCR (TCR^{MOG}) developing relapsing-remitting EAE (Pöllinger et al., 2009), or a double transgenic model with TCR^{MOG} and IgH^{MOG}, developing opticospinal EAE (Bettelli et al., 2006; Krishnamoorthy et al., 2006). The main advantage of these models is that the disease development depends on T cell - B cell cooperation, which mechanistically brings them closer to human MS.

1.3 *t*EAE in rat

Transfer EAE in rats can be induced by adoptive transfer of *in vitro* stimulated CD4⁺ CD8⁻ CNS-specific T cell blasts (Ben-Nun et al., 1981). The greatest advantage of the transfer EAE model in the rat is its high predictability and reproducibility. The disease is monophasic, and does not start immediately upon T cell transfer, but following a disease free period of 3-4 days. The disease peaks 5-6 days after T cell transfer and ends with a complete recovery around day 10 post transfer (p.t.) (Figure 1.1).

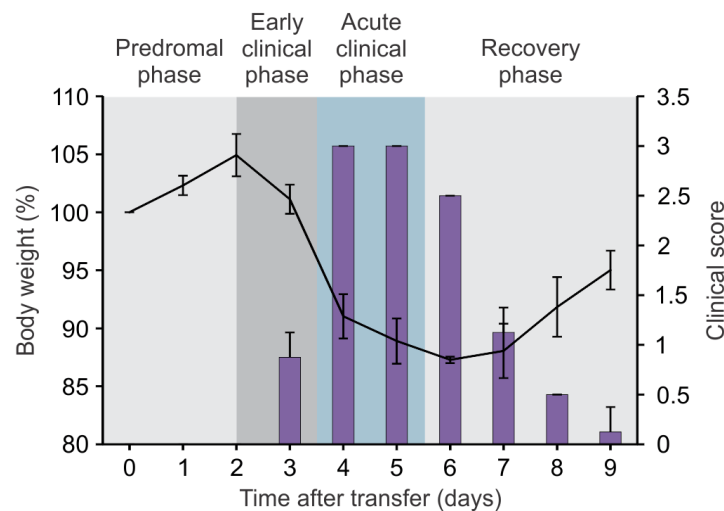


Figure 1.1 Clinical course of tEAE in Lewis rat. Body weight (line) and clinical symptoms (bars) following i.v. transfer of $T_{\text{MBP-GFP}}$ cells are depicted. Four different EAE phases can be distinguished: a disease-free prodromal period; developing clinical symptoms; disease maximum and recovery from paralytic disease (indicated by different background colors). Disease severity was scored as follows: 0, no disease; 1, flaccid tail; 2, gait disturbance; 3, complete hind limb paralysis; 4, tetraparesis.

The reason for delayed EAE onset is attributed to the specific immune situation of the brain (Hickey et al., 1991; Wekerle et al., 1986). The brain is considered to be an immune-privileged organ, due to the tight BBB, that restricts access of soluble molecules and cells, and therefore immune cells are rare. In addition, lymphatic vessels are sparse, and expression of factors needed for an efficient immune response, such as MHC and costimulatory molecules, is extremely low. By current hypothesis, encephalitogenic T cells overcome this obstacle by invading the brain in two waves. The first invasion occurs within hours after transfer, when very few activated “pioneer” T cell blasts can enter the brain and start to produce pro-inflammatory cytokines, to create immune permissive milieu, and enable second massive invasion of antigen-specific T cells (Flügel et al., 2007). Prior to this second invasion of the CNS, the T cells acquire a “migratory phenotype” in the peripheral lymphoid organs such as spleen, up-regulating chemokine receptors and down-regulating activation markers, (Flügel et al., 2001) and by this acquiring the capacity to migrate into the CNS. Upon arrival in the target organ, T cells are reactivated by local antigen presenting cells (APCs) presenting endogenous myelin antigen, (Bartholomäus et al., 2009; Kivisäkk et al., 2009), to produce abundant amounts of inflammatory cytokines. This recruits other non-specific immune cells such as

macrophages, which play a main role in causing the neurological disorder, by releasing toxic cytokines, which act on neurons and glial cells (Huitinga et al., 1990).

Like in other EAE models, *t*EAE in rats can also result in different neurological disorders, depending on the genetics of the experimental animals and on the T cell antigen-specificity used for induction. For example, the Dark Agouti (DA) strain is highly susceptible to *t*EAE induced by MOG-specific T cells (Storch et al., 1998). However, in a different genetic background, the Lewis (LE) strain, MOG-specific T cells have only a very mild effect (Weissert et al., 1998). Nevertheless, T cells specific for MBP, another myelin antigen, induce a severe neurological disorder in the same strain (Swanborg and Ames, 1971). Similar to human MS, this difference has been linked mainly to MHC gene region (Weissert et al., 1998), suggesting that T cell activation has crucial role for the disease development as shown by Kawakami and colleagues (Kawakami et al., 2004).

1.4 Breakage of the BBB

Brain-specific autoimmune T cells on their way to the CNS face a challenge of the BBB, which is a complicated composite of a central endothelial tube and two concentrically arranged basal laminas, in which pericytes and phagocytes are embedded (Sorokin, 2010). This barrier blocks most of the circulating blood components, but its impermeability is not absolute. Due to this, the T cells mediating EAE have developed an elaborate set of sequential interactions with different BBB components to access the brain tissue (Figure 1.2).

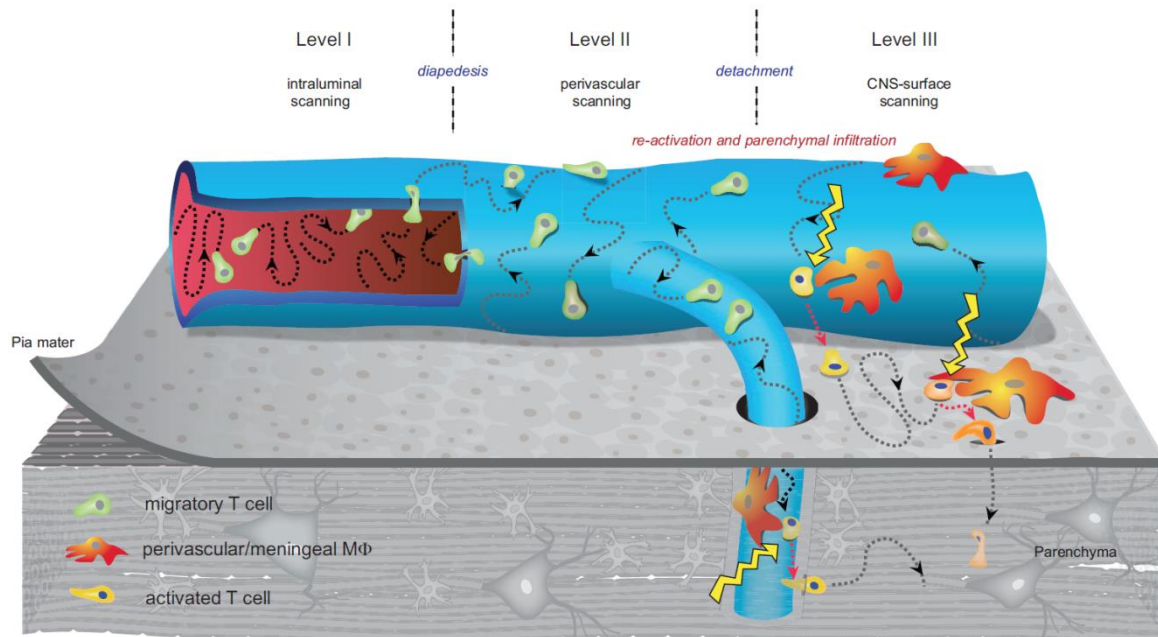


Figure 1.2. T cell invasion into the CNS. Schematic picture illustrating the invasion steps of $T_{\text{MBP-GFP}}$ cells in the CNS tissue. (Adopted from Bartholomäus et al., 2009)

The first contact between encephalitogenic T cells and the BBB occurs on the luminal surface of the endothelial tube. The T cells attach to the intraluminal surface of leptomeningeal vessels, first roll along, and then continue to crawl on the endothelial cells, scanning for extravasation site. Both modes of motion differ in the molecules used for the endothelial contacts. While rolling occurs along the blood stream and involves transient interactions between selectins and glycoproteins (Piccio et al., 2002), crawling is preferably against direction of blood flow and depends on the binding of α_4 and α_L integrins (Bartholomäus et al., 2009). Blocking of these adhesion molecules interferes with tight attachment, completely washing crawling T cells away, and dramatically ameliorates clinical EAE. Indeed, Natalizumab, the therapeutic humanized α_4 integrin blocking antibody is highly effective in reducing MS relapse rate (Lanzillo et al., 2012).

After extravagating from the blood vessels, T cells continue their scan on the albuminal vascular surface, where they can encounter perivascular phagocytes, able to present foreign as well as local antigens (Bartholomäus et al., 2009; Kivisäkk et al., 2009), make serial contacts with them, and eventually become activated. These observations led to the hypothesis, that the presentation of auto-antigens by those

perivascular antigen presenting cells (APCs) provides immigrant T cells with the critical cues that direct them into the CNS parenchyma. However, due to technical limitations, direct visualization of functional intercellular interaction leading to T cell activation has been lacking to date.

Strength of T cell reactivation determines infiltration rate and clinical outcome of the disease: in Lewis rat, for example, MBP-specific T cells are activated in the CNS by endogenous MBP, triggering classical acute EAE, which can be exacerbated by addition of exogenous MBP and following aggravated T cell activation (Odoardi et al., 2007a). On the other hand MOG-specific T cells display no activation, and hardly mediate any clinical defects (Kawakami et al., 2004). The reason for this is that T cell reactivation is accompanied by activation of the endothelium and loosening of the BBB, allowing further recruitment of immune cells. This massive immune cell infiltration into the CNS will eventually lead to a neurological disorder and the development of clinical symptoms.

1.5 T cell activation

In order to become activated, a T cell must engage in a productive interaction with an APC, leading to formation of an immunological synapse (IS) at the T cell-APC contact site. The IS is an highly organized structure, representing the simultaneous engagement of the TCR and costimulatory molecules on the T cell with the peptide-MHC complex and costimulatory molecules on the APC. Resulting TCR stimulation triggers a signaling cascade, leading eventually to the transcription of activation relevant genes.

1.5.1 T cell – APC contacts

To get activated, T cells must first make series contacts with APCs, each of which provide opportunity for antigen recognition to occur. Despite a good fundamental understanding of T cell activation, the way individual T cell experience their encounter with APC has been unknown for a long time. Experiments done *in vitro*, supported the idea that antigen recognition by T cells induces cell-arrest and formation of long lasting contacts with the presenting cell (Donnadieu et al., 1994;

Dustin et al., 1997; Negulescu et al., 1996). However, this was challenged by other *in vitro* finding showing that naive cells can become activated after establishing multiple short interactions (duration less than 10 min) with antigen-bearing DCs (Gunzer et al., 2000).

With development of two-photon laser scanning microscopy, it became possible for the first time to investigate the dynamic T cell – APC interactions *in vivo*. But instead of solving the controversy by providing a simple answer, it in fact documented a high diversity in T cell – APC contact dynamics (Bousso, 2008). Most experiments have so far been done in lymph nodes, the main environment where T cells are getting primed.

In the absence of the cognate antigen, T cells make serial transient contacts with DCs (duration of 3-5 min), resulting in infrequent Ca^{2+} signals (an early indicator of the activation stimulus) during these interactions (Asperti-Boursin et al., 2007; Wei et al., 2007). These contacts might still be functionally important for providing “tonic signals”, as naive T cells lose their motility in the lymph node if they are prevented from engaging MHCII molecules on the APC surface (Fischer et al., 2007).

In the presence of abundant amount of antigen that induces robust T cell activation, T cells are observed to make stable, long lasting contacts with DCs that often exceed imaging period of 30-60 min. It has been shown, that 6 h of stable interaction with DCs is needed to induce a clonal expansion of naive $CD4^+$ T cells (Celli et al., 2007), but what kind of signaling the T cells receive during this time and how their activation is affected, remains still unknown.

Apart from stable T cell – DC interactions, in presence of antigen T cells can be also engaged in contacts with DCs that are relatively short and hardly distinguishable from contacts with DCs without antigen to present. One reason could be that these contacts are simply unproductive, due to limiting amount of peptide-MHC complexes on APC surface, which T cells are then missing during the contact. However, there are data indicating that these interactions can also result in activation of both $CD4^+$ as well as $CD8^+$ T cells without inducing their arrest (Moreau et al., 2012; Skokos et al., 2007). Discriminating productive from nonproductive T cell – APC interactions remains a challenge for future studies.

1.5.2 Immunological synapse

Recognition of peptide-MHC complexes by the TCR results in a specialized membrane contact between T cell and APC, termed immunological synapse (IS). The IS is considered to have three functional layers (Figure 1.3A), based on receptor interactions, signal transduction and cytoskeletal transport (Dustin and Depoil, 2011). The receptor layer is defined by supramolecular activation complexes (SMACs), which are composed by centrally located TCR/CD3-MHC/peptide ligand pairs, along with costimulatory molecules such as CD28 and CTLA4. Additionally a ring of surrounding adhesion interaction partners, such as LFA1-ICAM1, ensures a tight T cell-APC interaction (Fig 1.3B).

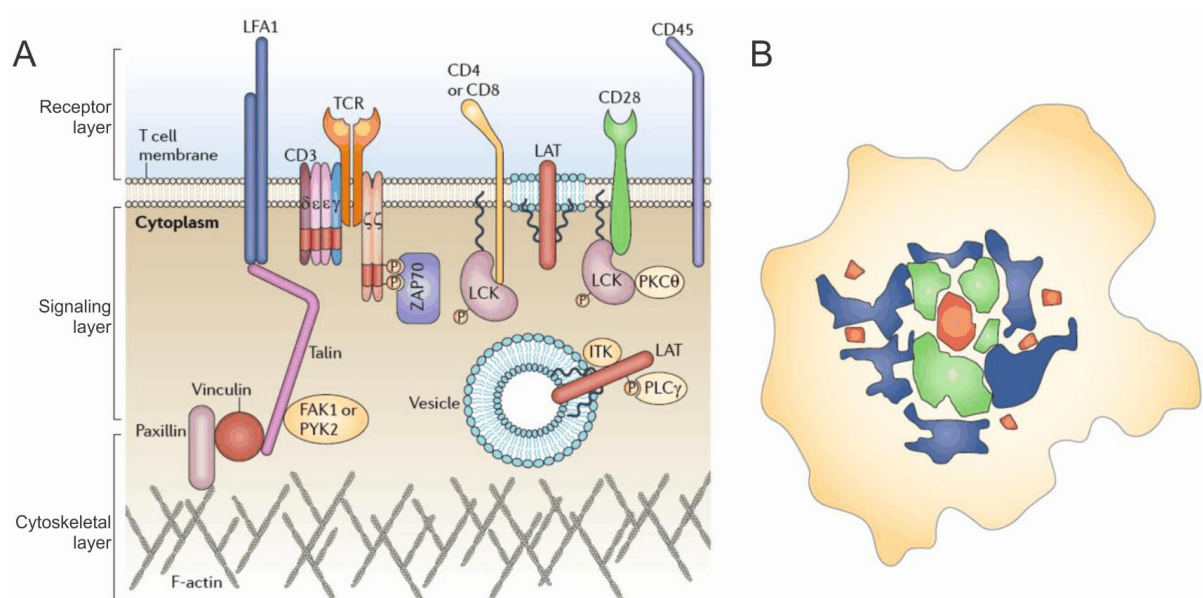


Figure 1.3. Structure of the Immunological Synapse. (A) Three layers of the Immunological Synapse (IS) on the T cell side. The receptor layer contains the TCR–CD3 complex, CD4 or CD8, CD28 and LFA1. The signaling layer includes LCK, ZAP70, ITK, PLC γ and PKC θ . The cytoskeletal layer contains F-actin, talin, paxillin and vinculin. (B) Supramolecular activation clusters (SMACs) of an IS, as seen looking down on a T cell. The TCR-rich central SMAC is shown in red, the CD28-rich periphery is depicted in green and the LFA1-rich peripheral SMAC is displayed in blue color. (Adopted from Dustin and Depoil, 2011)

Upon antigen recognition, stimulation of TCR induces series of intracellular signaling cascades. As the TCR has no intrinsic catalytic activity itself, it forms a complex with CD3, which itself has six subunits with long cytoplasmic domains, containing

immunoreceptor tyrosine-based activation motifs (ITAMs). ITAMs are phosphorylated by SRC family kinases LCK, and recruit ZAP70, a non-receptor tyrosine kinase, via a relatively high affinity interaction by binding to the tandem SH2-domains of ZAP-70. This binding leads to activation of ZAP-70, which subsequently phosphorylates a number of signaling proteins, including the linker for the activation of T cells (LAT). This leads to recruitment of the IL-2 inducible T cell kinase (ITK) and activation of phospholipase C γ (PLC γ).

TCR activation is also regulated by various costimulatory receptors such as CD28 and CD45. CD28 provides an essential co-stimulatory signal during T cell activation, which augments the IL-2 production, increases T cell proliferation and prevents the induction of anergy and cell death. Once ligated by B7 on the surface of the APCs, CD28 provides the T cell with an initial adhesion, bringing the T cell and APC membranes closer together. CD45 regulates TCR signaling by modulating the phosphorylation state of tyrosine kinases like Lck, and antagonizing inhibitory proteins, thereby favoring T cell activation (Dustin and Depoil, 2011).

The cytoskeletal layer is assembled by three filament forming proteins: actin, myosin II and tubulin. Integrin-dependent adhesion requires F-actin, and partially depends on myosin II. Integrins are linked to F-actin through proteins such as talin and vinculin (Figure 1.3A). TCR engagement induces actin polymerization with generation of forceful protrusions, and by recent finding, TCR can act as a mechanotransducer, meaning that it can generate signal transduction in response to forces (Dustin and Depoil, 2011).

1.5.3 Signal transduction in lymphocyte activation

Antigen binding to TCR leads, as mentioned, via activation of several layers of protein kinases, to activation of PLC γ which hydrolyses phosphatidylinositol-3,4-bisphosphate to diacylglycerol and inositol-1,4,5-trisphosphate (IP3). IP3 then binds to the IP3 receptor, which is a Ca²⁺-permeable ion channel, and Ca²⁺ is released from intracellular Ca²⁺ stores in the endoplasmic reticulum (ER). Ca²⁺ released from the ER results only in a moderate and transient increase of the intracellular Ca²⁺ concentration, due to the small volume of the ER. Importantly, the decrease of the Ca²⁺ concentration in the ER triggers the activation of a store-operated calcium entry

(SOCE) pathway, resulting in the opening of store-operated Ca^{2+} channels in the plasma membrane. In lymphocytes, the CRAC channel is the best described and the main store-operated Ca^{2+} channel. Ca^{2+} influx via CRAC channels results in a sustained Ca^{2+} signal and increased levels of intracellular Ca^{2+} are maintained (Feske, 2007). Ca^{2+} binds calmodulin, which in turn activates the calmodulin-dependent phosphatase calcineurin. Activated calcineurin dephosphorylates Nuclear Factor of Activated T cells (NFAT), which leads to its nuclear translocation and the induction of NFAT-mediated gene transcription (Figure 1.4) (Macian, 2005).

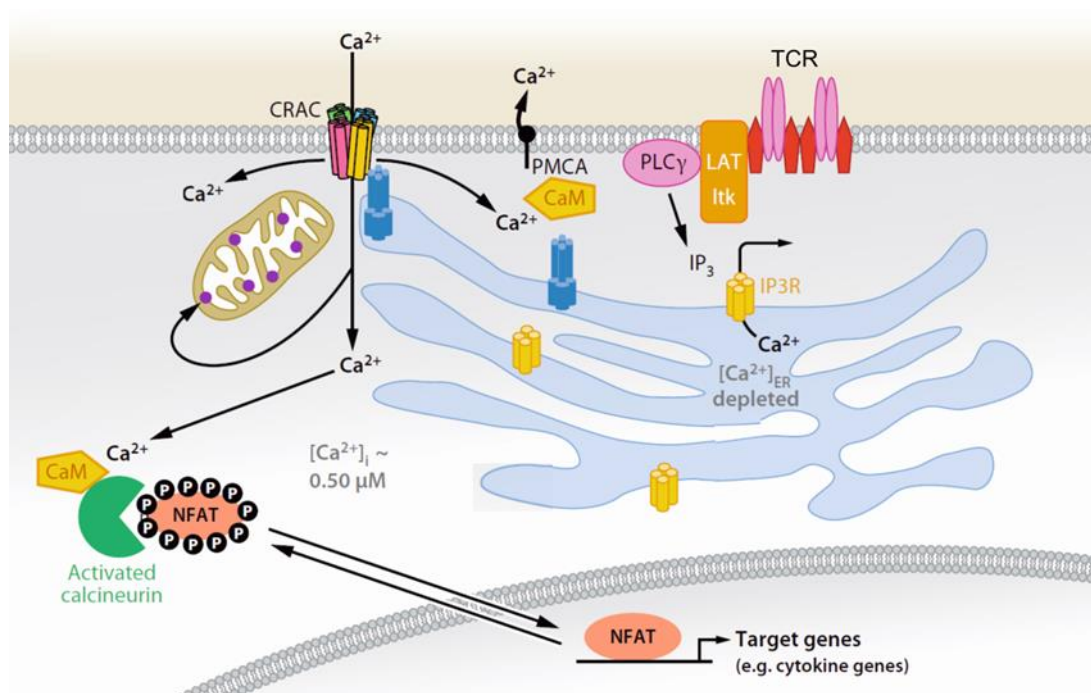


Figure 1.4. Signaling pathway connecting store-operated Ca^{2+} entry with NFAT-dependent gene transcription in T cells. T cell receptors assemble into signaling complexes that contain scaffold proteins such as LAT, tyrosine kinases such as Itk, and phospholipase C γ (PLC γ). IP₃ produced by PLC γ binds to receptors in the ER membrane, causing the release of Ca^{2+} from the ER. The depletion of ER Ca^{2+} stores, causes opening of CRAC channels. The resulting increase of intracellular Ca^{2+} causes the universal and abundant cytoplasmic Ca^{2+} sensor calmodulin (CaM) to bind to various channels and enzymes and modulate their activity. Among the targets of CaM is the phosphatase calcineurin, which dephosphorylates NFAT and causes its nuclear translocation, thus activating NFAT-dependent transcription (Adopted and modified from Hogan et al., 2010).

1.6 NFAT proteins

Initially, NFAT was identified as an inducible nuclear factor that could bind interleukin-2 (IL-2) promoter in activated T cells. However, it soon became clear that the expression of NFAT proteins was not limited to T cells, as at least one NFAT family member is expressed by almost every cell type. The NFAT family consists of five members (NFAT1-5), four of which are regulated by calcium signaling and have a highly conserved DNA-binding domain. Three of calcium regulated proteins (NFAT 1, 2 and 4) are expressed by T cells. Different NFAT proteins having selective roles in T cell differentiation has been a controversial idea. Current data suggest however, that NFAT1 and NFAT2 are functionally redundant (Avni et al., 2002), while NFAT4 seems to have preferential role in development of CD4⁺ and CD8⁺ T cells (Oukka et al., 1998).

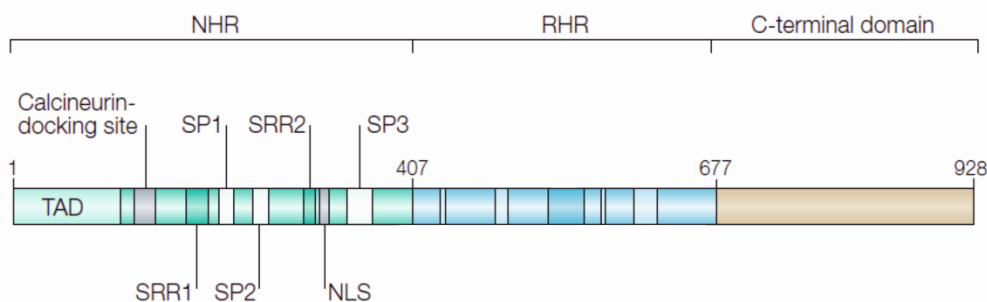


Figure 1.5. Scheme of NFAT and its domains. This schematic representation illustrates the location of the transactivation, regulatory, DNA-binding and carboxy (C)-terminal domains of NFAT1. Regulatory motifs in the NFAT homology region (NHR) and motives in REL-homology domain (RHR) are highly conserved among the calcium–calcineurin-regulated NFAT proteins (NFAT1–NFAT4). NHR includes the calcineurin-docking site, the nuclear localization signal (NLS), the serine-rich regions (SRRs) and the SPXX-repeat motifs (SPs), where X denotes any amino acid. An inducible phosphorylation site has also been described in the N-terminal transactivation domain (TAD) of NFAT1. The phosphoserines that are targeted by calcineurin dephosphorylation are located in the SP2, SP3 and SRR1 motifs. These serines are phosphorylated in the cytosol by maintenance kinases and in the nucleus by export kinases. (Adopted from Macian, 2005).

Each NFAT protein has two or more alternatively spliced forms. Splicing results in variations of the amino- (N) and carboxyl- (C) termini, with the core region being

conserved. The conserved core region of NFAT proteins consists of two tandem domains: a regulatory domain, which is also known as the NFAT-homology region (NHR); and the REL-homology domain (RHR), which binds DNA (Figure 1.5). The NHR contains many serine residues that are phosphorylated in resting T cells. It also includes the docking sites for calcineurin and the NFAT kinases, which regulate the activation of NFAT proteins by determining the phosphorylation status of the serines. All but one of the 14 phosphorylation sites, which have been mapped in NFAT1 and are conserved in all calcineurin-regulated NFAT proteins, are dephosphorylated by calcineurin. Dephosphorylation of the serine residues in these motifs leads to exposure of the NFAT1 nuclear localization signal and its nuclear import. Several kinases have been reported to phosphorylate NFAT proteins and control their nuclear shuttling, including glycogen-synthase kinase 3, casein kinase 1, p38 and JUN N-terminal kinase (Macian, 2005). The present data point to a complex model, in which different kinases phosphorylate the various serine-rich motifs in NFAT proteins. It is also necessary to distinguish between maintenance kinases, which act in the cytosol to keep NFAT proteins in a fully phosphorylated state and prevent their translocation into the nucleus in resting cells, and export kinases, which rephosphorylate NFAT in the nucleus and promote its nuclear export; thereby stopping NFAT-mediated transcription after T cell stimulation is withdrawn.

The importance of NFAT proteins in T cell activation is highlighted by genetic data. In two human families, failure to activate NFAT proteins because of a defect in store-operated calcium entry was associated with severe immunodeficiency (Feske et al., 2000). In mice, deficiency in both NFAT1 and NFAT2 in T cells results in grossly impaired production of many cytokines, including IL-2, IL-4, IL-10, IFN- γ , granulocyte/macrophage colony stimulating factor (GM-CSF) and TNF α . IL-5 expression is also notably diminished, as well as the expression of CD40L and CD95L (Peng et al., 2001), which confirms that the activation of NFAT proteins is essential for T cells to carry out many of their effector functions. The analysis of gene expression using DNA microarrays has also clearly shown that the activation-induced expression of most genes in T cells is blocked by calcineurin inhibitors (Feske et al., 2001; Macian et al., 2002).

Given the important role of NFAT proteins in the control of T cell activation, NFAT has always been considered to be an optimal target for therapeutic approaches that are aimed at regulating immune responses. Inhibitors of calcineurin, such as Cyclosporin A (CsA) and FK506, have been extensively used as immunosuppressive agents to improve graft survival and to treat autoimmune diseases (Macian, 2005)

OBJECTIVES

In experimental models of MS, clinical patterns can be determined by both, properties of myelin-specific auto-reactive effector T cells, and factors in the target tissue milieu (Ransohoff, 2009). These factors control the nature of interactions between effector cells and target tissue, from the earliest stages of the immune cell arrival to the terminal immune attack in the target tissue. Within this pathogenic cascade, entry of autoimmune effector T cells into the CNS target tissue plays a critical role in dictating the clinical outcome.

The present work was designed to unravel the role of locally presented neural auto-antigen in the formation of EAE lesions. We used three different T cell lines, which are indistinguishable in their general properties, but mediate EAE of different clinical intensity (Kawakami et al., 2004). By using *in vivo* two-photon imaging, we compared T cell migration patterns and local antigen presentation events between classical MBP-specific T cells of the Lewis rat, MOG-specific T cells of Dark Agouti rats (both highly encephalitogenic), and MOG-specific T cells of Lewis rats (weakly encephalitogenic).

To study the functional aspect of interactions between auto-reactive T cells with different encephalitogenic potential, and structures of the vascular BBB, a fluorescent derivative of truncated NFAT (Δ NFAT-GFP) was introduced as an indicator of *in vivo* and *in situ* T cell activation. Due to the lack of suitable markers so far, autoimmune activation events were never shown formally *in vivo* before, and this drawback should be overcome by this project.

2 MATERIAL AND METHODS

2.1 Material

2.1.1 Reagents and Buffers

Medium	Specified amount	
DMEM	13.4 g/L	DMEM powder
	3.7 g/L	NaHCO ₃
Freezing medium	50 % Vol.	Horse serum (inactivated)
	40 % Vol.	TCM
	10 % Vol.	DMSO
EH	97.5 % Vol.	DMEM
	2.5 % Vol.	HEPES solution, 1M
Lysis buffer	150 mM	NH ₄ Cl
	1 mM	KHCO ₃
	0.1 mM	Na ₂ EDTA
Restimulation medium (RM)	99 % Vol.	TCM
	1 % Vol.	Rat serum
TCGF	80 % Vol.	TCM
	10 % Vol.	Horse serum (inactivated)
	10 % Vol.	Supernatant from ConA stimulated mouse splenocytes
TCM	ad 1 L	DMEM
	2 mM	L-Glutamine
	100 IU/ml, 100 µg/ml	Penicillin/Streptomycin
	3.6 g/l	Asparagine
	1 mM	Sodium-Pyruvate
	10 ml/L	Non-essential amino acids
	4 µl/L	2-Mercaptoethanol

Medium	Specified amount	
TCM + FCS	90% Vol.	TCM
	10% Vol.	Fetal calf serum (inactivated)
PBS (pH 7.4)	12 mM	Na ₂ HPO ₄ / NaH ₂ PO ₄
	137 mM	NaCl
	2.7 mM	KCl
FACS buffer	95 % Vol.	PBS
	5 % Vol.	Rat serum
	0.05 %	NaN ₃
CNS density gradient reagent	10.8 mL	Isotonic Percoll (1.124g/mL)
	10 mL	Underlay Percoll (1.077g/mL)
Blood lymphocyte gradient reagent	100 µL	Heparin (5000U/mL)
	0.63 mL for 5 mL blood	Optiprep
Ca ²⁺ imaging buffer (pH 7.4)	140 mM	NaCl
	5 mM	KCl
	1 mM	MgSO ₄ * 7 H ₂ O
	1 mM	CaCl ₂
	1 mM	NaH ₂ PO ₄ * H ₂ O
	5.5 mM	Glucose
	20 mM	HEPES

2.1.2 Antibodies

Antibody (clone, isotype)	Host and specificity company	Applications
isotope control (MOPC31c, IgG1)	mouse Sigma	Flow cytometry, primary antibody
CD4 (W3/25, IgG1)	mouse anti-rat Serotec	Flow cytometry, primary antibody
$\alpha\beta$ TCR (R73, IgG1)	mouse anti-rat Serotec	Flow cytometry, primary antibody
CD134 (OX40)	mouse anti-rat Serotec	Flow cytometry, primary antibody
CD25 (OX39, IgG1)	mouse anti-rat Serotec	Flow cytometry, primary antibody
IFN γ (DB-1, IgG1)	Mouse anti-rat eBiosciences	Flow cytometry, primary antibody
IL-17 (TC11-18H10, IgG1)	PE-conjugated rat anti-mouse BD	Flow cytometry, primary antibody
integrin α L (WT.1, IgG2a)	mouse anti-rat provided by Dr. Masayuki Miyasaka	Flow cytometry, primary antibody
integrin α 4 (TA-2, IgG1)	mouse anti-rat Serotec	Flow cytometry, primary antibody
ICAM-1 (1A29, IgG1)	mouse anti-rat provided by Dr. Masayuki Miyasaka	Flow cytometry, primary antibody
VCAM-1 (MR106, IgG1)	mouse anti-rat Serotec	Flow cytometry, primary antibody
CD62L (HRL2, IgG)	Armenian hamster anti-rat provided by Dr. Masayuki Miyasaka	Flow cytometry, primary antibody
MHCII (OX6, IgG1)	mouse anti-rat Serotec	Flow cytometry, primary antibody
APC IgG	Goat anti-mouse Jackson Laboratory	Flow cytometry, secondary antibody

Antibody (clone, isotype)	Host and specificity company	Applications
PerCP IgG	Rabbit anti-mouse Santa Cruz	Flow cytometry, secondary antibody
APC IgG	Goat anti-armerian hamster Jackson Laboratory	Flow cytometry, secondary antibody
laminin α 1 (polyclonal)	rabbit anti-rat serum provided by Dr. Takako Sasaki	Histology primary antibody
CD43 (W3/13, IgG2b)	Mouse anti-rat Serotec	Histology primary antibody
Cy3 IgG	Goat anti-rabbit Jackson Laboratory	Histology secondary antibody

2.1.3 Antigens

MBP was prepared from guinea pig brain homogenates as reported (Campbell et al., 1973), and recombinant MOG (amino acids 1-120) was produced as described (Adelmann et al., 1995).

2.1.4 Animals

Lewis rats were obtained from the animal facility at the Max Planck Institute of Biochemistry. Dark Agouti rats were purchased from Harlan. LE and DA rats were interbred to obtain the F1 generation. All animals were kept and bred in the animal facility at the Max Planck Institute of Neurobiology and all experiments were conducted according to Bavarian state regulations for animal experimentation and approved by the appropriate authorities.

2.2 Methods

2.2.1 Cell culture

Cultivation of cell lines. T cell lines were cultivated in fully complemented DMEM medium in standard cell culture-treated plastic dishes (BD) in a humidified incubator (Heraeus) at 37°C and 10%CO₂, respectively. Cells growing in suspension were harvested by repeatable pipetting, and adherent cells were treated with Trypsin-EDTA (PAA Laboratories) for 3-5 min at 37°C. Cell densities were determined using a Neubauer hemocytometer (Neubauer). Cultures were kept subconfluent by regular dilution with fresh medium. Cells were pelleted by centrifugation at 250 rcf for 7 min at 4°C.

Freezing and thawing of cell stocks. For preparation of long-term stocks, 20-30×10⁶ cells were harvested and resuspended in 1.5 mL of Freezing medium. Stocks were frozen in a dedicated Freezing Container (Thermo Fisher Scientific) at -80°C and subsequently stored in liquid nitrogen. For thawing, stocks were transferred to 37°C and washed once with 10 ml of EH to remove DMSO, before resuspension in 10 ml of warm medium.

Generation of retrovirally transduced, antigen-specific T cell lines. Antigen-specific T cells were generated using the method of Flügel et al. (Flügel et al., 1999). Rats were immunized by subcutaneous injection of antigen (100 µg), emulsified in complete freunds adjuvant (CFA, Difco) containing *Mycobacterium tuberculosis* strain H37RA (4 mg/mL). Cells from the draining lymph nodes were isolated 10 days after immunization and co-cultured with GP+E-86 cells (2×10⁵ of T cells with 1.5×10⁴ GP+E cells per well, in 96 well round-bottom plate), which were transfected to produce a GFP gene-coding retrovirus. Alternatively, GP+E-86 cells transfected with pMSCV-ΔNFAT-GFP (aa 1-460 of mouse NFAT1) were used and cultured with a modified limiting dilution method. The T cells were positively selected by specific antigen stimulation (10 µg/mL), and negatively using an antibiotic resistance gene included in the retroviral vector. During the first two days, T cells were stimulated with their specific antigen in RM and afterwards IL-2 conditioned medium (TCGF) was added for expanding and maintaining selected cells until next stimulation. For

the following restimulation, T lymphocytes were incubated with irradiated (5000 rad) syngeneic thymocytes in the presence of antigen. At least three rounds of stimulation with the antigen, followed by expansion in the conditional medium were completed before the cells were used for the experiments.

In vitro T cell proliferation assays. To evaluate the specificity of the established T cell lines for their respective antigen, *in vitro* proliferation assays were performed. 2×10^4 T cells were cultured with 1×10^6 irradiated thymocytes in 100 μ l of RM in a 96-well flat-bottomed plate for 48 h. Series of diluted antigens were used. Then, ^3H -thymidine was added to the culture and the plate was incubated for an additional 16 h. ^3H uptake was measured using a β -counter (Coulter). In some experiments, meningeal APCs, prepared as described (Bartholomäus et al., 2009), were used. Briefly, CNS meninges were dissected mechanically and homogenized. Then 10^6 meningeal cells were co-cultured with 10^4 antigen-specific T cells. For some experiments meningeal APCs were pretreated with exogenous antigens (10 $\mu\text{g}/\text{ml}$ for 1 h) and co-cultured with T cells. Production of IFN γ was examined by flow cytometry 48 h after co-culturing.

2.2.2 Flow cytometric analysis (FACS)

Quantification of cell numbers. At the indicated time points, animals were sacrificed by CO_2 . Spleen, CNS meninges and parenchyma were isolated, homogenized and suspended in EH, before used for further analysis. For cell quantifications, defined amounts of the cell suspension were mixed with a defined number of fluorochrome conjugated micro-beads (BD) and analyzed by FACSsort (BD). Values are shown as cells per gram of organ.

Surface staining. For the T cell surface marker staining, additional purifications were performed. Cells from the spleen were treated with lysis solution to remove erythrocytes, while T cells from the CNS parenchyma were purified by density gradient centrifugation (Percoll, GE Healthcare). Thereafter 1×10^6 cells per staining were used. To prevent nonspecific antibody binding, cells were incubated with FACS buffer in a 96-well plate for 10 min on ice. Subsequently, cells were incubated with the primary antibody (1 $\mu\text{g}/\text{sample}$) for 30 min on ice. After washing twice with FACS buffer, cells were incubated with fluorescently labeled secondary antibody (diluted

1:200 in FACS buffer) for 30 min on ice. Finally, the cells were washed once with FACS buffer and once with PBS.

Intracellular staining. For intracellular stainings, cells were fixed in 2 % PFA for 20 min followed by washing in PBS. Permeabilization was carried out using BD Perm/Wash buffer during incubation on ice for 15 min. All further steps were conducted in BD Perm/Wash buffer. The primary antibody for IFN γ (diluted 1:200) was added and incubated on ice for 30-60 min. After three washings with BD Perm/Wash, the secondary antibody (1:200 dilution) along with PE-IL-17 (1:400 dilution) antibody were added and incubated for 90 min on ice followed by one washing with BD Perm/Wash, one with PBS and final resuspension in PBS.

Stained cells were measured using a FACSCalibur flow cytometer (BD) and the data were analyzed by FlowJo software (Tree Star).

2.2.3 Histology

Organs from PFA-perfused rats were fixed in 4%PFA in PBS for 24 h and immersed in 40% sucrose. Tissues were embedded in Tissue-Tek O.C.T. Compound (Sakura), and 10 μ m sections were cut on a CM3050 S Cryocutter (Leica).

Tissue sections were thawed, fixed in 4%PFA for 20 min, and blocked with 5% Rat serum in PBS for 1 h at room temperature. This buffer was used for all further steps. Incubation with primary antibody (dilution 1:200) was done for 1 h at room temperature or at 4°C overnight, and with secondary (Cy3-conjugated anti-rabbit Ig dilution 1:500) for 1-3 h at room temperature. Three washings for 10 min were done in between.

In vitro cultured resting T_{MBP-NFAT-GFP} cells were labeled with PKH26 red fluorescent cell linker kit for general cell membrane labeling (Sigma-Aldrich). Part of the cells was treated with ionomycin (1 μ M) for 3 min, and then stimulated and non-stimulated cells were incubated on collagen coated glass slides for 15 min to immobilize. Cells were fixed in 4%PFA and stained with DAPI (5 μ g/ml) for 10 min.

All slides were then left to dry and embedded in anti-fading mounting medium (Dianova).

All images were acquired on an inverted SP2 confocal microscope (Leica) equipped with a 20x objective lens (N.A: 0.7) or 40x oil immersion lens (N.A: 1.25) (both from Leica).

2.2.4 Animal experiments

Adoptive transfer EAE. Transfer EAE was induced by intravenous injection of $5-10 \times 10^6$ encephalitogenic T cell blasts into 8-12 weeks old animals. The animals were monitored for weight loss and clinical symptoms daily. Clinical evaluation was done by grading clinical scores as follows: 0.5, loss of tail tonus; 1, tail paralysis; 2, gait disturbance; 3, hind-limb paralysis; 4, tetraparesis; 5, death.

Intrathecal injection. Animals were anesthetized by intramuscular injection of fentanyl/midazolam/medetomidin (5 $\mu\text{g}/\text{kg}$, 2 mg/kg and 150 $\mu\text{g}/\text{kg}$, respectively) and mounted in a stereotactic device. For labeling of meningeal APCs, 6 μg of Texas Red or tetramethylrhodamine conjugated dextran (molecular size: 70 kDa or 2 MDa respectively from Molecular Probes) was injected into the cisterna magna between C1 and C2 using a 27G needle (BD). For meningeal APC-pulsing, meningeal APCs were prepared from naive Lewis rats by mechanical homogenization. Cells were then incubated with antigen (10 $\mu\text{g}/\text{ml}$) in RM for 1 h at 37°C. Finally, cells were washed three times and then injected intrathecally. In some experiments, local APCs were visualized by intrathecal injection of DQ-MOG (custom synthesis by Molecular Probes). 1 μg of DQ-MOG was injected into anesthetized animals 2 h before imaging. For inducing inflammation in the leptomeninges, 30 ng LPS were injected.

Splenocyte retransfer and SNARF-1 labeling. The “migratory” encephalitogenic T cells were prepared from host spleens 3 days after transfer. Erythrocytes were removed from the suspensions by osmotic lysis and the macrophages by adhesion on culture dishes by incubating for 1 h at 37°C. Prior to SNARF-1 labeling, splenocytes were enriched for CD4⁺ T cells using the MagCollect Rat CD4⁺ T cell Isolation Kit (R&D Systems). On average, 20-30% of the T cells were GFP/ Δ NFAT-GFP expressing cells. T cells were labeled with SNARF-1 (Molecular Probes) by incubating for 15 min at the concentration of 1.25 μM . SNARF-1 labeling results in a strong signal in the nucleus, whereas cytoplasm staining is often weaker.

2.2.5 Fluorescent video-microscopy

Resting *in vitro* T_{MBP-NFAT-GFP} cells were resuspended in buffer for Ca²⁺ imaging and incubated in a μ -slide I 0.4 collagen coated microscopy chamber (ibidi). T cells were stimulated by 1 μ M ionomycin during image acquisition, and imaging was continued for 15 min after stimulation. Cells were then collected, washed from ionomycin, plated again in new Microscopy chamber, and imaged for another 2-3 h. Images were acquired every 30 s. Time-lapse recordings were performed using an inverted Axiovert 200 M microscope, equipped with a 40x oil immersion objective (N.A. 1.3, Zeiss). Images were acquired by using a Coolsnap-HQ camera (Photometrics, Roper Scientific) and processed by MetaMorph software (Molecular Devices).

2.2.6 *In vivo* two-photon microscopy

Image acquisition. Time-lapse two-photon laser-scanning microscopy was performed using a SP2 confocal microscope (Leica) equipped with a 10 W Millennia/Tsunami laser (Newport Spectra Physics). Excitation wavelength was tuned to 880 nm and routed through a 20x water-immersion objective (N.A. 0.95, Olympus) or 25x water-immersion objective (N.A. 0.95, Leica). Imaging was done with 1x or 2x zoom and 30-50 μ m z-stacks were acquired with 3-4 μ m step size. Acquisition rate was 25.219 s time interval, with images averaged twice. Fluorescent signals were detected using non-descanned photomultiplier tube detectors (Hamamatsu) equipped with 440/40 nm (detection of second harmonic), 525/50 nm (GFP), 579/34 nm (tetramethylrhodamine dextran), 630/69 nm (Texas Red dextran and SNARF), and 685/40 nm (SNARF) band-pass filters (Semrock).

Animal preparation. Animals were anesthetized by intramuscular injection of fentanyl/midazolam/medetomidin (5 μ g/kg, 2 mg/kg and 150 μ g/kg, respectively), orotracheally intubated, and ventilated with 2% isoflurane. Animals were placed on a custom-made microscope stage and the body temperature was regulated by a heated pad and thermo-sensor (37.5°C). Electrocardiograms were recorded and physiological parameters, such as concentrations of inspiratory and expiratory gases, and ventilation pressure were constantly monitored during imaging.

Spinal cord imaging. For spinal cord imaging a spinal cord window was prepared at level Th12/L1. After midline skin incision, the paravertebral musculature was detached from the spine and laminectomy on one spine disc was performed using a dental drill (FOREDOM). For reducing artifacts caused by heart beats and breathing of the animal, the laminectomized spine disc along with two neighboring discs was fixed using a custom made fixation mounted on the stage (Figure 2.1). Around the imaging window, an agarose ring was mounted, retaining the buffer in which water objective was embedded. Blood vessels and CNS meningeal APCs were visualized by intravenously and intrathecally injected fluorescent dextran conjugates.

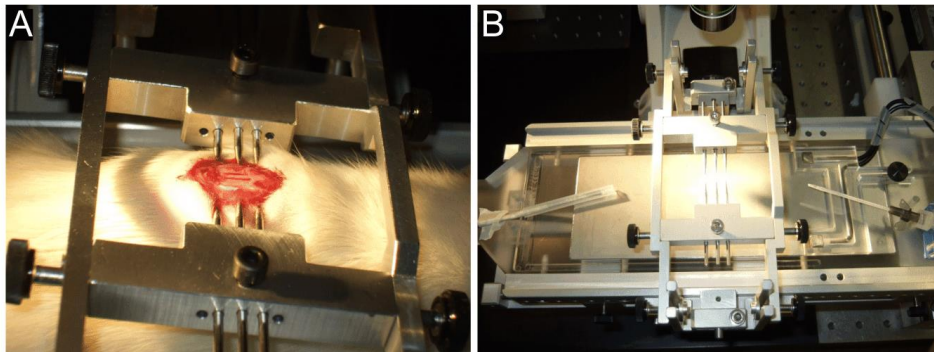


Figure 2.1. Fixation and stage for intravital microscopy of the spinal cord. (A) Rat prepared for spinal cord imaging. In the middle, the imaging window is opened and the spine is stabilized using a custom-made fixation. (B) Stage for intravital microscopy. Metal plate is heated and temperature regulated with a thermo-sensor on the left. ECG pads and a tube for the intratracheal intubation are depicted on the right. Fixation is mounted on the stage and its position can be adjusted in all dimensions. (Adopted from Bartholomäus, 2011).

Spleen imaging. For spleen imaging, a skin incision was made and the spleen was gently pulled out of the animal, taking care that its blood connection is not disrupted. The organ was placed on a custom-made stage with an opening for the blood vessels, that was mounded as close to the animal as possible to reduce tension on the vessels. The spleen was embedded in warmed buffer and pressed slightly by a glass bottom culture dish for stabilization.

Local injections into the imaging window. For local injections a microcapillary (tip diameter of 13 μm , Biomedical Instruments) was used, and hold by a micro-manipulator (Luigs & Neumann). The capillary was pushed through the arachnoidea

through a hole cut by a high-energy two-photon laser. For the injection, the microcapillary was filled with a solution of 10 µg/ml of protein and 0.2 µg/ml tetramethylrhodamine dextran. A volume of 3-4 µl of this solution was injected.

Image analysis. Time-lapse images were acquired using Leica LCS software (Leica), and subsequently processed and analyzed by ImageJ (NIH). To obtain two-dimensional movies, a Gaussian blur filter was applied, the contrast was adjusted by linear rescaling, and maximum intensity z-projections were made. In some videos the noise was removed additionally using a Median filter. The position of T cells in the three-dimensional space was analyzed using Imaris software (Bitplane). For analyzing perivascular localization, T cells located further than 10 µm (thickness of endothelial cell plus attached T cell) from the blood vessels in the maximum projection were considered as detached and then correlated with the total cell number. The instantaneous T cell velocity was calculated by combining the cell coordinates with the time interval of imaging. Trajectory lines were drawn based on the coordinate information obtained. The calculation of the mean square displacement (MSD) was done for a 10 min time interval and only the cells present for the entire period of time were considered (Beltman et al., 2009). Cells were considered to be stationary if their displacement did not exceed 10 µm in 10 min. The T cell/APC contacts were analyzed manually, and all of the physical interactions between the T cells and labeled meningeal APCs in the three-dimensional volume were defined as contacts. The meandering index was calculated as $(cell\ displacement)/(track\ length)$.

2.2.7 Statistical analysis

The statistical evaluation was performed using Prism software (GraphPad). $p < 0.05$ was considered significant. n.s.: not significant. Test used, as well as the resulting p value is specified for each experiment separately in the figure legends.

3 RESULTS

3.1 Infiltration of leptomeninges and parenchyma

In this study, the early interactions of myelin-specific autoimmune T cells with target structures in the CNS were examined. Three types of GFP-labeled CD4⁺ T cell lines, distinguished by their encephalitogenic potential (Kawakami et al., 2004) were investigated: MBP-specific T cells from Lewis rats (T_{LE-MBP}) and MOG-specific T cells from DA rats (T_{DA-MOG}) were highly aggressive and induced a severe neurological disorder (EAE^{hi}), while MOG-specific T cells from Lewis rats (T_{LE-MOG}) hardly induced any symptoms (EAE^{lo}) (Figure 3.1.1).

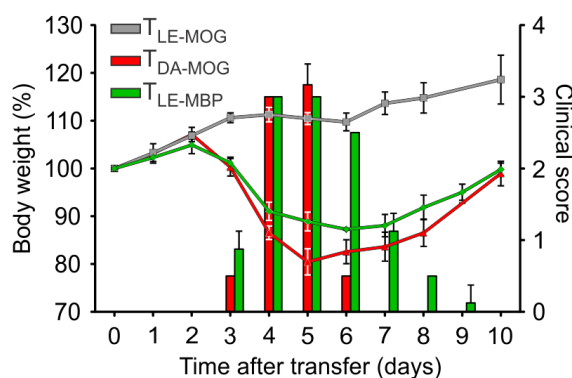


Figure 3.1.1 Representative clinical EAE course induced by GFP labeled T_{LE-MOG} , T_{DA-MOG} , and T_{LE-MBP} cells. Lines depict the body weight (day 0 set to 100%, left y-axis) and bars indicate clinical scores (right y-axis). Data of three animals per group were averaged and representative data of at least three independent experiments are shown.

However, all T cell lines were highly specific against their cognate antigen, and secreted TNF α , IL-10, MCP-1 and MIP-1 at comparable levels, but did not produce IL-4 (Kawakami et al., 2004). Additionally, their intracellular production of IFN γ /IL-17 was very similar (Figure 3.1.2A), and expression of surface molecules including MHC class II, adhesion molecules and activation markers, by the three T cell lines was indistinguishable (Figure 3.1.2B).

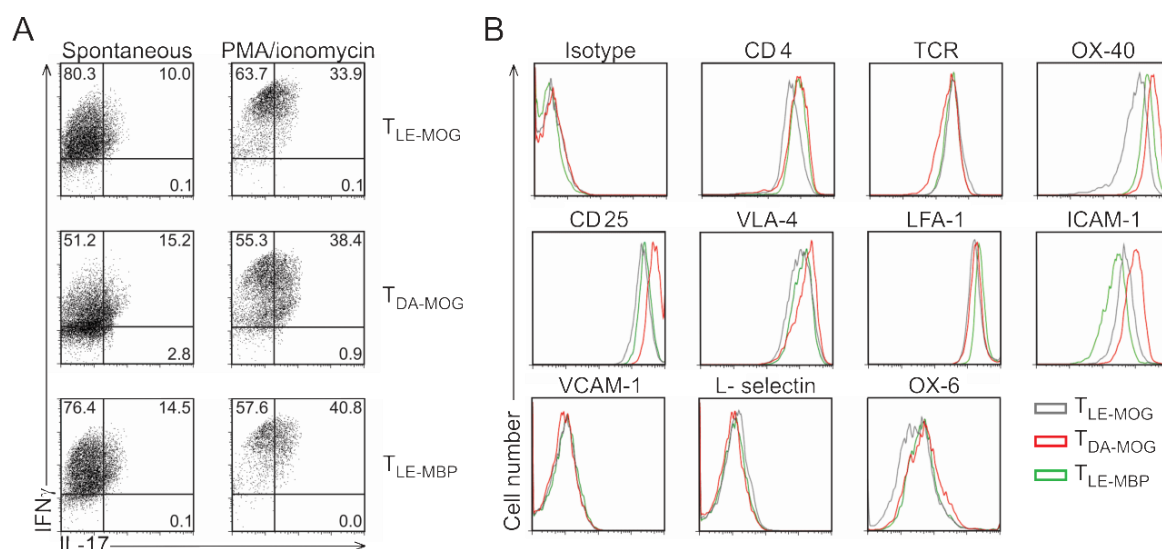


Figure 3.1.2. Profiling of *in vitro* cultured auto-reactive T cells. (A) Dot plots of IFN γ /IL-17 intracellular staining with or without PMA/ionomycin stimulation. The inserted numbers indicate the proportion of cells in each quadrant. Representative results are shown from four independent experiments. (B) Histograms depict expression of cell surface markers on *in vitro* activated GFP-labeled T cells. T_{LE-MBP} (green lines), T_{LE-MOG} (grey lines) and T_{DA-MOG} (red lines) cells were stained with specific antibodies as indicated and analyzed by flow cytometry. Representative results from two independent experiments are shown.

Both, EAE^{lo} as well as EAE^{hi}, T cells showed similar infiltration kinetics into the leptomeninges (Figure 3.1.3A). All T cell lines appeared on day two post transfer (p.t.), and then continued to massively infiltrate the meningeal area on day three and four in comparable numbers, regardless of their encephalitogenicity. As previously described (Bartholomäus et al., 2009), meningeal infiltration is followed by an infiltration of the parenchyma. Large numbers of highly encephalitogenic T cells penetrate into the CNS parenchyma on day three, increasing further on day four (Figure 3.1.3B). In striking contrast, EAE^{lo} T_{LE-MOG} cells also appeared in the CNS parenchyma but in much lower numbers, reaching only 10% of EAE^{hi} T cell numbers on both day three and four (Figure 3.1.3B). Histology confirmed that T_{LE-MOG} cells remained in the leptomeninges and the Robin Virchow space at a time when T_{LE-MBP} cells and T_{DA-MOG} cells became evenly distributed within the CNS parenchyma (Figure 3.1.3C).

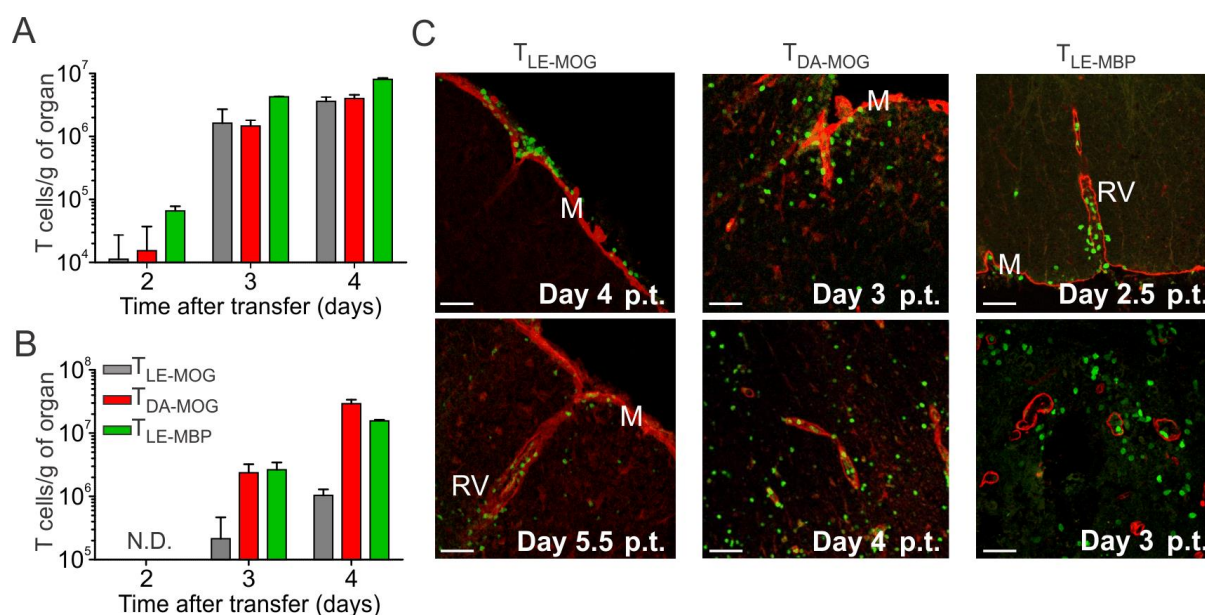


Figure 3.1.3. Infiltration of self-reactive effector T cells into the CNS. (A and B) T cell infiltration within CNS leptomeninges (A) and parenchyma (B) was quantified by flow cytometry at the indicated time points. Means \pm S.D. of two animals, triplicate measurements per animal, are shown. Each graph includes six animals per group. Representative results from at least three independent experiments are shown. N.D.: not detected. (C) Spinal cord cryosections were prepared at indicated time points after transfer of auto-reactive GFP-labeled T cells (green). Sections were stained with anti-laminin $\alpha 1$ antibody (red). Images were acquired by confocal microscopy. M: CNS meninges, RV: Robin Virchow space. Scale bar: 50 μ m.

3.2 Intraluminal crawling is unaffected by pathogenic potential

Upon arrival in the CNS, EAE^{hi} T_{LE-MBP} cells have been shown to dock on the luminal surface of the leptomeningeal vessels and then crawl there, preferably against the blood flow, potentially looking for suitable extravasation sites (Bartholomäus et al., 2009). Two-photon imaging documented that while they are within the vascular lumen, initially the weakly encephalitogenic T_{LE-MOG} cells behave in a similar way to their pathogenic counterparts, T_{LE-MBP} and T_{DA-MOG} cells (Figure 3.2.1A). About 40% of the observed T cells migrated against blood flow, whereas 20% moved along the blood stream, regardless of antigen specificity (Figure 3.2.1B). Furthermore, all T cell types crawled for a similar duration of time (Figure 3.2.1C) and with similar velocity (Figure 3.2.1D), again regardless of their antigen specificity and pathogenic

potential. Overall, the intraluminal locomotion of EAE^{hi} and EAE^{lo} cells was indistinguishable.

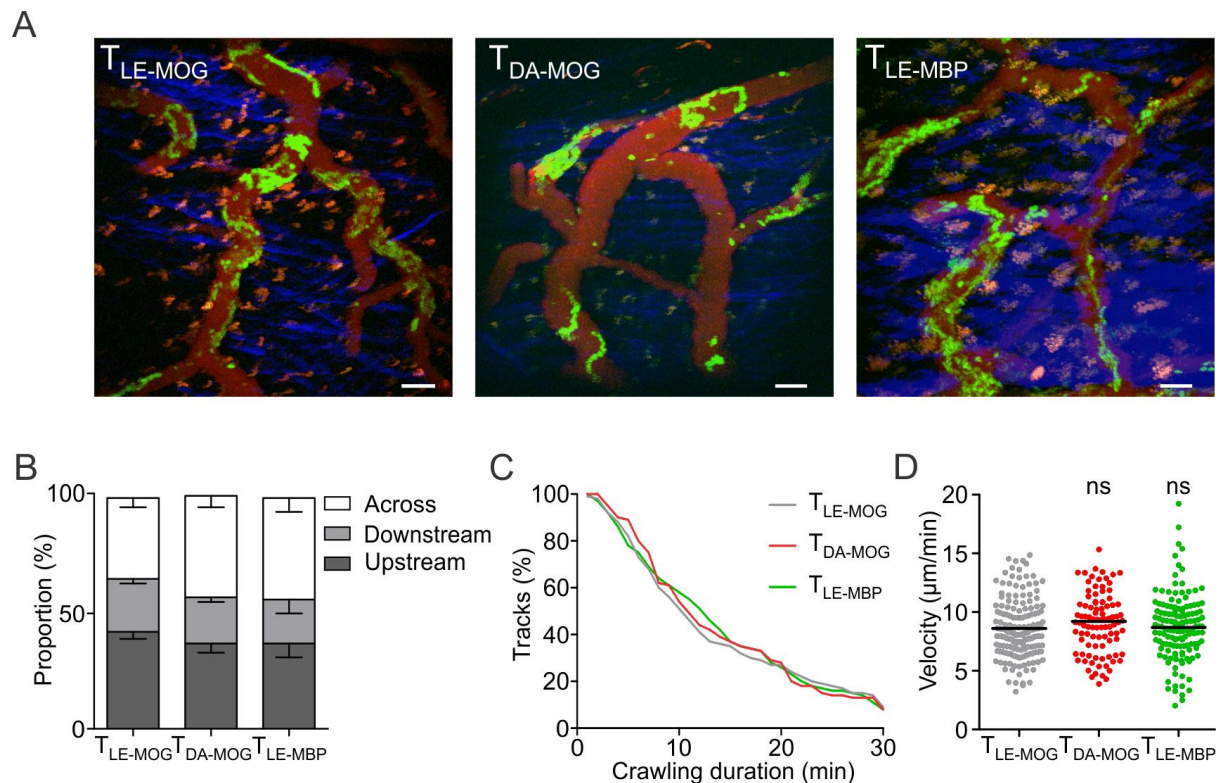


Figure 3.2.1. Intraluminal motility in the leptomeningeal vessels. Intraluminal T cell motility was analyzed from intravital recordings. (A) Time projections of 30 min are shown for T_{LE-MOG}, T_{DA-MOG}, and T_{LE-MBP} cells (green) on day two p.t., when all cells are scanning the intraluminal surface of the blood vessels (red). Collagen fibers (blue) were detected by second harmonic generation. Scale bar: 50 μm. (B) Intraluminal T cell movements were categorized relative to the direction of blood flow as follows: Downstream: moving with the blood flow, Upstream: moving against the blood flow, and Across: moving at an angle of >45° of the vessel axis, or arrested, and their relative representation was calculated. Results were obtained from at least four different videos per cell line. Means +/- S.D. are shown. (C) Durations of intraluminal crawling. Fractions of T cell tracks are plotted as a function of their crawling duration. (D) Intraluminal velocity of GFP-expressing T cells. (C and D) Results are sum of at least three different experiments per cell line. ns: not significant (One-way ANOVA, Kruskal Wallis test - Dunn's multiple comparison test).

3.3 Perivascular detachment is impaired in EAE^{lo} T cells

After extravasation, effector T cells continued to crawl on the abluminal surface of the vessels and finally detached to spread through the leptomeningeal space

(Bartholomäus et al., 2009). To compare the infiltration kinetics of EAE^{hi} and EAE^{lo} T cells in more detail, 24 h long panoramic time-lapse imaging (one panoramic image per hour), was performed, starting on day two after T cell transfer, when the T cells just start to appear in leptomeninges, until the time when they are fully infiltrated.

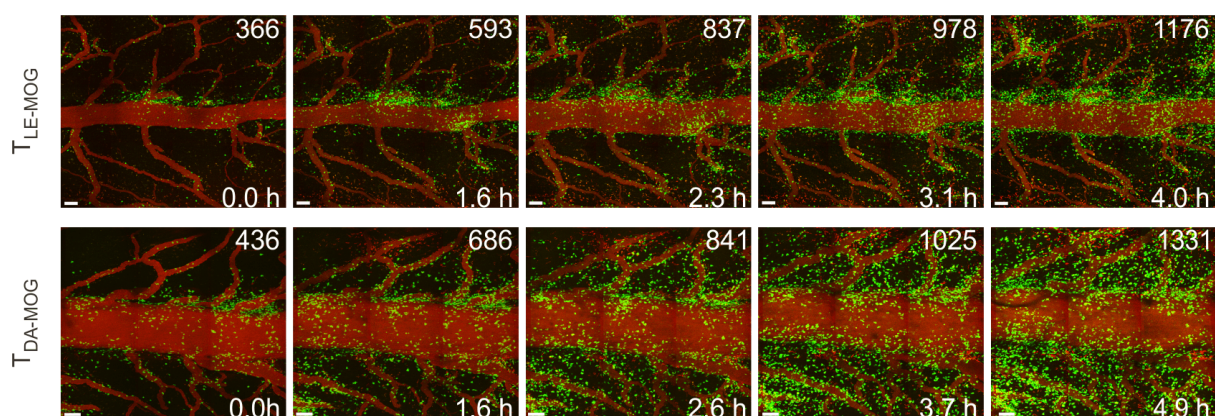


Figure 3.3.1. Meningeal infiltration of EAE^{hi} and EAE^{lo} T cells. Representative panoramic views of the meningeal infiltration by T_{LE-MOG} (upper panels) or T_{DA-MOG} cells (lower panels). Blood vessels are indicated in red. Inserted numbers represent the number of cells/mm² and time after start of imaging. Scale bar: 100 μ m.

Confirming flow cytometric results, all T cell lines penetrated into the leptomeninges with similar kinetics, regardless of their encephalitogenic potential (Figure 3.3.1 and Figure 3.3.2A). However, the cell types' subsequent behavior was remarkably different. While EAE^{hi} cells (T_{LE-MBP} and T_{DA-MOG}) detached from the perivascular surfaces and distributed evenly in the sub-leptomeningeal area, EAE^{lo} cells (T_{LE-MOG}) failed to do so and tended to, after extravasation, accumulate in close proximity to the blood vessels (Figure 3.3.1 and Figure 3.3.2, B and C).

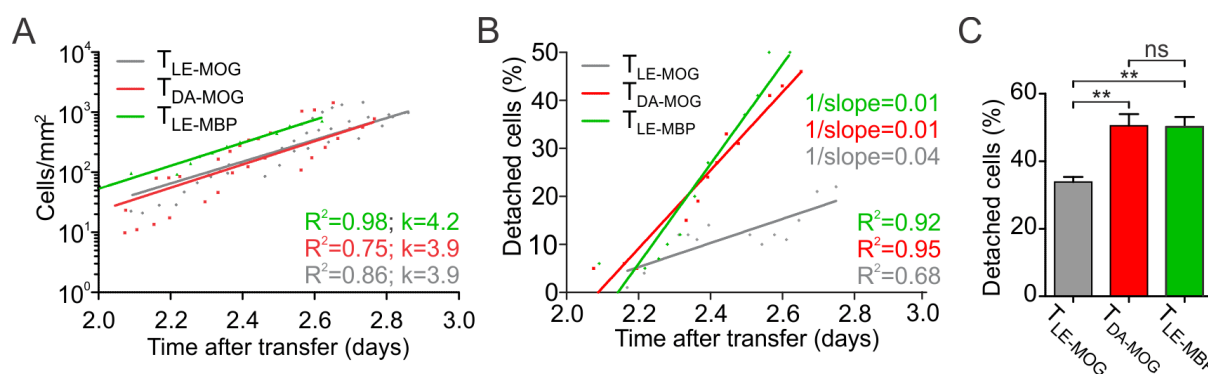


Figure 3.3.2. Infiltration and vessel detachment kinetics of EAE^{hi} and EAE^{lo} T cells into CNS meninges. (A) The numbers of T cells that have infiltrated the CNS meninges were counted from long-term intravital recordings. The cell numbers at indicated time points were normalized by area. Results were obtained from at least three animals per cell line, and combined from two independent experiments for $T_{LE-MOG-GFP}$ and $T_{DA-MOG-GFP}$ cell lines, and one experiment for the $T_{LE-MBP-GFP}$ cell line. (B) Kinetics of T cell detachment from leptomeningeal vessels: Detached cells were defined as $>10\ \mu\text{m}$ distance from the closest vessels. At least three animals per cell line were used. Representative data from two independent experiments are shown. In A and B, trend lines were calculated by GraphPad Prism software. R^2 describes how well the trend line fits the data. k and 1/slope indicate the exponential or linear trend line slope, respectively. (C) The proportions of detached cells from leptomeningeal vessels at day three p.t. At least four animals were used for each cell line. **p < 0.01 (One-way ANOVA, Tukey's multiple comparison test).

3.4 After extravasation, EAE^{hi} T cells have lower motility compared to EAE^{lo} T cells

Next, the motility of different auto-reactive T cells upon extravasation was compared by analyzing their basic motility parameters. EAE^{lo} T cells (T_{LE-MOG}) moved with higher velocity compared to EAE^{hi} T cells (T_{DA-MOG} and T_{LE-MBP}), while the motility of different EAE^{hi} cell lines was indistinguishable (Figure 3.4.1A). EAE^{hi} T cells had a higher percentage of stationary cells (Figure 3.4.1C) (see material and methods), and were more confined comparing to EAE^{lo} (T_{LE-MOG}) cells, indicated by their lower meandering index and lower mean square displacement (Figure 3.4.1, B and D).

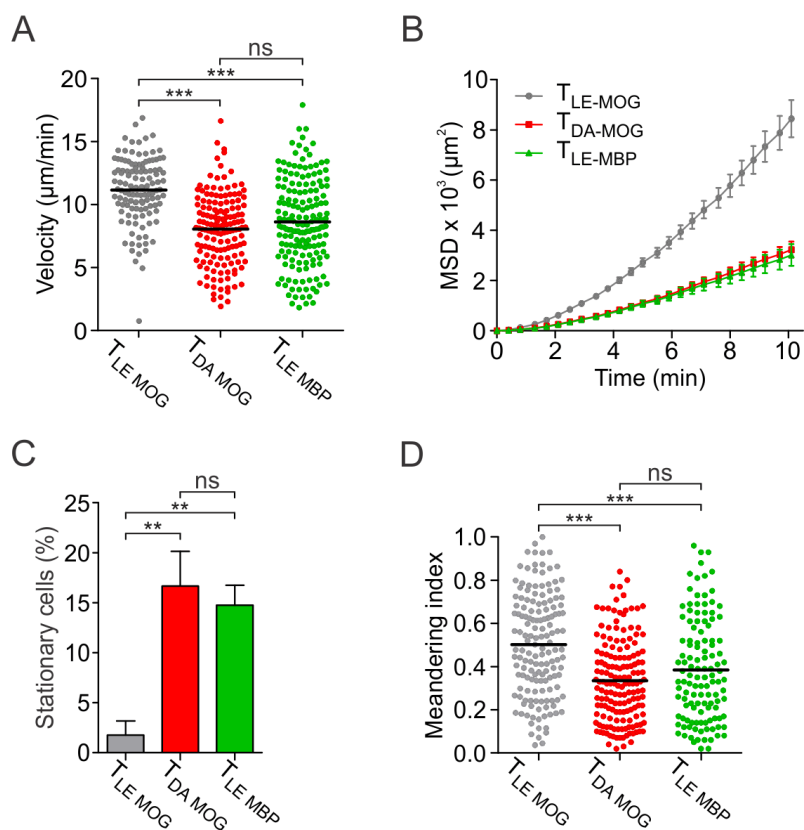


Figure 3.4.1 Motility of EAE^{hi} and EAE^{lo} T cells after extravasation from leptomeningeal vessels. Velocity (A), mean square displacement (B), frequency of stationary cells (C) and meandering index (D) of T_{LE-MOG}, T_{DA-MOG} and T_{LE-MBP} cells were calculated from intravital recordings. A and D are sum, B is representative and C display means with S.D. of at least three independent experiments per cell line. A and D, ***p<0.001 (One-way ANOVA, Kruskal Wallis test - Dunn's multiple comparison test). C, **p<0.01 (One-way ANOVA, Tukey's multiple comparison Test).

3.5 EAE^{hi} T cells stay longer in contact with perivascular APCs compared to EAE^{lo} T cells.

After crossing the vascular wall, the myelin-specific T cells have been shown to establish contacts with local APCs (Bartholomäus et al., 2009). To test the hypothesis that difference in motility of EAE^{hi} and EAE^{lo} T cells might be due to their different interactions with local APCs, T cell/APC contacts were analyzed in more detail. Meningeal phagocytes were labeled by intrathecal injection of Texas-Red conjugated dextran. These phagocytes exhibit mostly macrophage and not DC markers, and a substantial proportion expresses MHC class II molecules on their surface, qualifying them as APCs (Bartholomäus et al., 2009). The EAE^{lo} T_{LE-MOG}

cells largely ignored the local APCs, moving continuously along straight trajectories (white line in upper panel of Figure 3.5.1). In contrast, the EAE^{hi} T_{DA-MOG} and T_{LE-MBP} cells halted upon contact with APCs, drawing trajectories that twisted around an anchoring point (white line in the middle and lower panel of Figure 3.5.1, respectively).

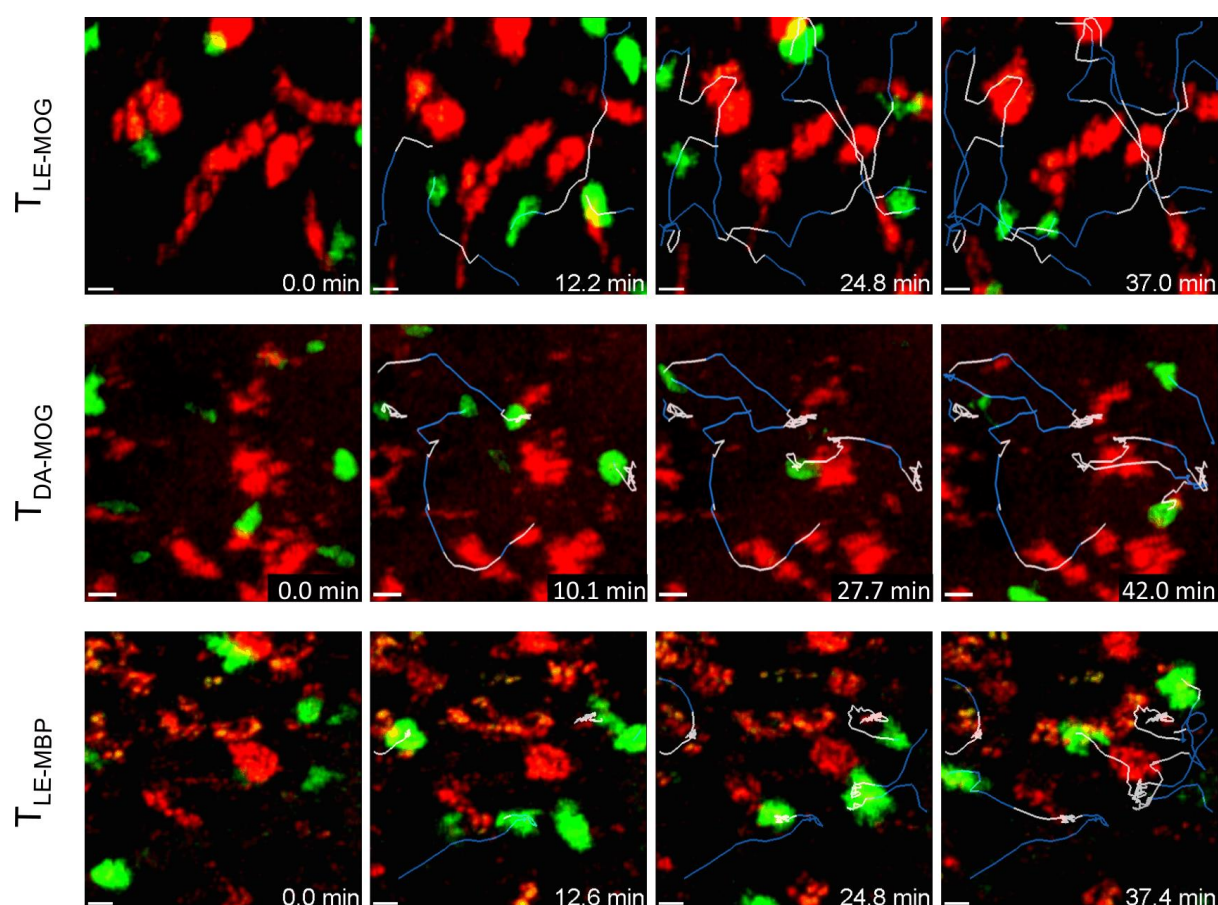


Figure 3.5.1. Contacts between infiltrated T cells (green) and perivascular/meningeal APC (red). Still images of representative T cell/APC contacts in the leptomeninges: T_{LE-MOG-GFP}, T_{DA-MOG-GFP} and T_{LE-MBP-GFP} cells are shown in green, together with local APCs (red). Trajectories of the T cell movement are overlaid with the images. White lines represent phases when the T cell contacts an APC, while blue lines indicate when T cell is freely moving. EAE^{lo} (T_{LE-MOG-GFP} cells, upper panels) or EAE^{hi} (T_{DA-MOG-GFP} and T_{LE-MBP-GFP} cells, middle and lower panels, respectively) are shown. Time scales are indicated. Scale bar: 10 μ m.

Detailed analysis showed that T cell/APC contacts made by EAE^{hi} T cells were significantly longer lasting (average duration 7 min for T_{DA-MOG}, and 6 min for T_{LE-MBP}), compared to those of EAE^{lo} T cells (3 min average duration) (Figure 3.5.2A).

The contacts of EAE^{hi} T cells were also less frequent, but lasted longer than those of EAE^{lo} T cells, which instead made repeated short contacts (Figure 3.5.2B).

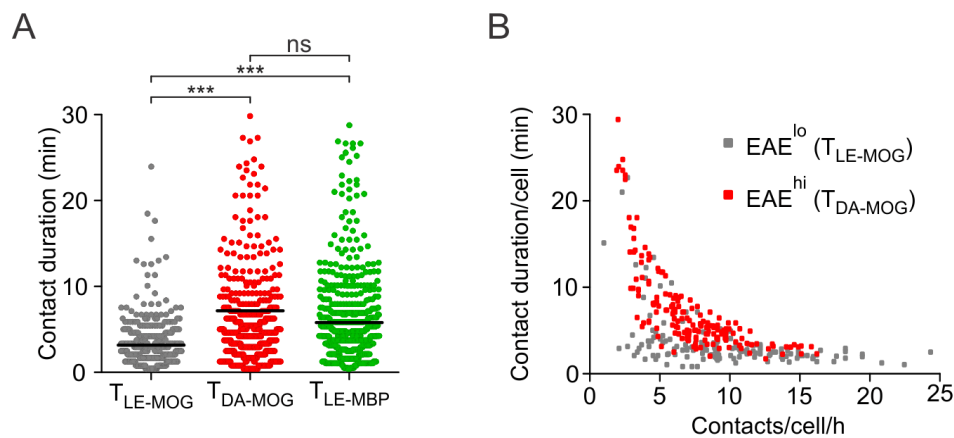


Figure 3.5.2. Quantification of T cell/APC contacts. (A) Contact duration of T_{LE-MOG-GFP}, T_{DA-MOG-GFP} and T_{LE-MBP-GFP} cells was calculated from intravital recordings. (B) Graph of T cell-based contacts, where each dot represents a single T cell plotted for the number of contacts per hour (x-axis) and average duration of contacts (y-axis). A and B, results are sum of at least three independent experiments per cell line. ***p<0.001 (One-way ANOVA, Kruskal Wallis test - Dunn's multiple comparison test).

Since contacts with local APCs lead to T cell activation (Bartholomäus et al., 2009; Kawakami et al., 2005), the expression of surface activation marker CD134 (OX40 antigen), as well as spontaneous production of IFN γ and IL-17 by all T cell lines, was monitored using flow cytometry. As expected, T_{LE-MBP} and T_{DA-MOG} cells were strongly activated in the CNS leptomeninges compared to those in the spleen, and were further activated within the CNS parenchyma. In contrast, activation of T_{LE-MOG} cells remained marginal (Figure 3.5.3), similar to OVA-specific control T cells (Flügel et al., 2001).

in vitro, was monitored. EAE^{lo} T cells were slightly less sensitive to limiting antigen doses than EAE^{hi} T cell lines (Figure 3.6.1). However, at saturating concentrations of antigen, T_{LE-MOG} cells proliferated with similar rates to T_{DA-MOG} and T_{LE-MBP} cells.

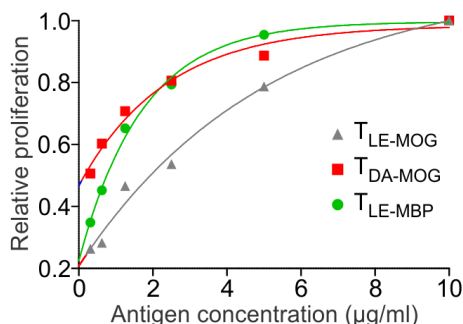


Figure 3.6.1. Sensitivity of T cells against specific antigen. Antigen-specific T cells were stimulated by serial dilution of antigens *in vitro*. Proliferation was quantified by ³H-labeled thymidine up-take. Means of triplicate measurements were calculated. Results are presented as a proliferation index (relative ³H uptake, with 10 µg/ml antigen concentration normalized as 1.0). Trend lines were inserted by GraphPad software. Cumulative results, from at least four independent experiments, are shown.

Another limiting factor for EAE^{lo} T cells could also be availability of local myelin auto-antigens in the leptomeninges. As shown before, leptomeningeal APCs are not saturated with locally produced MBP antigen and addition of exogenous antigen can further activate T_{LE-MBP} cells *in vivo* (Odoardi et al., 2007a). Thus, marginal antigen availability could especially affect immune responses against MOG, a minor myelin protein component (less than 0.1%) (Johns and Bernard, 1999). If this is the case, introduction of exogenous MOG into leptomeninges should provide sufficient activation stimulus for even low sensitive T_{LE-MOG} cells.

To test this, meningeal APCs from CNS leptomeninges of naive rats were prepared, loaded with antigen *in vitro* (MOG or control OVA), and then transferred intrathecally into animals, two days after i.v. transfer of T_{LE-MOG-GFP} cells, the time point when they start to appear in leptomeningeal area. Intravital panoramic views and quantification by flow cytometry confirmed that transferred MOG-pulsed APC intensified recruitment of T_{LE-MOG-GFP} cells by three-fold compared to the effect of control OVA-

pulsed APCs, and enhanced infiltration into CNS parenchyma to an even greater extent (Figure 3.6.2).

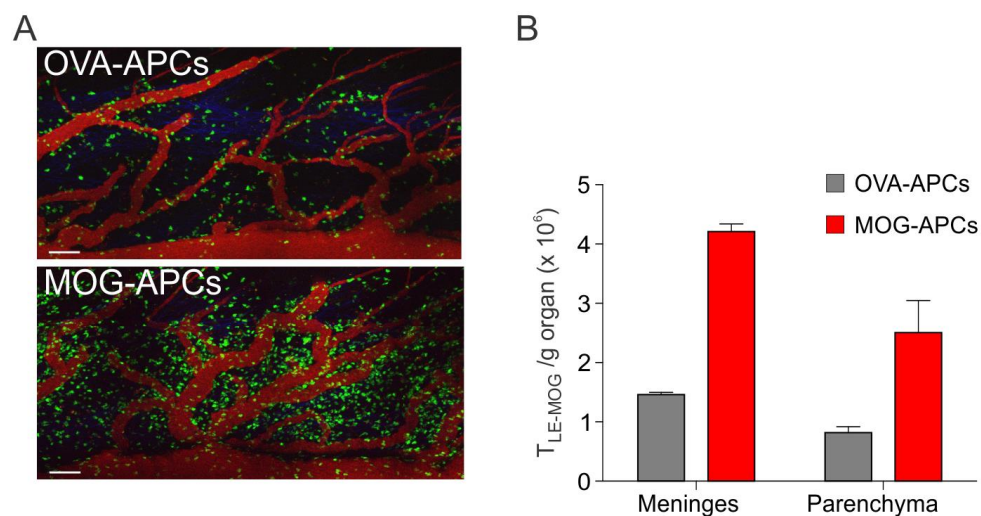


Figure 3.6.2. Intensified recruitment of $T_{LE-MOG-GFP}$ cells within the CNS meninges after MOG-pulsed APC intrathecal application. (A) Overview of CNS infiltrated $T_{LE-MOG-GFP}$ cells after intrathecal application of MOG- or OVA-pulsed meningeal APCs. Intravital imaging was performed 12 h after APC intrathecal injection. $T_{LE-MOG-GFP}$ cells (green) were visualized together with Texas Red conjugated dextran infused blood vessels (red). Scale bar: 100 μ m. (B) Quantification of infiltrated $T_{LE-MOG-GFP}$ cells by flow cytometry 12 h after intrathecal MOG- (red bars) or OVA-pulsed (grey bars) APC injection. Means and S.D. of triplicates measurements from two animals are shown.

Motility of T_{LE-MOG} cells after application of MOG-pulsed APCs was reduced, as shown by their lowered velocity (Figure 3.6.3A), and lowered mean square displacement (Figure 3.6.3B). They also became more confined (Figure 3.6.3C), and percentage of stationary cells increased (Figure 3.6.3D) to values characteristic for EAE^{hi} T cells (Figure 3.4.1C).

T_{LE-MOG} cells interacted with local APCs very much like highly encephalitogenic T cells did. They made less frequent but longer lasting contacts with APCs (Figure 3.6.3E), with average contact duration extending from 3 to 6 min (Figure 3.6.3F).

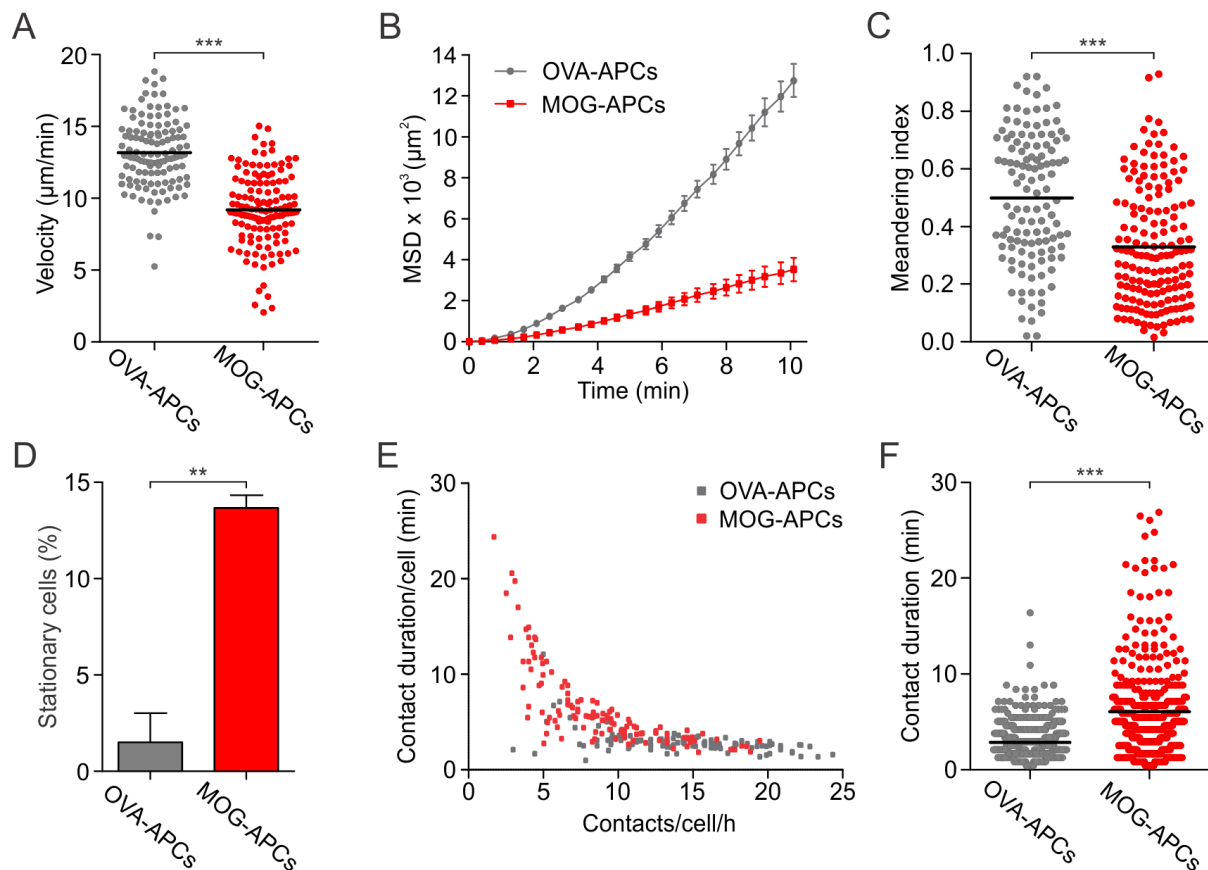


Figure 3.6.3. Motility of $T_{LE-MOG-GFP}$ cells within the CNS meninges after MOG or OVA-pulsed APCs intrathecal application. Velocity (A), mean square displacement (MSD) (B), meandering index (C), and percentage of stationary cells (D), were calculated from intravital recordings. (E) Graph of T cell-based contact where each dot represents a single T cell plotted for the number of contacts per hour (x-axis) and average duration of contacts (y-axis). (F) $T_{LE-MOG-GFP}/APC$ contact duration. Imaging was done 12 h after intrathecal injection of MOG- or OVA-pulsed APCs. A, C, E, F are sum, B is representative, and D display means with S.D. of two and three independent experiments after OVA and MOG APC-pulsing, respectively. A, C and F, $***P < 0.0001$ (nonparametric t test). D, $**p < 0.01$ (unpaired t test).

Finally, T_{LE-MOG} cells were activated in the leptomeninges, after application of exogenous antigen (Figure 3.6.4, A and B), and they triggered clinical EAE, as reflected by weight loss and neurological signs (Figure 3.6.4C). Taken together, the increased availability of MOG by exogenous application changed the behavior of the T_{LE-MOG} cells from an EAE^{lo} to an EAE^{hi} pattern.

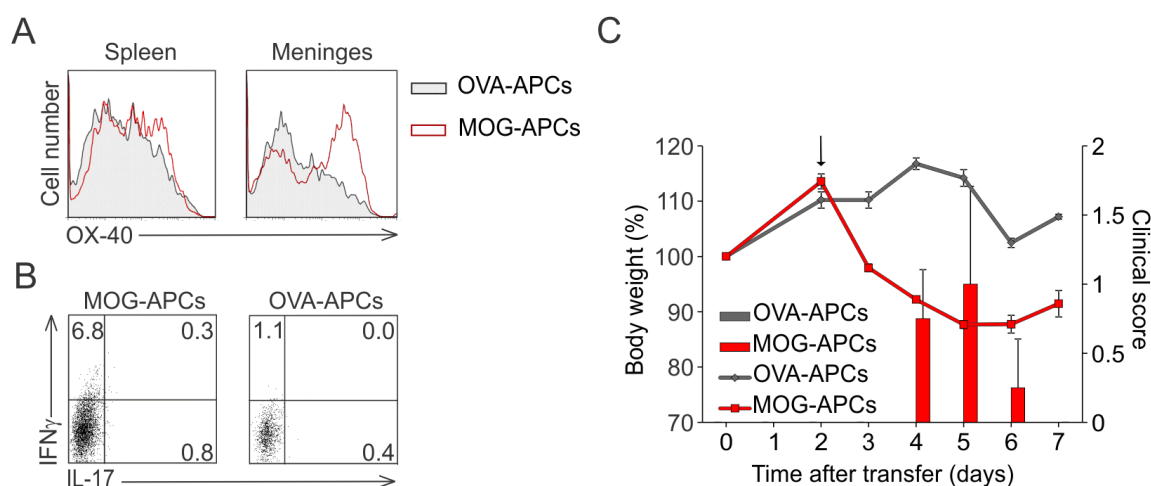


Figure 3.6.4. Activation status and encephalitogenic potential of T_{LE-MOG} cells after MOG-pulsed APC intrathecal application. (A) CD134 expression (OX40) as T cell activation marker was examined. Staining on T cells derived from OVA-pulsed APC-treated animals (filled histogram) were overlaid with results obtained from MOG-pulsed APC-treated (red lines) animals in the spleen and CNS meninges. (B) Production of IFN γ and IL-17 in the T cells after OVA- or MOG-pulsed APC treatment. (C) Clinical outcome after antigen-pulsed meningeal APC intrathecal injection was evaluated. Relative body weight (lines, left y-axis) and clinical score (bars, right y-axis) after OVA- (grey) or MOG- (red) pulsed APC treatments are shown. The arrow indicates the time point of intrathecal antigen-pulsed APCs injection; two animals per group. Representative data of four independent experiments are shown (means \pm S.D.).

The disadvantage of the approach using antigen-pulsed APCs is that quantification of T cell/APC contacts is performed with all APCs, as pulsed and non-pulsed APCs are indistinguishable, due to technical limitation. To identify leptomeningeal phagocytes actively involved in processing local antigen, self-quenched MOG (MOG_{DQ}) was injected intrathecally. In its native conformation, MOG_{DQ} quenches itself, and is unable to emit fluorescent signal. However, once taken up by APCs and cleaved by intracellular proteases, MOG_{DQ} becomes brightly fluorescent (Lewis and Cobb, 2010). MOG_{DQ} or OVA_{DQ} was injected intrathecally on day 2.5 after $T_{LE-MOG-GFP}$ cell transfer, and motility and contact duration between $T_{LE-MOG-GFP}$ cells and stained APCs were analyzed. $T_{LE-MOG-GFP}$ cells showed confined movement during the contact with APCs that had processed MOG_{DQ}, resulting in zig-zag traces within small area (Figure 3.6.5A). Their velocity was reduced and they became more confined, as shown by lowered MSD (Figure 3.6.5, B and C). Additionally, the

duration of contacts with local APCs was extended to a period characteristic for EAE^{hi} T cells (Figure 3.6.5D).

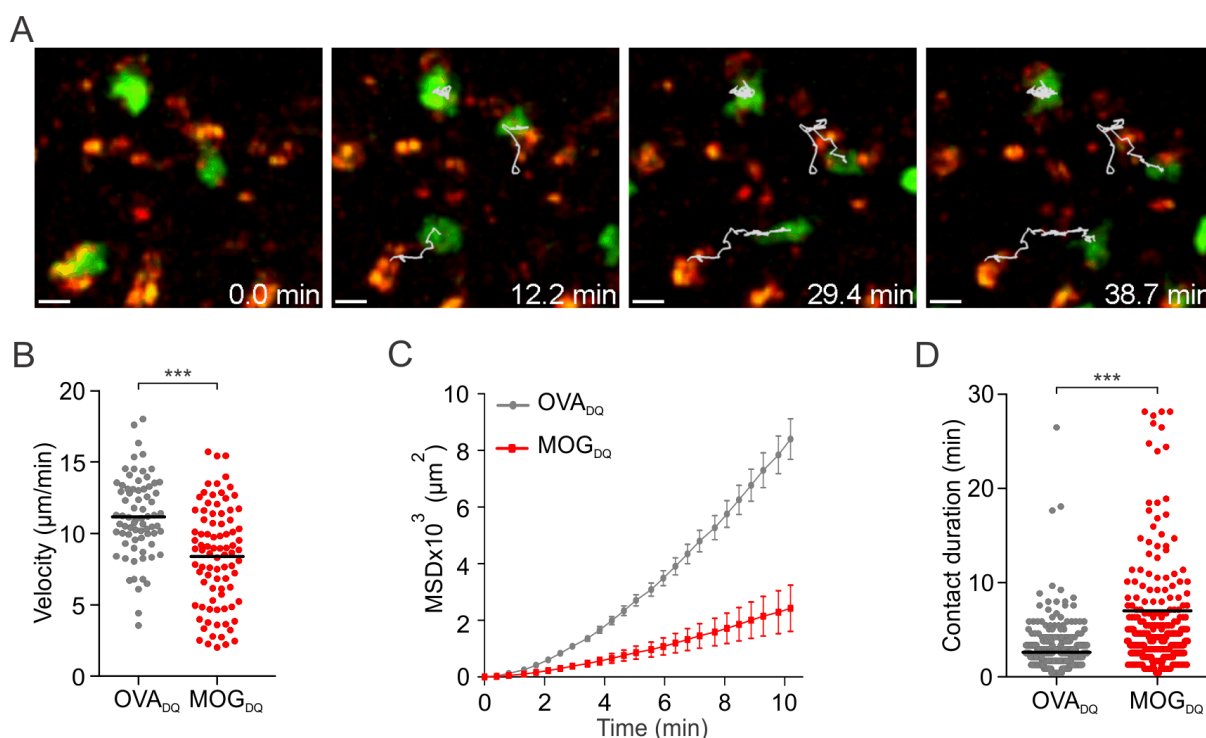


Figure 3.6.5. T_{LE-MOG-GFP} cell motility in the CNS meninges after intrathecal MOG_{DQ} or OVA_{DQ} application. (A) Images are taken from representative video for T_{LE-MOG-GFP}/APC contacts after application of MOG_{DQ}. Trajectory lines were overlaid. Inserted numbers indicate relative time after the start of image acquisition. Scale bar: 10 µm. (B,C, and D) Instantaneous velocity (B), Mean square displacement (MSD) (C), and T/APC contact duration (D) were analyzed. Results were summed (B and D) or representative (C) from two and four different experiments after OVA^{DQ} or MOG^{DQ} application respectively. ***P<0.0001 (nonparametric t test)

In vivo observations were supported by *in vitro* experiments. T_{LE-MOG} cells were confronted by APC freshly prepared from CNS meninges with or without exogenous antigen. Expression of intracellular IFN γ was used as a sensitive marker of rat T cell activation (Kawakami et al., 2004). Although naive meningeal APCs alone failed to stimulate IFN γ production in T_{LE-MOG} cells, addition of exogenous MOG induced the cytokine in a substantial proportion of cells (Figure 3.6.6). Thus, T_{LE-MOG} cells essentially behaved like OVA-specific T cells. In contrast, encephalitogenic T_{LE-MBP} cells and T_{DA-MOG} cells produced IFN γ upon contact with meningeal APCs even in the absence of exogenous antigen, i.e. in response to endogenous MBP and MOG,

respectively. All T cell lines were stimulated to produce high levels of IFN γ when appropriate antigen was presented by thymus derived professional APCs (DCs) (Figure 3.6.6)

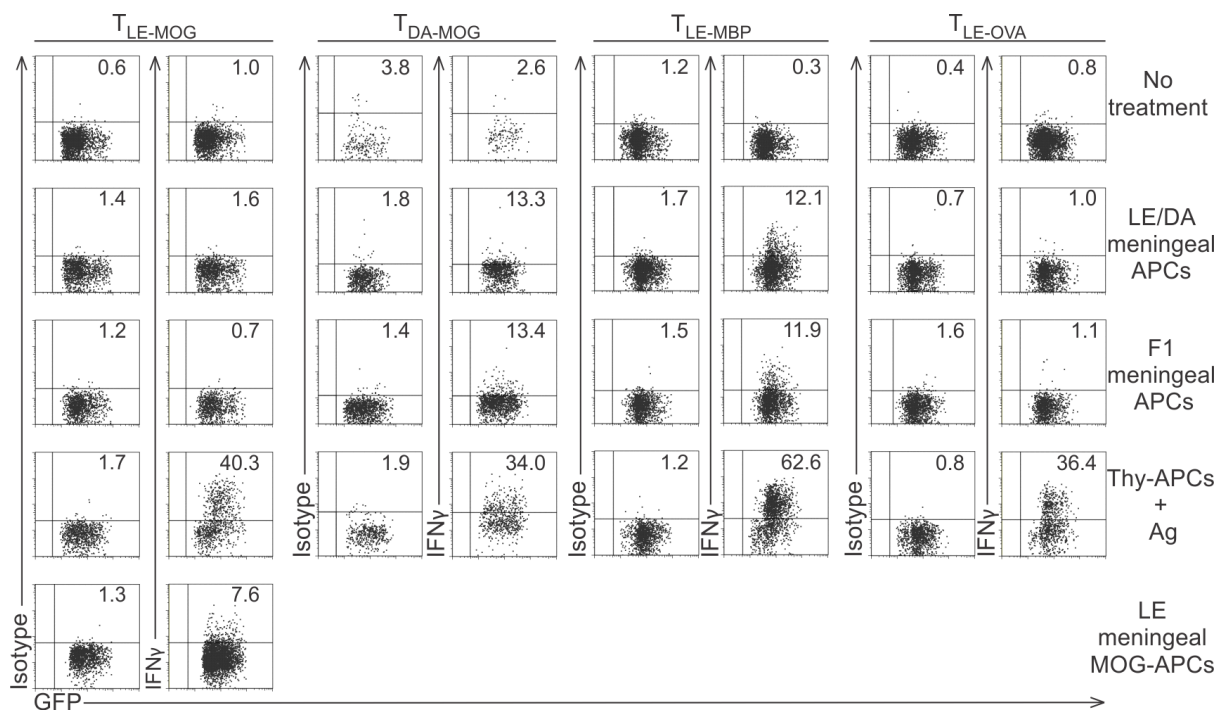


Figure 3.6.6. *In vitro* stimulation of encephalitogenic T cell lines by CNS local APCs. Encephalitogenic T cell lines were cultured with CNS-APCs in the absence of exogenous antigens. CNS-APCs were prepared from either syngeneic or F1 rats. Thymocytes together with exogenous antigens served as positive controls. Additionally $T_{LE-MOG-GFP}$ cells were stimulated with MOG-pulsed CNS-APCs. 48 hours after co-culture, T cells were stained with anti IFN γ antibody and analyzed by flow cytometry. Representative results from three independent experiments are shown.

3.7 Transfer into F1 recipients

According to a previous report, Lewis rat myelin contains lower levels of MOG than myelin from rats with high encephalitogenic responsiveness (Pagany et al., 2003), and this difference may be a reason for low encephalitogenic potential of T_{LE-MOG} cells in the Lewis rat. To explore this possibility, T_{LE-MOG} or T_{DA-MOG} cells were separately transferred into F1 (LE x DA) rats, and their behavior was followed *in vivo* by intravital imaging. The behavior of both effector cells in F1 recipients replicated their activities in parental hosts. In F1 rats, EAE^{hi} T_{DA-MOG} cells showed a low and confined motility (Figure 3.7.1, A and B), and formed extended contacts with local APCs (Figure 3.7.1C). Conversely, EAE^{lo} T_{LE-MOG} cells transferred into F1 rats had higher velocity and MSD (Figure 3.7.1, A and B), and showed shorter APC contacts (Figure 3.7.1C).

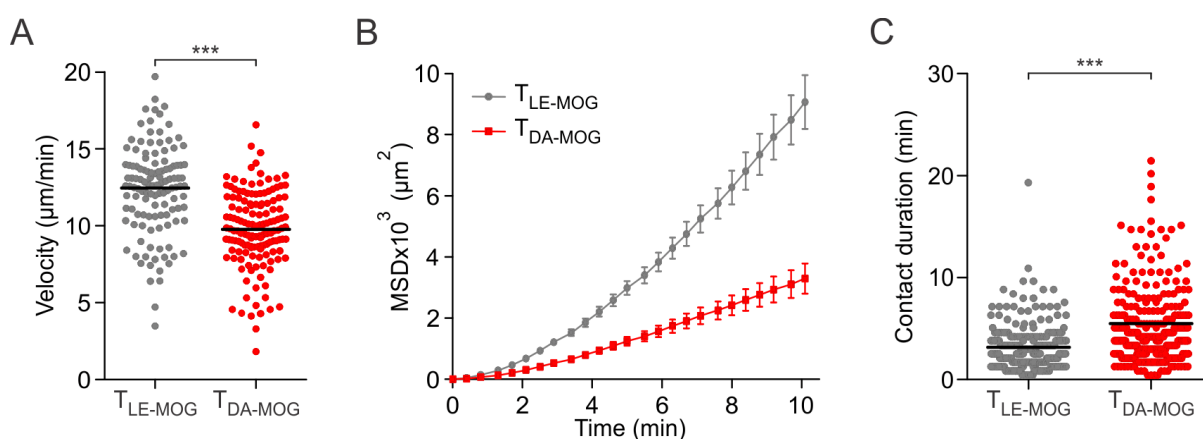


Figure 3.7.1. $T_{LE-MOG-GFP}$ and $T_{DA-MOG-GFP}$ cells in the CNS meninges of F1 (LExDA) rats. Velocity (A), mean square displacement (MSD) (B), and duration of T cell/APC contacts (C), was calculated from intravital recordings. Results are sum from three different experiments per cell line. *** $P < 0.0001$ (nonparametric t test)

Additionally, T_{DA-MOG} cells were activated within the CNS of F1 recipients, like they were in DA recipients, while T_{LE-MOG} cells in F1 also like in Lewis rats remained resting (Figure 3.7.2A). T_{DA-MOG} , in contrast to T_{LE-MOG} cells, induced clinical EAE in the F1 hosts (Figure 3.7.2B). The milder neurological disorder mediated by T_{DA-MOG} in F1 rats, compared to DA rats, can be attributed to a gene dosage effect of DA-derived MHC II RT1 (Ben-Nun et al., 1981). *In vitro* experiments also confirmed that

CNS-derived APCs from F1 rats, presenting endogenous myelin antigens, can activate EAE^{hi} T_{LE-MBP} and T_{DA-MOG} cells, but not EAE^{lo} T_{LE-MOG} cells, as evaluated by intracellular IFN γ production (Figure 3.6.6). The similar activity of T_{LE-MOG} cells and T_{DA-MOG} cells in parental as in F1 hosts argues against different MOG-expression levels as an explanation for different T cell encephalitogenicity between LE and DA hosts.

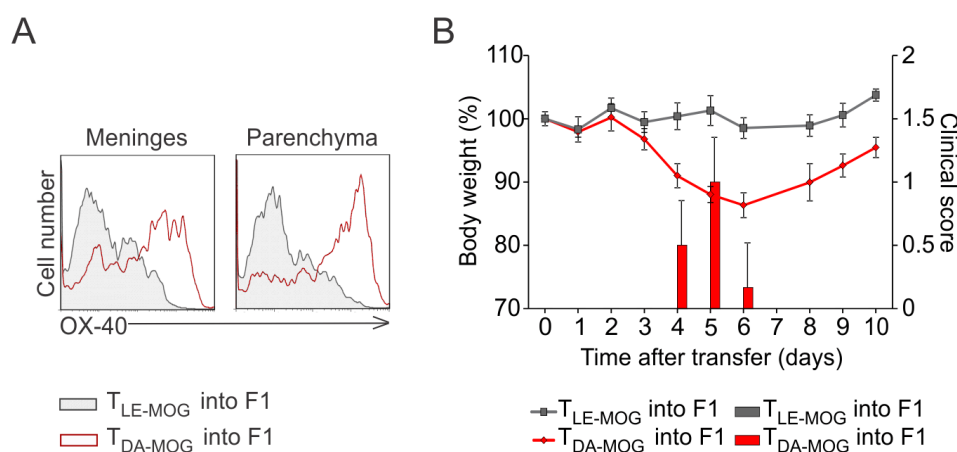


Figure 3.7.2. Activation status and encephalitogenic potential of MOG-specific T cells in F1 recipients. (A) Expression of the surface T cell activation marker (OX40) was analyzed by flow cytometry. Expression on T_{DA-MOG-GFP} cells (red overlaid lines) was compared to T_{LE-MOG-GFP} cells (filled histograms) in both CNS meninges and parenchyma. Representative results from two independent experiments are shown. (B) EAE clinical course evaluated by body weight change (lines, left y-axis) and clinical score (bars, right y-axis) after transfer of T_{DA-MOG-GFP} cells (red) or T_{LE-MOG-GFP} cells (grey) are shown. Results are means \pm S.D. of three animals. Representative results from four independent experiments are shown.

3.8 The effect of a pro-inflammatory milieu

The interaction of effector T cells with BBB and CNS parenchyma can be also influenced by the local microenvironment. To test the effect of a pro-inflammatory milieu on the behavior of EAE^{lo} T cells, LPS was intrathecally injected, opening the BBB and activating local phagocytes. However, this did not change the motility of T_{LE-MOG} cells (Figure 3.8.1A) or duration of their contacts with meningeal APCs (Figure 3.8.1B). Accordingly, T_{LE-MOG} cells were not activated in the CNS (Figure

3.8.1C). These results suggest that the duration of interactions between T cells and APCs is highly antigen-dependent and does not depend on inflammatory conditions.

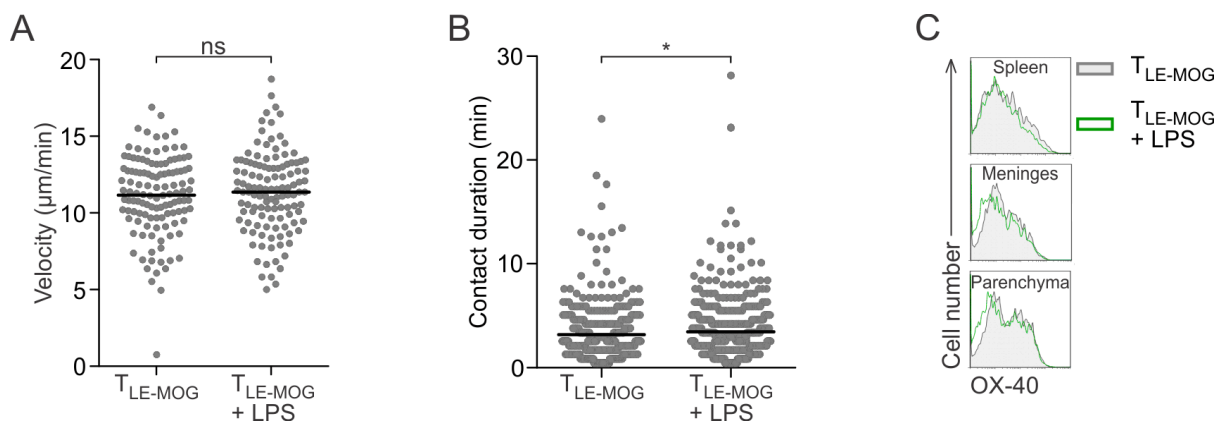


Figure 3.8.1. Motility and activation of T_{LE-MOG} cells under inflammatory conditions induced by LPS. Animals were intrathaceally injected with LPS two days after i.v transfer of $T_{LE-MOG-GFP}$ cells. Imaging was performed 12 h later. Velocity (A), and T cell/APC contact duration (B) were calculated from intravital recordings. Results are sum of at least two different experiments per condition. (C) Expression of surface T cell activation marker (OX40) was analyzed by flow cytometry. $T_{LE-MOG-GFP}$ cells were isolated 16 h after LPS treatment from spleen, CNS meninges and parenchyma. Expression without treatment (field histograms), was overlaid with expression after LPS treatment (green lines). Results are representative from two independent experiments. ns: not significant, * $p < 0.01$ (nonparametric t test).

3.9 Δ NFAT-GFP as fluorescent marker of T cell activation *in vivo*

Previous experiments suggest that auto-reactive T cells receive an activation stimulus from meningeal/perivascular APCs, and that longer lasting contacts provide a sufficient signal for the T cell activation. However, with this experimental approach distinguishing productive from non-productive interactions was not possible. To directly link T cell/APC contacts with T cell activation, a truncated NFAT fused to GFP (Δ NFAT-GFP) was introduced as fluorescent “functional” tag, and used to visualize activation events in auto-reactive T cells interacting with structures of the BBB.

The Δ NFAT-GFP construct contained the regulatory domain of NFAT1, which is necessary for phosphorylation, cytoplasmic sequestration, and calcium-induced and

calcineurin-mediated dephosphorylation. Dephosphorylation induces a conformational change, which exposes a nuclear localization signal leading to the translocation of NFAT from the cytoplasm to the nucleus (Hogan et al., 2003; Okamura et al., 2000). The NFAT construct was truncated to delete the DNA-binding domain of native NFAT (Aramburu et al., 1998) (Figure 3.9.1A), so as not to interfere with the gene regulation by endogenous NFAT. To visualize the subcellular localization of truncated NFAT, GFP was fused to C-terminal. Upon T cell activation, Δ NFAT-GFP is translocated from the cytoplasm to the nucleus, similar to native NFAT1 (Shaw et al., 1995) (Figure 3.9.1B).

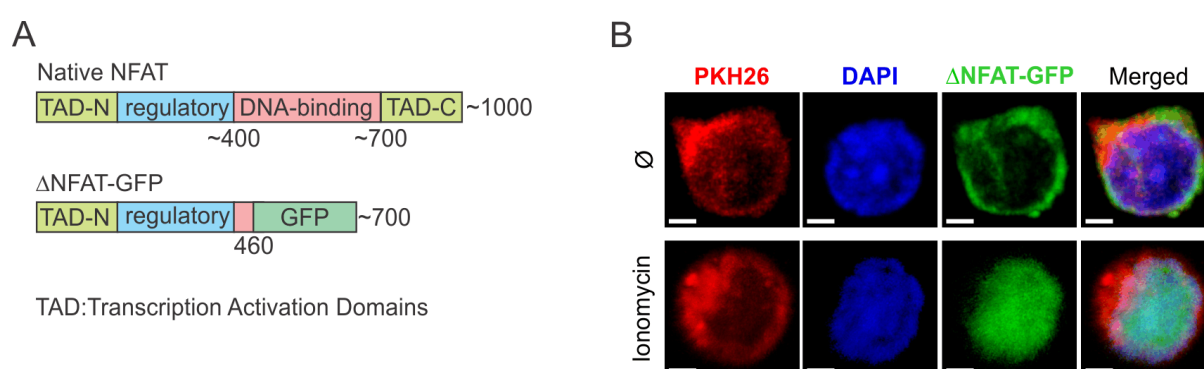


Figure 3.9.1. Δ NFAT-GFP as activation marker of T cells. (A) Schematic of naive and truncated version of NFAT. Numbers indicate amino acid. (B) Confocal images of a resting *in vitro* $T_{MBP-NFAT-GFP}$ cell stained with the red membrane dye PKH26 and DAPI, before and after application of ionomycin. Scale bar: 2 μ m.

Two-photon microscopy can only resolve processes of a certain temporal range (few seconds to few hours). Therefore, the *in vitro* kinetic of the Δ NFAT-GFP translocation, from cytosol to the nucleus (c-n) upon stimulation, as well as back to the nucleus (n-c) after removing the activation stimulus, was investigated. Translocation of Δ NFAT-GFP from cytosol to nucleus happened within only few minutes upon ionomycin stimulation; however, the reverse transport took much longer (around 1 h) (Figure 3.9.2).

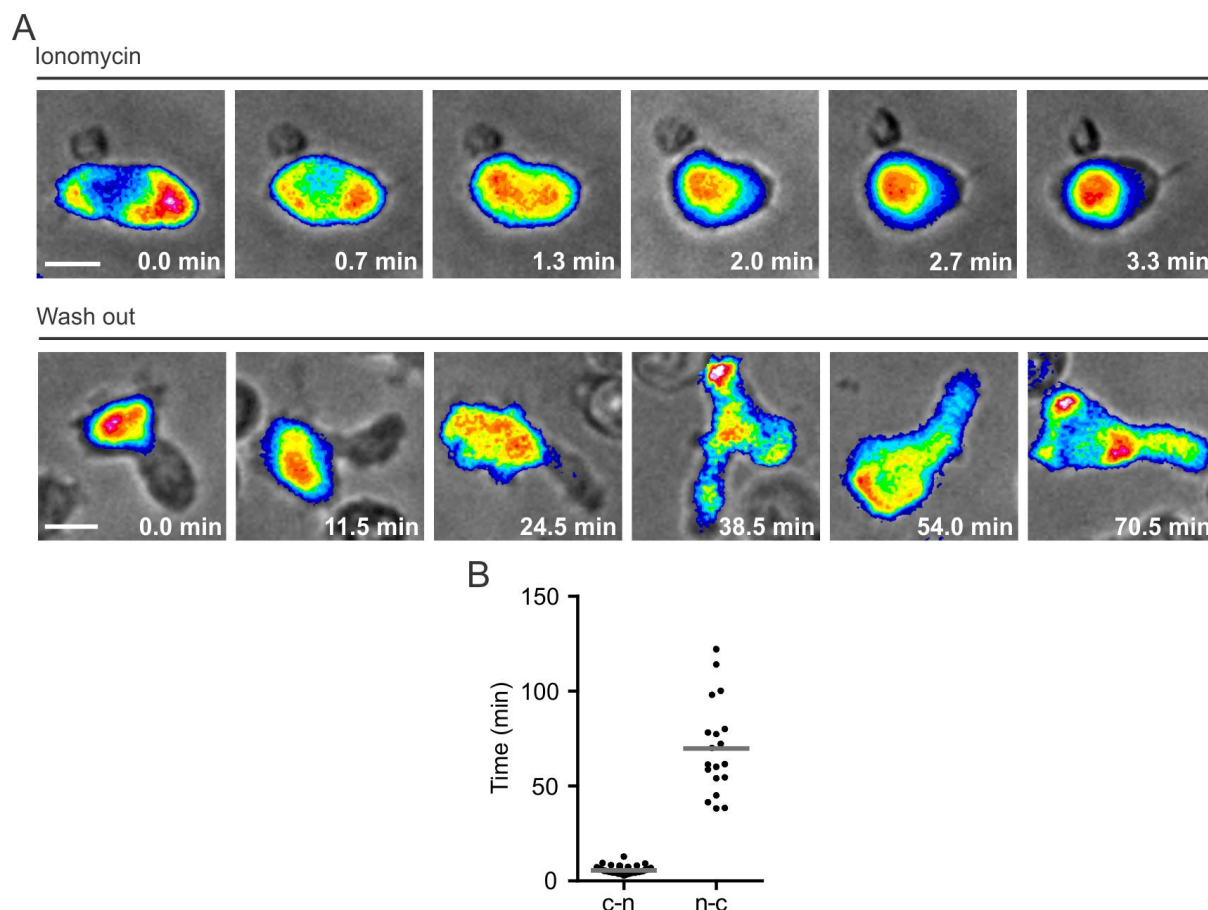


Figure 3.9.2. Dynamics of Δ NFAT-GFP translocation. (A) Fluorescent video-microscopy of Δ NFAT-GFP translocation from cytosol to nucleus (upper panel) upon ionomycin stimulation, and back to the cytosol (lower panels) after washing out the ionomycin, in representative resting *in vitro* $T_{MBP-NFAT-GFP}$ cells. Bright field images (grey) were overlaid with pseudo color images depicting GFP intensity distribution (from blue - low intensity, to red - high intensity). Inserted numbers indicate the relative time after addition or removal of ionomycin, respectively. Scale bar: 5 μ m. (D) Δ NFAT-GFP translocation times from cytosol to nucleus (c-n) after addition of ionomycin, and back to the cytosol (n-c) after washing ionomycin out. Each dot represent single cell. Result is sum of at least three independent experiments per condition.

Δ NFAT-GFP-expressing T cells behaved like their GFP-expressing counterparts; especially, their encephalitogenic potential remained unimpaired (Figure 3.9.3). All these facts indicated that Δ NFAT-GFP can serve as a reliable genetic indicator of T cell activation for two-photon imaging without disturbing cellular function.

As no difference between the two investigated EAE^{hi} T cell lines (T_{DA-MOG} and T_{LE-MBP}) was seen previously, $T_{LE-MBP-NFAT-GFP}$ cells were chosen as EAE^{hi} and $T_{LE-MOG-NFAT-GFP}$ cells as EAE^{lo} , for the study of differential T cell activation *in vivo*, using

Δ NFAT-GFP as a marker. For clarity, they will from now on be referred to as T_{MBP} and T_{MOG} , as they have the same recipient rat strain.

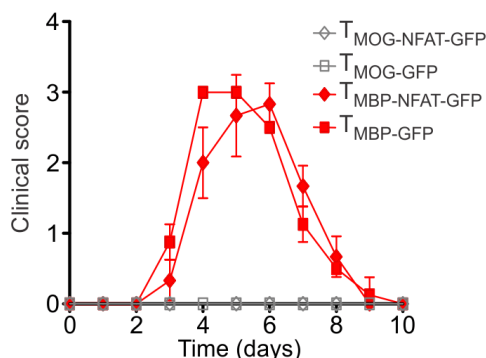


Figure 3.9.3. Comparison of the EAE-course induced by Δ NFAT-GFP-expressing T cells and their GFP-expressing counterparts. EAE clinical course induced by transfer of $T_{MOG/MBP-GFP}$ cells as well as $T_{MOG/MBP-NFAT-GFP}$ cells. Means \pm S.D. from at least three animals per group are shown. Representative data from three independent experiments per cell line are shown.

3.10 Activation status of intraluminal T cells

The marker was first used to investigate activation status of intraluminal auto-reactive T cells, during their initial encounter with the BBB. T cells attach to the intraluminal surface, first roll and then crawl on the endothelial cells. Both modes of motion differ in the molecules used for endothelial contacts. Rolling involves transient interactions between selectins and glycoproteins (Engelhardt, 2006), and crawling depends on the binding of integrins (Bartholomäus et al., 2009). These interactions appear to involve some stimulation effect of the T cells (Engelhardt, 2006); however, it is not clear which of the endothelial contacts trigger activation, and to what level of stimulation the T cells are driven within the vascular lumen. Two-photon imaging showed, that regardless of their pathogenic potential (EAE^{hi} vs. EAE^{lo} T cells), both the crawling and the rolling T cells restricted Δ NFAT-GFP to their cytosol (Figure 3.10.1). This result indicates that, if there is any stimulation of intraluminal T cells, it is not sufficient to translocate NFAT into the nucleus, and further initiate gene activation.

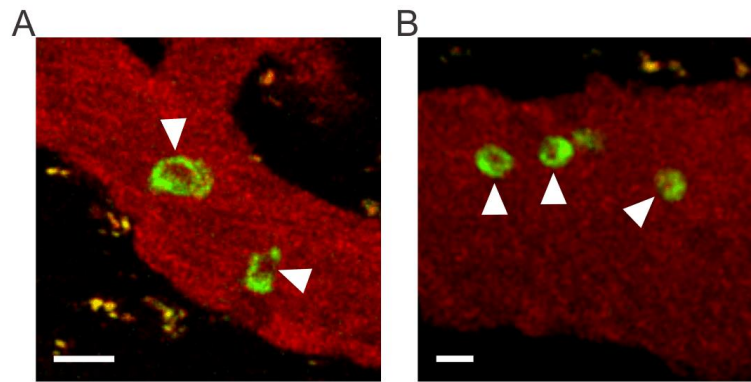


Figure 3.10.1. Activation status of auto-reactive T cells within leptomeningeal blood vessels. Images taken from representative videos, showing crawling (A) and rolling (B) of $T_{\text{MBP-NFAT-GFP}}$ cells. White arrowheads: Δ NFAT-GFP-spared nuclei. Scale bar: 10 μm .

3.11 Δ NFAT-GFP translocation in perivascular T cells

Next, Δ NFAT-GFP localization in EAE^{hi} ($T_{\text{MBP-NFAT-GFP}}$) and EAE^{lo} ($T_{\text{MOG-NFAT-GFP}}$) cells was compared upon their extravasation. For improving the visualization of the marker's subcellular location, the cells were additionally stained with SNARF-1 (Bouso et al., 2002), which labels both the cytosol and nucleus. To avoid the dilution of SNARF-1 staining by the extensive cell division in first three days after T cell transfer, the CD4^+ T cells isolated from spleen, 3 days after transfer of NFAT-GFP T cells, were labeled and then transferred into wild type recipients (Figure 3.11.1). At this time, the T cells have already assumed their migratory phenotype, and the retransferred T cells infiltrate the CNS quicker than *in vitro* activated T cells (Flügel et al., 2001).

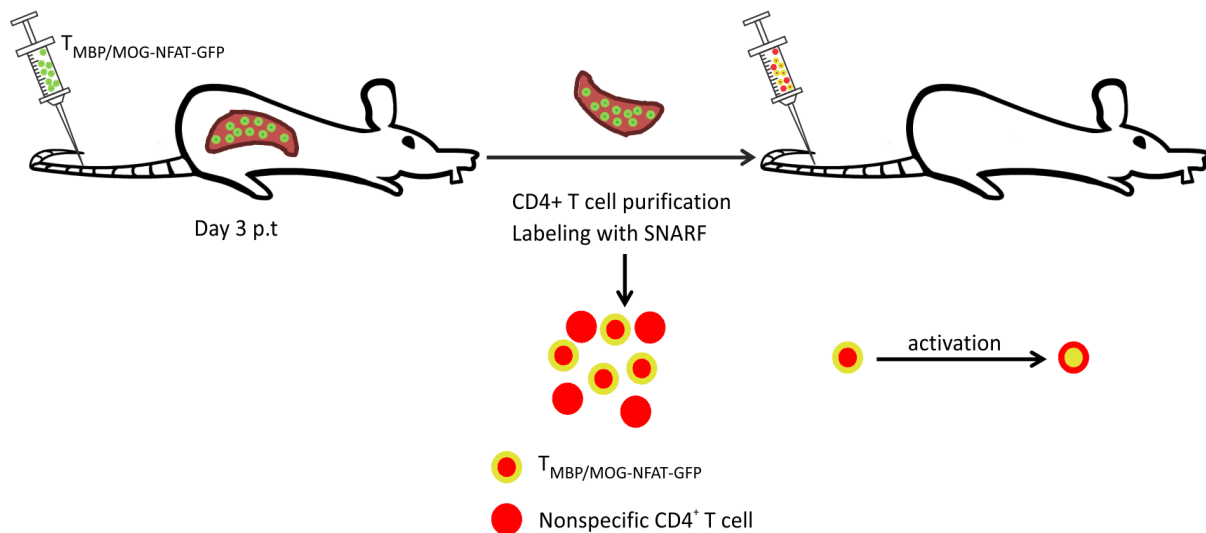


Figure 3.11.1. Schematic overview of “migratory” $T_{\text{MBP/MOG-NFAT-GFP}}$ cells retransferred from the donor spleen into wild type recipient. Spleens were collected from donor animals three days after the i.v. transfer of the $T_{\text{MBP/MOG-NFAT-GFP}}$ cells. $CD4^+$ T cells were purified from the spleen, using a $CD4^+$ T cell isolation kit, and were labeled with SNARF-1. This mixed population of SNARF-labeled antigen-nonspecific (no $\Delta\text{NFAT-GFP}$ expression) single positive (red), and antigen-specific $\Delta\text{NFAT-GFP}$ - and SNARF-labeled double-positive (red/green) cells, was injected into WT recipients. Imaging was performed 12 h after re-transfer.

SNARF-1 counterstaining allowed the determination of the $\Delta\text{NFAT-GFP}$ location in up to 90% of all cells and facilitated the distinction of three $\Delta\text{NFAT-GFP}$ patterns: cytoplasmic (c), located in the cytosol and not the nucleus in resting T cells; nuclear (n), in the nucleus and not the cytosol in activated cells; and both in the cytoplasm and nucleus (nc) of transitional cells (Figure 3.11.2A).

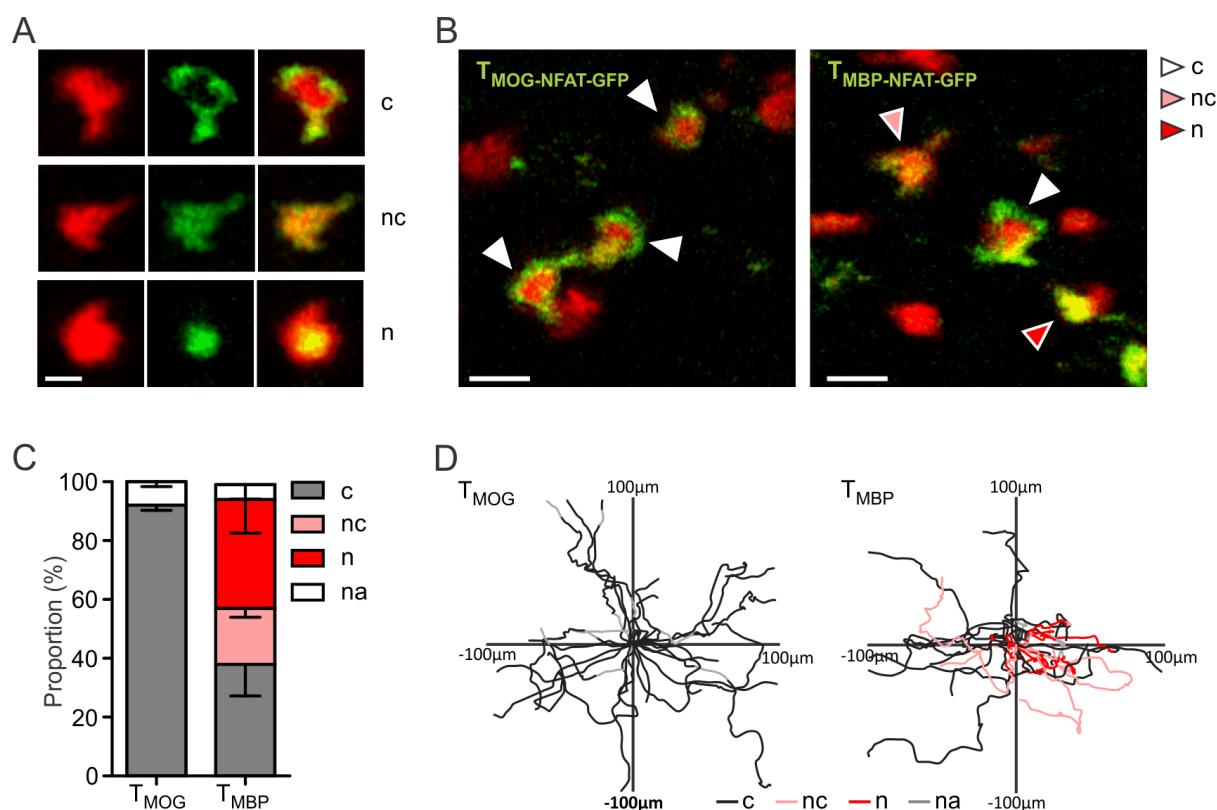


Figure 3.11.2. Perivascular T cell activation indicated by the cellular localization of the Δ NFAT-GFP marker. (A) Three patterns of Δ NFAT-GFP (green)/SNARF-1 (red) in double-labeled T cells. Cytosolic (c), nuclear (n), and nuclear/cytosolic (nc). Scale bar: 5 μ m. (B) Snapshots of T_{MOG}/MBP-NFAT-GFP cells in the CNS. Scale bar: 10 μ m. (C) Δ NFAT-GFP patterns (A) in the T_{MOG}/MBP-NFAT-GFP cells were categorized, and their relative occurrence calculated. n.a.: not analyzable. (D) T cell trajectories from representative movies were superimposed; each line starts at the coordinate origin. Lines were colored to indicate the Δ NFAT-GFP location. Results for B, D are representative and for C are mean with indicated S.D, from at least three different experiments per cell line.

Unlike intraluminal T cells, more than 30% of the extravasated EAE^{hi} T_{MBP-NFAT-GFP} cells showed a nuclear localization of Δ NFAT-GFP (n), and another 20% had the marker located both in the cytosol and nucleus (nc). However, the EAE^{lo} T_{MOG-NFAT-GFP} cells restricted Δ NFAT-GFP to the cytoplasm (Figure 3.11.2, B and C). Subcellular localization of the marker correlated to the locomotion behavior of T cells. Regardless of their antigen-specificity and encephalitogenic potential (EAE^{hi} or EAE^{lo}), T cells with cytosolic Δ NFAT-GFP were highly motile, with nearly straight trajectories (black lines in Figure 3.11.2D). In contrast, T cells with nuclear Δ NFAT-GFP showed a confined zig-zag movement (red lines in Figure 3.11.2D).

T cell velocity was also tightly related with the Δ NFAT-GFP localization. T cells having Δ NFAT-GFP in the cytosol (c) moved at high velocity (average 10 $\mu\text{m}/\text{min}$), again regardless of their encephalitogenic potential, whereas T cells with Δ NFAT-GFP in the nucleus (n) traveled at a slow velocity (mean 4.5 $\mu\text{m}/\text{min}$). Finally, T cells with both nuclear and cytosolic Δ NFAT-GFP (nc) moved with an intermediate speed (mean 6.5 $\mu\text{m}/\text{min}$) (Figure 3.11.3A). As shown by one representative cell (Figure 3.11.3B), the Δ NFAT-GFP translocation correlated with the changes in T cell velocity.

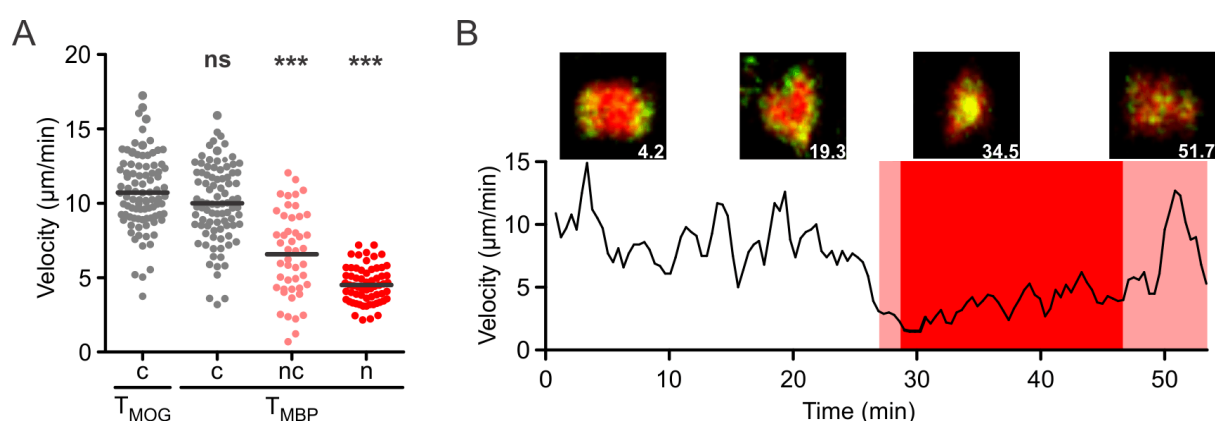


Figure 3.11.3. T cell velocity correlates with the subcellular Δ NFAT-GFP localization. (A) Velocity of T cells with different Δ NFAT-GFP localizations was calculated from intravital recordings. Results are the sum of at least three different experiments per cell line. (B) Velocity (averaged over three time points) of a representative $T_{\text{MBP-}\Delta\text{NFAT-GFP}}$ cell changing the Δ NFAT-GFP localization. Light and dark red colors indicate Δ NFAT-GFP in the nucleus/cytosol (nc) and the nucleus (n), respectively. Top-row images depict the Δ NFAT-GFP localization in a SNARF-1-labeled $T_{\text{MBP-}\Delta\text{NFAT-GFP}}$ cell (red/green) at the indicated time points (in min). *** $p < 0.001$ (One-way ANOVA, Kruskal-Wallis test - Dunn's multiple comparison test).

3.12 Contacts with local APCs are crucial for T cell activation

The nuclear translocation of Δ NFAT-GFP in the T cells correlated with their contacts to the local APCs (Figure 3.12.1). Note that in Figure 3.12.1 the same APC that had activated T cell #1 interacted with T cell #2, triggering Δ NFAT-GFP translocation. In fact, sequential T cell activation by one APC was not unusual. This indicates that APCs differ in their capacity to activate T cells, and some particular APCs are more potent in activating T cells than the others. This is in harmony with our previous

results, showing that only a fraction of the dextran-labeled cells expressed MHC class II (Bartholomäus et al., 2009).

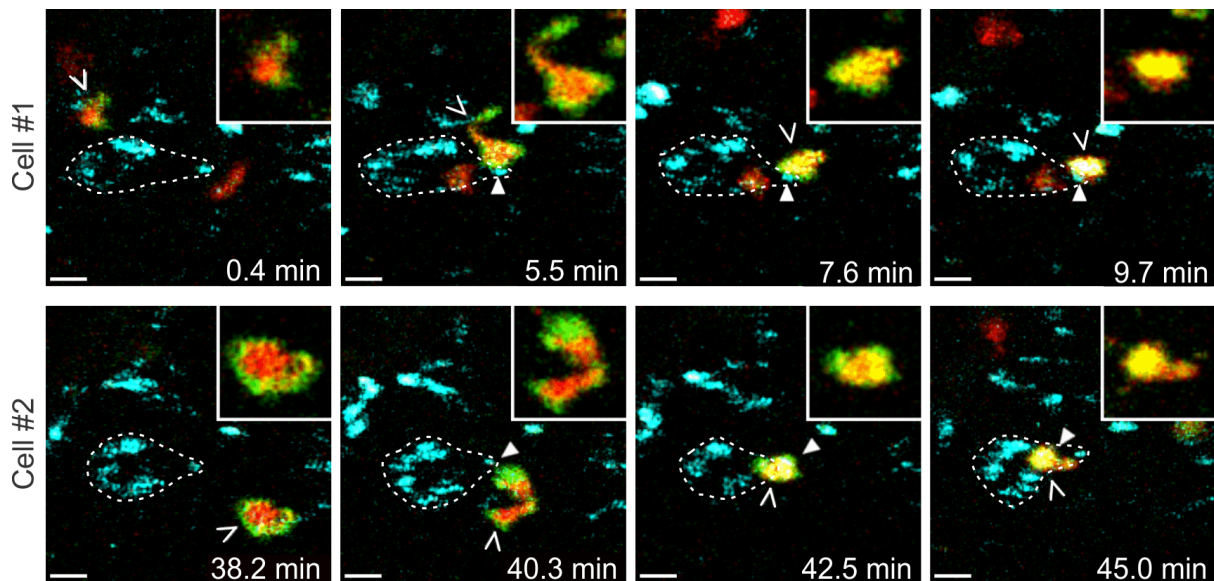


Figure 3.12.1. Δ NFAT-GFP translocation correlates with T cell/APC contacts. Images from a representative movie, showing two SNARF-labeled $T_{MBP-NFAT-GFP}$ cells (red/green) getting successively activated (nuclear translocation of Δ NFAT-GFP) following the contact with the same APC (cyan, speculated outline indicated by a dotted line). Closed arrowheads point to the T cell/APC interaction leading to Δ NFAT-GFP translocation from cytosol to nucleus (c-n), and the open arrows indicate the T cell of interest. Relative time after start of acquisition is indicated. Inserts show snapshots of the T cells (in green and red channel only) at a higher magnification. Scale bar: 10 μ m.

Prolonged APC contacts (average duration 20 min) were required to translocate Δ NFAT-GFP from cytosol to the nucleus (c-n), whereas brief interactions (average duration 3 min) did not affect the Δ NFAT-GFP localization (it remained in cytosol – c), irrespective of the T cell antigen-specificity, and pathogenic potential (EAE^{hi} vs. EAE^{lo}) (Figure 3.12.2A). Additionally, analysis showed that the cytoplasmic-nuclear translocation of Δ NFAT-GFP occurred shortly after the contact with an APC (mean lag time 4 min), whereas the average duration of this contact was still extended to 20 min (Figure 3.12.2B). Although the longest T cell/APC contacts were the ones leading to translocation of Δ NFAT-GFP from cytosol to nucleus (c-n), extended interactions were also observed to be formed with the APCs (average duration 10 min) by the T cells having acquired a nuclear Δ NFAT-GFP (n) elsewhere (Figure 3.12.2A). This suggests that already activated T cells continue to visit successively

other local APCs and that these interactions either maintain their activation state at a particular level or intensify it.

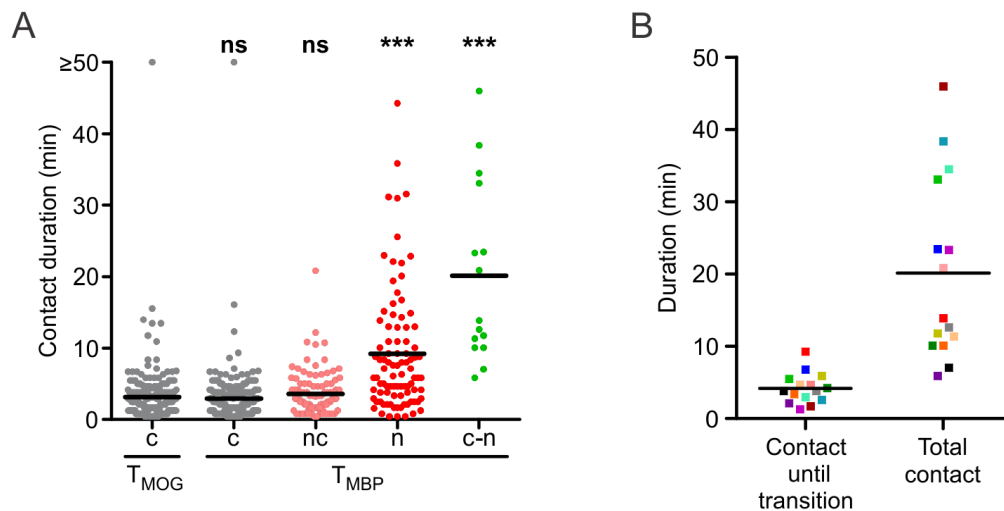


Figure 3.12.2. Quantification of T cell/APC contacts. (A) Duration of the T cell/APC contacts by cells with different Δ NFAT-GFP locations (c, nc, and n) and contacts leading to cytosol-nuclear Δ NFAT-GFP translocation (c-n). (B) Time required for the Δ NFAT-GFP translocation, starting at the beginning of the T cell/APC contact, as compared to the total duration of the same contact. Each color represents the same contact. Results are the sum of three independent experiments per cell line. *** $p < 0.001$ (One-way ANOVA, Kruskal-Wallis test - Dunn's multiple comparison test)

Unlike the cytosol-nuclear (c-n) translocation of Δ NFAT-GFP, which happened within minutes after T cell/APC contact, the reverse transport of Δ NFAT-GFP from the nucleus to the cytoplasm (n-c) required a longer period of time. Once detached from the APC, Δ NFAT-GFP was gradually translocated back to the cytosol, a process requiring approximately 30 min (Figure 3.12.3). Thus, Δ NFAT-GFP translocation kinetics observed *in vivo* (both c-n as well as n-c) correlated with *in vitro* obtained results (Figure 3.9.2).

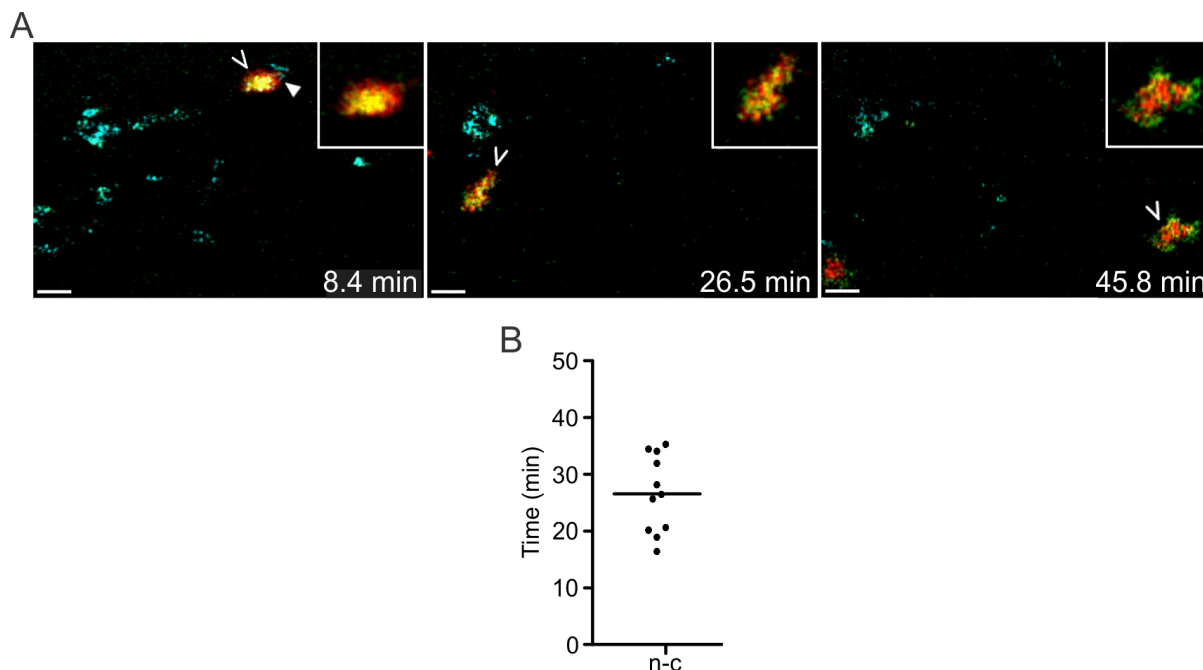


Figure 3.12.3. Translocation of Δ NFAT-GFP from the nucleus back to the cytosol (n-c). (A) Images taken from a representative movie show SNARF-labeled $T_{MBP-NFAT-GFP}$ (red/green) cell, translocating Δ NFAT-GFP from the nucleus back to the cytosol (n-cn-c in images) after detachment from a local APC (cyan). Closed arrowheads point to the T cell/APC interaction, and the open arrows indicate the cell of interest. Relative time after start of the acquisition is indicated. Inserts show magnifications of the T cells (in green and red channel only). Scale bar: 10 μ m. (B) Time required for the Δ NFAT-GFP to be translocated from nucleus back to the cytosol (n-c). Each dot represents a single cell. Results are the sum of three independent experiments.

Finally the question was addressed, if rather sequential or stable T cell/APC interactions induce the T cell activation. Each T cell makes two types of contact, “non activating” and “activating”, which can be distinguished by the Δ NFAT-GFP localization. “Non activating” contacts that precede the “activating” ones were analyzed in more detail. “Non activating” contacts are short lasting (average duration 3 min, Figure 3.12.4) compared to “activating” ones (average duration 20 min, c-n in Figure 3.12.2 and Figure 3.12.4), and during this “non activating” contacts, T cells keep their motility high (average 9 μ m/min, Figure 3.12.4). Although the possibility that a cell is receiving some stimulus during these APC visits cannot be excluded, the results indicate that single, long contacts are more important for T cell activation.

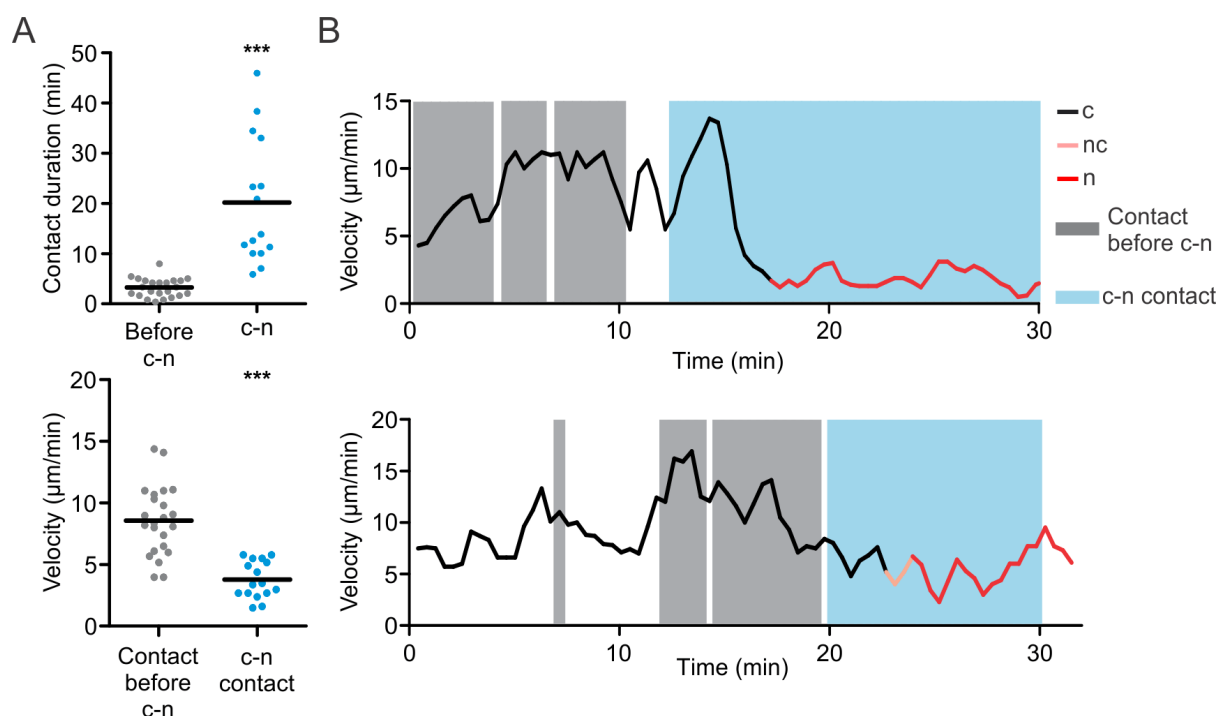


Figure 3.12.4. Characterization of T cell-APC interactions prior to $T_{\text{MBP-NFAT-GFP}}$ cell activation.

(A) Contact duration, and T cell velocity during contact, was quantified for “non activating” (before c-n) and “activating” (c-n) contacts. Duration of activating (c-n) contacts was taken from Figure 3.12.2, and plotted here for better comparison. Results are the sum of five videos from three independent experiments. (B) Instantaneous velocity (averaged over three time points) for two representative $T_{\text{MBP-NFAT-GFP}}$ cells, making various “non-activating” (before c-n) contacts with APCs and finally making the “activating” one (c-n). Line color indicates Δ NFAT-GFP subcellular localization, and background color indicates T cell/APC interaction. *** $p < 0.0001$ (nonparametric t test).

3.13 Antigen availability and T cell activation in the CNS meninges

As shown by the GFP-expressing T cells, EAE^{lo} T_{MOG} cells are not reactivated in the leptomenigeal area (Figure 3.5.3); they are highly motile, and only briefly interacting with perivascular APCs (Figure 3.4.1 and Figure 3.5.2). However, once antigen was externally provided, either by application of MOG-pulsed APCs (Figure 3.6.3) or by injection of MOG protein itself (Figure 3.6.5), they became activated (Figure 3.6.4), their motility was reduced and the duration of the T cell/APC contacts was extended. This suggested that the discrepant interactions may reflect a difference in the availability of presented auto-antigen. To explore the effect of the auto-antigen

availability on the Δ NFAT-GFP expressing T_{MOG} cells, CNS-APCs were saturated with exogenous MOG by local infusion into the imaging window using a microcapillary.

The effect of the exogenous auto-antigen on the subcellular Δ NFAT-GFP localization in $T_{\text{MOG-NFAT-GFP}}$ cells was drastic and immediate. The injection of MOG induced the nuclear translocation of Δ NFAT-GFP in up to 60% of the analyzed cells (Figure 3.13.1, A and B), which was more than in $T_{\text{MBP-NFAT-GFP}}$ cells without the exogenous antigen (Figure 3.11.2C), leaving hardly any cells in intermediate state (nc).

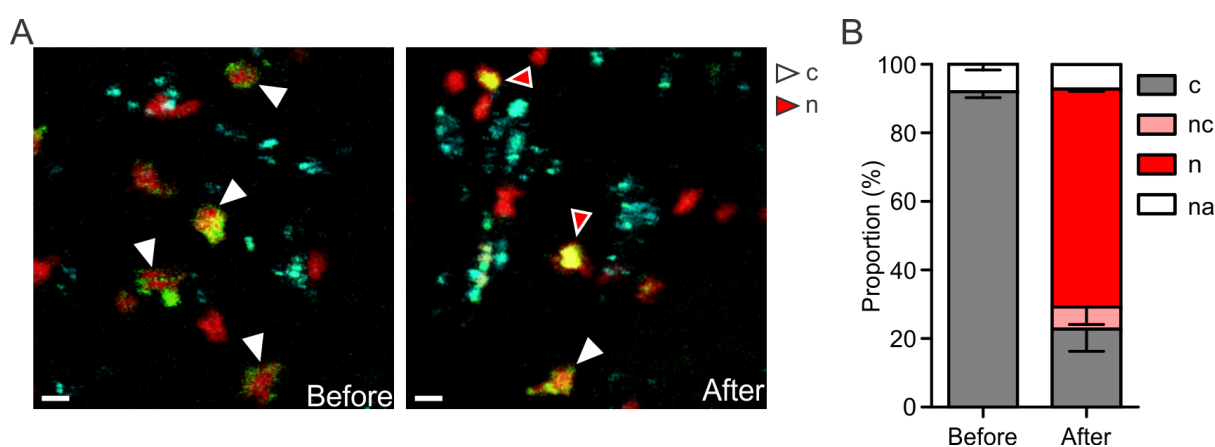


Figure 3.13.1. $T_{\text{MOG-NFAT-GFP}}$ cell activation by exogenous supply of antigen. (A) Representative images of SNARF-labeled $T_{\text{MOG-NFAT-GFP}}$ cells (red/green) interacting with local APCs (cyan) before and after the local application of MOG-protein. Scale bar: 10 μm . (B) Proportion of Δ NFAT-GFP patterns (cytosolic-c, nuclear-n, cytosolic and nuclear-nc) in $T_{\text{MOG-NFAT-GFP}}$ cells analyzed before and after the local application of MOG-protein. Results show mean values with S.D. of at least three independent experiments per condition. na: not analyzable.

The locomotion of $T_{\text{MOG-NFAT-GFP}}$ cells was influenced by exogenous MOG only in cells receiving an activation stimulus (translocation of Δ NFAT-GFP into nucleus - n), showing confined coiled tracks (red lines in Figure 3.13.2A), while cells retaining Δ NFAT-GFP in their cytosol were highly motile before and after antigen application (black lines in Figure 3.13.2A). The cell velocity was also changed by MOG infusion accordingly (Figure 3.13.2B). Similar to EAE^{hi} $T_{\text{MBP-NFAT-GFP}}$ cells, $T_{\text{MOG-NFAT-GFP}}$ cells with cytosolic Δ NFAT-GFP (c) moved at an average of 10 $\mu\text{m}/\text{min}$, before and after antigen application, whereas the cells with nuclear Δ NFAT-GFP (n) slowed down

drastically (average velocity 3 $\mu\text{m}/\text{min}$), which again supports that T cell motility directly correlates with $\Delta\text{NFAT-GFP}$ localization and hence T cell activation.

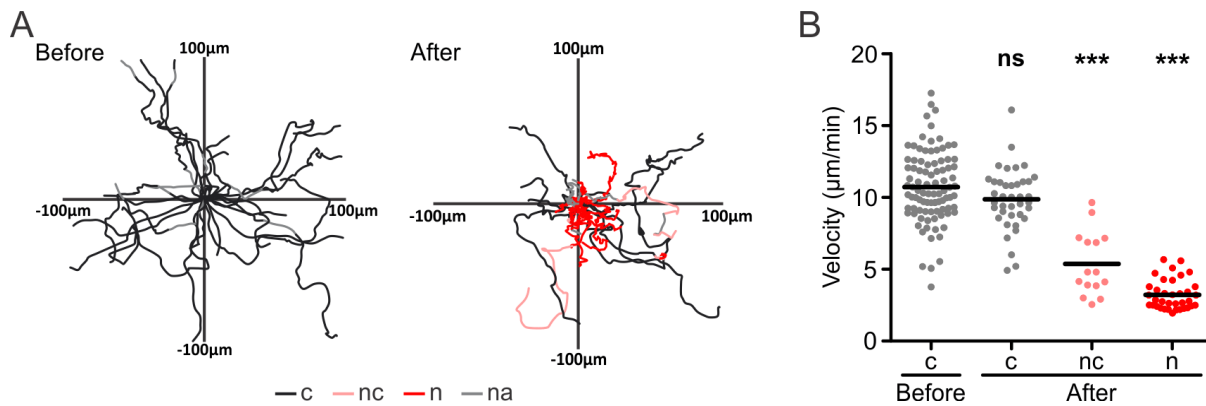


Figure 3.13.2. $T_{\text{MOG-NFAT-GFP}}$ cell motility before and after MOG infusion. (A) T cell trajectories from representative movies before and after MOG infusion, were superimposed on the coordinate origin. Lines were colored to indicate the $\Delta\text{NFAT-GFP}$ location. na: not analyzable. (B) Velocity of T cells with different $\Delta\text{NFAT-GFP}$ locations were calculated from intravital recordings, before and after antigen application. Results are the sum of three different experiments per condition. *** $p < 0.001$ (One-way ANOVA, Kruskal-Wallis test - Dunn's multiple comparison test)

T cell/APC contact of resting $T_{\text{MOG-NFAT-GFP}}$ cells (c) remained brief, regardless of the antigen availability; while the ones that led to $\Delta\text{NFAT-GFP}$ nuclear translocation (c-n) were long lasting, as well as the contacts made by T cells which had previously acquired activation (n) (Figure 3.13.3A). This suggests that the T cells displaying nuclear $\Delta\text{NFAT-GFP}$ (n) were contacting the APCs to maintain their activation status, similar to the APC interactions observed with MBP-specific T cells. Since NFAT nuclear translocation leads to gene transcription, the T cell activation was confirmed by flow cytometry. As shown in Figure 3.13.3B, T_{MOG} cells were activated only after the soluble MOG treatment. Taken together, the increased availability of exogenous MOG translocated $\Delta\text{NFAT-GFP}$ into the nucleus of EAE^{lo} $T_{\text{MOG-NFAT-GFP}}$ cells and changed their motility accordingly, following the same patterns as EAE^{hi} $T_{\text{MBP-NFAT-GFP}}$ cells.

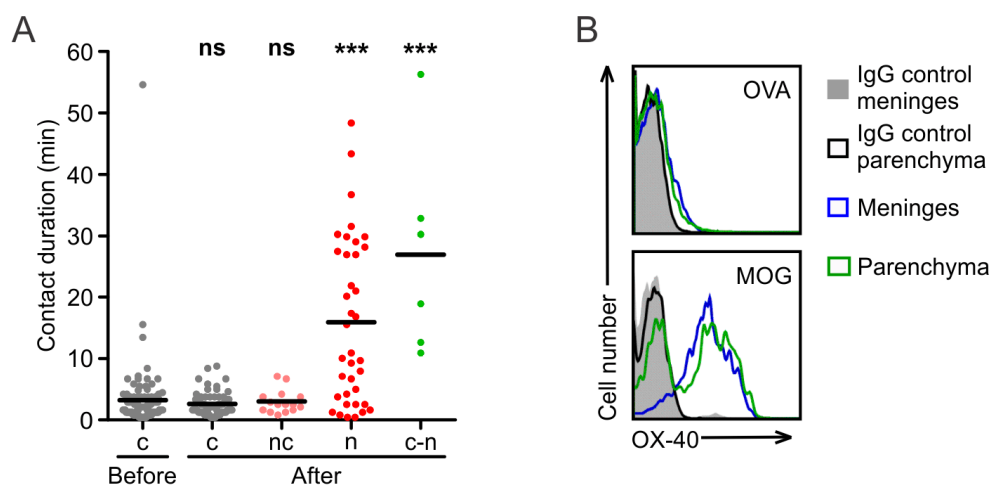


Figure 3.13.3. Contact duration of $T_{MOG-NFAT-GFP}$ cells before and after antigen injection, and their following activation. (A) Duration of the APC contacts made by $T_{MOG-NFAT-GFP}$ cells with different $\Delta NFAT-GFP$ locations (c, nc, and n) and contacts leading to cytosol-nuclear $\Delta NFAT-GFP$ translocation (c-n), was quantified before and after MOG infusion. Results are the sum of three independent experiments per condition. (B) Expression of the activation marker (OX40) on CNS-infiltrating $T_{MOG-NFAT-GFP}$ cells after intrathecal application of OVA or MOG antigen. Representative results from three independent experiments. *** $p < 0.001$ (One-way ANOVA, Kruskal-Wallis test - Dunn's multiple comparison test).

3.14 T cell activation state in peripheral lymphoid organs and CNS parenchyma

On their way to the CNS, T cells acquire a “migratory phenotype” in peripheral lymphoid organs such as spleen, down-regulating activation markers, and up-regulating chemokine receptors (Flügel et al., 2001). Therefore, the subcellular localization of $\Delta NFAT-GFP$ in $T_{MBP-NFAT-GFP}$ cells was investigated in peripheral organs just before they invade the CNS.

In peripheral lymphoid organs, $\Delta NFAT-GFP$ was restricted to the cytosol of EAE^{hi} $T_{MBP-NFAT-GFP}$ cells (Figure 3.14.1, A and C). However, the marker was translocated into the nucleus within minutes upon i.v. application of MBP protein (Figure 3.14.1A). This is in line with previous reports, describing T cell activation in the spleen upon antigen application, detected by flow cytometry and quantitative PCR (Odoardi et al., 2007b). $T_{MBP-NFAT-GFP}$ cells that infiltrated deep into the CNS parenchyma had similar patterns of $\Delta NFAT-GFP$ cellular localization (c, cn, and n) as those in leptomeninges

(Figure 3.14.1B), confirming that reactivation in leptomeninges guides immigrant T cells further into the CNS parenchyma.

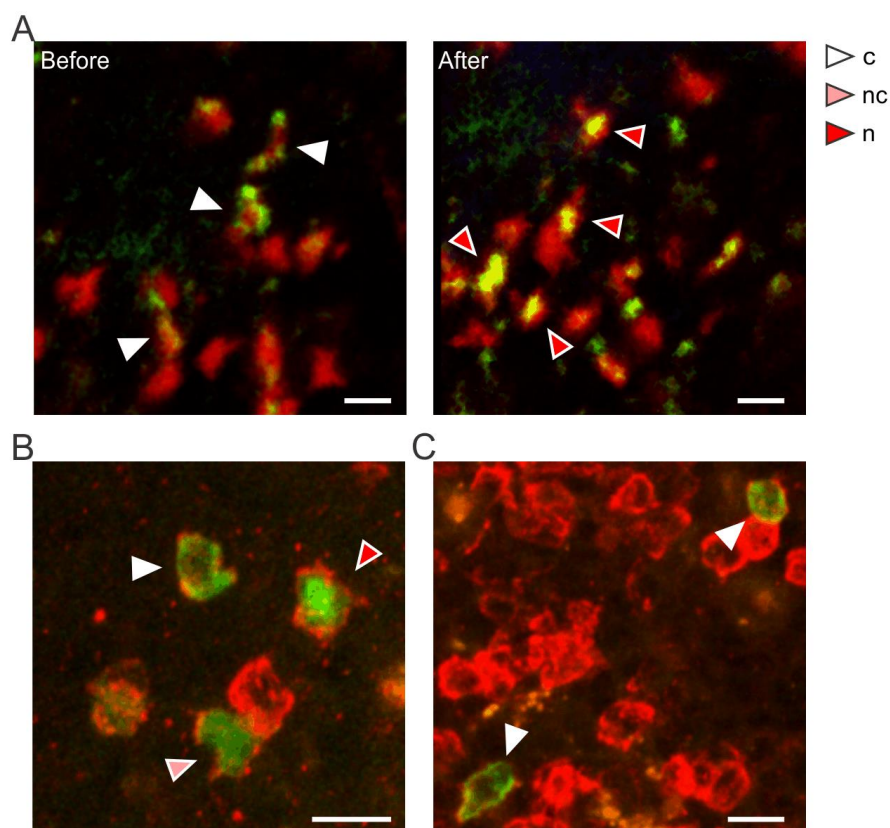


Figure 3.14.1. Subcellular localization of Δ NFAT-GFP in peripheral lymphoid organs and the CNS parenchyma. (A) Images of SNARF-labeled T_{MBP-NFAT-GFP} cells (red/green) in spleen, before and after i.v. application of MBP protein. (B and C) Confocal images of CNS parenchyma (B), and parathymic LN (C), stained with the T cell marker W3/13 (red), three days after transfer of T_{MBP-NFAT-GFP} cells (green). Scale bar: 10 μm. (A, B, and C) Results are representative of at least three independent experiments.

3.15 Modeling of T cell/APC interactions in the leptomeningeal area

This work was designed to model T cell activation in leptomeningeal area, by a theoretical physics approach, using the previously generated two-photon imaging data.

There are two hypotheses, explaining how T cells can receive their activation signal:

- 1) A T cell can scan APCs until it finds the one presenting the right antigen, and make long contact which induces T cell activation
- 2) A T cell can scan APCs, staying with each of them for relatively short periods of time (even with the ones that carry the specific antigen), thereby accumulating an activation signal along the way, until a certain threshold is exceeded, which leads to T cell activation.

Both of these hypotheses will be considered, starting from the assumption that the T cells would evolutionary prefer a concept that is energetically cheaper for them, and theoretically obtained values will be compared with the experimental results.

3.15.1 Basic model assumptions

In order to become activated, T cells must first scan many APCs until they find the one presenting their specific antigen and they receive the activation signal while interacting with it. It is considered here that, in order to become activated, T cells must first spend energy to find a right APC (E_{find}), and then spend energy to become activated (E_{act}). It is assumed that energy consumption is linear over time ($\Delta E/\Delta t$).

The total energy that a T cell will spend in each of the two suggested hypotheses is:

Hypothesis I:

$$E_{total} = \frac{\Delta E_{find}}{\Delta t} T_{find} + \frac{\Delta E_{act}}{\Delta t} T_{act}$$

Hypothesis II:

$$E_{2total} = N \frac{\Delta E_{find}}{\Delta t} T_{find} + N \frac{\Delta E_{act}}{\Delta t} T_{2act}$$

T_{find} Time that a T cell needs to find the APC with the right antigen

T_{1act} Average length of one contact that would lead to full activation

T_{2act} Average length of many short accumulating contacts

N Number of short activating contacts that a T cell must make until activation threshold is exceeded

In the next section, the finding and the activating component of the total energy a T cell must spend on its activation, will be discussed in more detail.

3.15.2 T cell in search of an activating APC

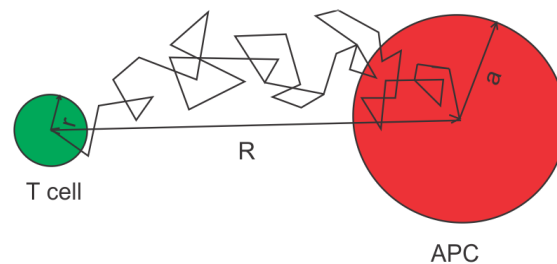


Figure 3.15.1. Schematic illustration of the basic model assumptions. A T cell of radius r and its closest APC of radius a . R is a distance between them and irregular line represent the path T cell will take until it reaches an APC assumed it follows a random walk.

Imaging data show that, in the process of scanning, T cells are moving randomly in a Brownian motion. An average time (τ) that a T cell of radius r needs to spend to contact the closest APC of radius a (Figure 3.15.1) is given as:

$$\tau = \frac{R^3}{3Dt(r+a)} \quad (\text{Castro, 2011})$$

R is an average distance between the T cell and the closest APC, and Dt represents the diffusivity of T cells and can be experimentally calculated as:

$$Dt = \frac{\sum \Delta x^2}{n} * \frac{1}{\Delta t} \text{ (Lythe, 2011)}$$

Δx represents the cell displacement and Δt is the time between two imaging frames.

Upon T cell/APC contact, the T cell needs to scan the surface of the APC, in search for the one that can activate it. For simplicity it is assumed, that a T cell is able to do this while simply passing by an APC. The time the T cell will need for this is:

$$ts = \frac{\pi l^2}{16Dt} \text{ (Lythe, 2011)}$$

$l = 2a + 2r$ – Distance T cell must travel while passing by (scanning) an APC.

If P is the probability that the T cell/APC contact is activating one, then the T cell must contact in average:

$$n = \frac{1}{P} \text{ APCs, to find the activating one.}$$

For this a T cell needs to spend time according to the following equation:

$$T_{find} = n(\tau + ts)$$

$$T_{find} = \frac{1}{P} \left(\frac{R^3}{3Dt(r+a)} + \frac{\pi(2a+2r)^2}{16Dt} \right)$$

It can be assumed, that during its migration the T cell spends energy per time unit:

$$\frac{\Delta E_{find}}{\Delta t} = F_{friction} * v = 6\pi\mu r v^2 \text{ (Castro, 2011)}$$

μ represent viscosity of the medium (we can consider that is water), and v is average T cell velocity. The total energy that a T cell spends for finding an activating APC is:

$$E_{find} = \frac{\Delta E_{find}}{\Delta t} T = 6\pi\mu r v^2 \frac{1}{P} \left(\frac{R^3}{3Dt(r+a)} + \frac{\pi(2a+2r)^2}{16Dt} \right)$$

v can be experimentally calculated from $v = \frac{\sum \Delta x}{n} * \frac{1}{\Delta t}$, and Dt from $Dt = \frac{\sum \Delta x^2}{n} * \frac{1}{\Delta t}$

Putting this back to the equation for E_{find} gives:

$$E_{find} = \frac{\pi\mu r (\sum \Delta x)^2}{2Pn\Delta t \sum \Delta x^2} \left(\frac{4R^3}{r+a} + 3\pi(a+r)^2 \right)$$

Since Δt can be considered as constant, (during two-photon imaging, the time between two scans is constant), E_{find} depends on the cell displacement as $\frac{(\sum \Delta x)^2}{\sum \Delta x^2}$

This part of the system was modeled based on two-photon imaging data. Values for R , r and a could be obtained from experimental data. Also, from experiments where $\Delta NFAT$ -GFP was used as T cell activation indicator, the probability of a T cell getting activated upon a random APC contact could be calculated as:

$$P = \frac{\text{No of activating contacts}}{\text{Total No of contacts}} = 0.06$$

Knowing these parameters, it was modeled in MATLAB, how v , Dt , T , and E_{find} depend on different mean displacements. The idea is, that one value of Δx is chosen as a mean displacement, and others around it are modeled by Gaussian distribution (with random possibility that any of them occurs). This was performed for a range of mean displacements, and dependency graphs were obtained (Fig. 3.15.2).

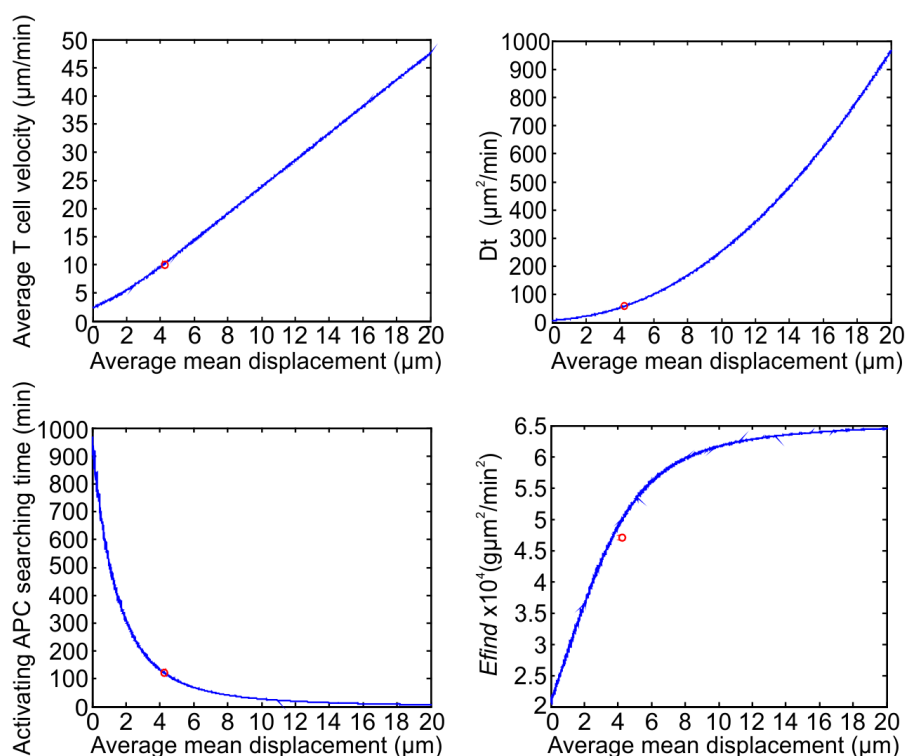


Figure 3.15.2. Mean displacement (Δx) dependency graphs modeled in MATLAB. Dependency of T cell velocity (v), diffusivity (Dt), activating APC searching time (T) and the energy a T cell spends on finding a right APC (E_{find}) from mean cell displacement (Δx) were modeled in mat lab using previously described formulas. Red circles on graphs represent values for experimental mean displacement (4.23 μm).

This indicated that E_{find} has an exponential dependency on the mean cell displacement, suggesting that, for increasing its speed, the T cell spends exponentially more energy, but in contrast less time for APC searching. Nevertheless, there is a plateau when the increase of speed stops being energetically expensive for the T cell, from which the T cell could theoretically benefit. However, the experimentally calculated value (red circles in Figure 3.15.2) is not on the plateau. Based on the current model, the time a T cell needs to just pass by an APC (t_s) could be calculated to be 3 min, which fits very well with the experimental values of the average EAE^{lo} T cell/APC contact duration (3 min). It could also be estimated that a T cell would need an average of 16 contacts until it finds an APC being able to activate it, and for this it would need around 2 h.

3.15.3 Correlation between *Tfind* and *Tact*

As discussed before, the influx of Ca^{2+} ions is one of the first crucial steps in the cascade of T cell activation. The time course of this influx is depicted in figure 3.15.3:

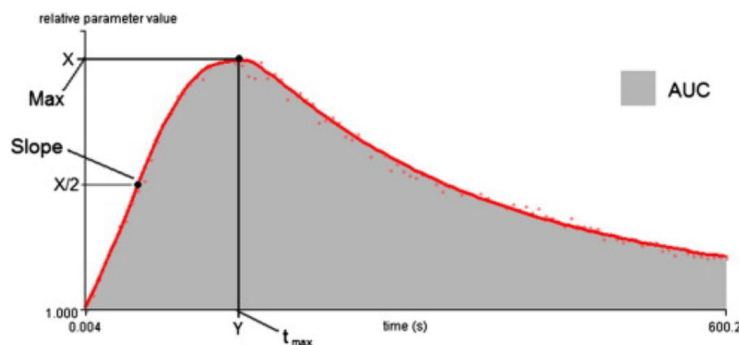


Figure 3.15.3. Scheme of Ca^{2+} influx into a lymphocyte. The maximum value represents the peak value of the Ca^{2+} influx curve upon lymphocyte activation, thus it reflects the maximal amount of $[\text{Ca}^{2+}]_{\text{cyt}}$ in the course of activation. The time to reach the maximum value (Y, t_{max}) describes, how soon the peak value is reached. The slope reflects how rapidly the peak of Ca^{2+} influx is reached. The area under the curve (AUC) describes the full amount of $[\text{Ca}^{2+}]_{\text{cyt}}$ during the whole period of lymphocyte activation. AUC values correspond to the sum $[\text{Ca}^{2+}]_{\text{cyt}}$ increase, which further corresponds to the level of lymphocyte activation. (Adopted from Toldi et al., 2011)

According to the second hypothesis on T cell activation, the lymphocyte must encounter several APCs presenting its specific antigen in the context of the MHC II. However, each of these contacts alone is insufficient to exceed the cytosolic calcium threshold concentration required for the final activation of the T cell. As illustrated in Figure 3.15.3, the rise in cytosolic calcium triggered by a single APC has a limited life time. This duration is a critical variable for modeling the T cell activation, as the gap between successful interactions of T cells and APCs needs to be shorter in order to steadily increase the intracellular calcium level.

Experimental data on this time differ, depending on the method and cell type used (Lioudyno et al., 2008; Toldi et al., 2011). Most measurements were done for 10-15 min, the time in which Ca^{2+} values significantly dropped. However, in the previously modeled scenario, a T cell needs an average time of 127 min to find an activating APC, which would be too long for second hypothesis to possibly lead to an activation event. To find a second activating APC in 10-20 min, the T cell would

require moving with a velocity of 25-40 $\mu\text{m}/\text{min}$, which is extremely fast (experimental velocity is 10 $\mu\text{m}/\text{min}$). It can be concluded that second hypothesis is not very likely, based on the assumptions that have been made.

However, the experimental data used for the probability calculation are based on $\Delta\text{NFAT-GFP}$ as a sensor for the final T cell activation event. Therefore, it does not indicate the Ca^{2+} influx, an early step of the activation pathway. However, the second hypothesis assumes, that T cells receive sub-maximal signals from different APCs on the way. If this is taken into consideration, the probability for finding the right APC would be much higher.

For the second hypothesis to be possible, a T cell must find a stimulating APC in approximately 20 min or less. If the searching time is considered to be constant (20 min), it can be modeled how P (probability that a T cell/APC contact is stimulating), depends on mean displacement (Figure. 3.15.4).

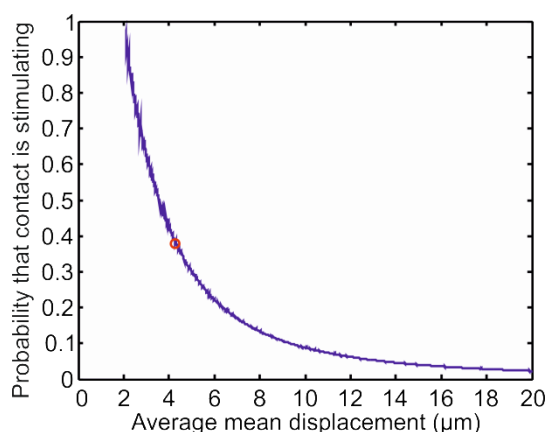


Figure 3.15.4. Mean displacement (Δx) dependency graph modeled in MATLAB with a constant T_{find} of 20 min. Dependency of the probability (P) that a T cell/APC contact is stimulating from mean displacement with the assumption that the APC searching time is constant (20 min). Red circle on the graph represents the experimentally observed mean displacement (4.23 μm).

The red circle in figure 3.15.4 indicates probability for experimentally determined velocity, and is 0.39, meaning that every 2-3 T cell/APC contacts must lead to Ca^{2+} influx, for the T cell to be able to accumulate a stimulus on the way.

3.15.4 Modeling T cell activation during antigen recognition and signal transduction

It was assumed that besides for finding an APC, the T cell also has to spend energy on the process of activation during antigen recognition and signal transduction. It was defined before, that the total energy a T cell needs to spend on becoming activated, in the two discussed hypotheses is:

Hypothesis I:

$$E1total = \frac{\Delta E_{find}}{\Delta t} T_{find} + \frac{\Delta E_{act}}{\Delta t} T1act$$

Hypothesis II:

$$E2total = N \frac{\Delta E_{find}}{\Delta t} T_{find} + N \frac{\Delta E_{act}}{\Delta t} T2act$$

N Number of short activating contacts that T cell must establish until the activation threshold is exceeded, leading finally to a full activation.

From these equations can be concluded that, for the second hypothesis to be possible, the energy a T cell spends on antigen recognition and signal transduction must here be much less compared to the first case. Since it is considered that energy has linear dependency over time, these will be true if a T cell spends much less time for activation process itself in the second compared to the first hypothesis. It is also clear that in the second case the T cell will always spend N time more energy on finding the right APC. This imply that the T cell can benefit in the second scenario only if the antigen recognition and signal transduction process is energetically more expensive than process of APC searching. In equations this would be:

$$E2total < E1total \text{ if}$$

$$T1act > N * T2act \quad \text{and} \quad \frac{\Delta E_{find}}{\Delta t} \ll \frac{\Delta E_{act}}{\Delta t}$$

The first condition was modeled to test the feasibility of this scenario. For this, the Ca^{2+} influx kinetic graph was used (Fig. 3.15.3). Please note that t_{max} describes

how soon the peak value of the Ca^{2+} influx curve is reached, and that the Area Under the Curve (AUC), which corresponds to the sum of $[\text{Ca}^{2+}]_{\text{cyt}}$ increase, further relates to the level of lymphocyte activation (Toldi et al., 2011).

It is assumed here that a certain AUC is needed for the full activation of T lymphocyte. Using experimental data it was also suggested that the duration of one contact, leading to full T cell activation ($T1_{act}$), should be approximately 20 min. For further modeling in MATLAB, the approximation of the Ca^{2+} influx curve was used (Figure 3.15.5).

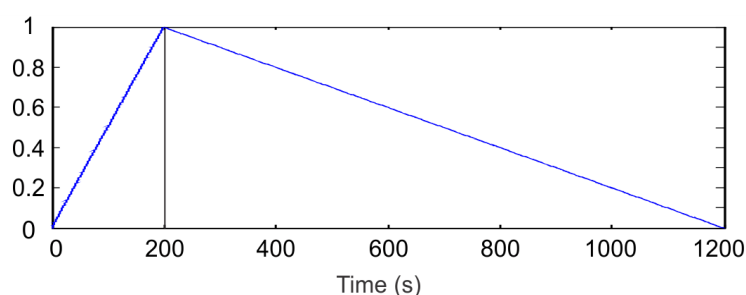


Figure 3.15.5. Approximation of the Ca^{2+} influx curve, as used for modeling the activation in MATLAB. Graph depicts approximated kinetics of the Ca^{2+} influx and decay in one T cell/APC contact that would lead to a full activation. The area under the curve (AUC) was used as a constant needed for full activation, and the line at 200 s indicates t_{max} , which was variable in our model.

Here, the AUC does not depend on t_{max} (only on height), implying that for one long activating contact it is not relevant how fast the maximum value is reached. However, this can be crucial for receiving a stimulus upon a short contact, why it was modeled how is N (Number of short activating contact needed for full activation) depending on t_{max} . This would directly give us information of the total time that T cells need to spend on their activation according to the second hypothesis ($T2_{act}$), which can then be compared to $T1_{act}$ (assumption is 20 min). An average short contact between a T cell and an APC is, as it was already calculated, the time the T cell needs to simply pass by an APC ($t_s = 3.23$ min). It is suggested that even during simple scanning whether or not the APC is presenting the appropriate antigen, the T cell will get a certain stimulus as Ca^{2+} influx. The stimulus intensity would correspond with the AUC value. The dependence of N and t_{max} (time needed for Ca^{2+} to reach its maximum value) was modeled in MATLAB (Figure 3.15.6).

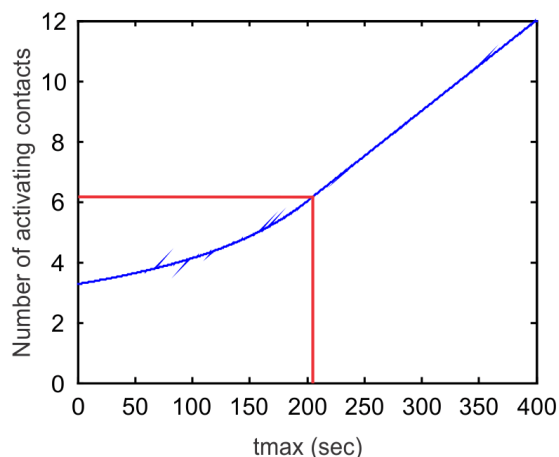


Figure 3.15.6. tmax dependency graph. Graph depicts how the number of short contacts ($t_s=3.23$ min) needed for full activation (AUC from the Figure 3.15.3), is depending on t_{max} . Red lines set the borders for second hypothesis to be possible using calculations ($N \cdot t_s < T1_{act}$). The calculation was performed using MATLAB.

Figure 3.15.6 illustrates that for small t_{max} (Ca^{2+} influx reaches maximum value fast), the T cell would need just a few contacts and hence less time ($T2_{act}$), to become fully activated, comparing to one long contact ($T1_{act}$). All this would imply that T cells can energetically benefit from the second hypothesis, presuming that Ca^{2+} influx reaches its maximum fast.

It should also be mentioned, that the T cells would always spend more energy for an APC search in the second hypothesis ($N \times$ more). Therefore, in order to energetically benefit from the second scenario, the equation $\frac{\Delta E_{find}}{\Delta t} \ll \frac{\Delta E_{act}}{\Delta t}$ must also be satisfied.

4 DISCUSSION

In this study, T cell lines with distinct antigen-specificities, inducing either severe (EAE^{hi}), or marginal (EAE^{lo}) neurological disorder, in different rat strains (LE vs DA), were used as a paradigm to investigate the role of CNS-associated antigen presentation in early stages of disease development. Intravital two-photon imaging approach demonstrated that the interaction between infiltrated T cells and local APCs residing in the leptomeninges are crucial for the formation of tissue infiltrates and for induction of clinical disease. In addition, a new fluorescent marker of T cell activation, truncated NFAT fused to GFP (Δ NFAT-GFP) was applied, allowing, for the first time to visualize the autoimmune T cell activation *in vivo*. This approach unambiguously documented that T cell interactions with perivascular phagocytes, and not with endothelial cells, are essential for T cell activation. This work further emphasizes the impact of auto-antigen availability on the locomotor behavior and pathological capacity of CNS autoimmune T cells.

Entry of myelin-reactive autoimmune T cells into the CNS involves a complex set of sequential interactions between T lymphocytes and their surrounding milieu, first in the periphery and then at the BBB. Following adoptive transfer, *in vitro* activated T cells first enter lymphatic organs where they assume a “migratory” phenotype, down-regulating activation markers and up-regulating chemokine receptors, which renders them competent to home into the CNS (Flügel et al., 2001). A recent study showed that T cells can also acquire migratory phenotype in the lung (Odoardi et al., 2012). Once they arrive at their CNS entry port, the leptomeningeal vessels (Bartholomäus et al., 2009; Kivisäkk et al., 2009), the T cells attach to the luminal surface of the local vessels, first roll along, and then crawl, preferentially against the blood flow, before they pass through the endothelial wall (Bartholomäus et al., 2009). After extravasation the immigrant T cells continue to crawl on the abluminal side where they make contacts with perivascular phagocytes. It was hypothesized that these interactions facilitate the presentation of locally released auto-antigen to auto-reactive T cells, directing them further into the CNS parenchyma.

The first structure encountered by CNS-homing T cells is the luminal membrane of meningeal vessels. In the CNS, blood vessel endothelium is highly specialized structure of the BBB. Apart from tight junctions, endothelial cells express a spectrum of surface molecules allowing them to attract blood leukocytes and communicate with them (Nourshargh et al., 2010). For instance, T cell rolling involves transient interactions between selectins and glycoproteins (Piccio et al., 2002), while crawling depends on the binding of integrins LFA-1 and VLA-4 (Bartholomäus et al., 2009). Here it was documented, that myelin-specific T cells, interact with the cerebrovascular endothelium remarkably similar, regardless of their encephalitogenic potential. They appear in the leptomeninges with similar kinetics, and show an undistinguishable locomotive behavior. All T cell types attached to intraluminal surfaces and crawled there with similar velocities and track patterns. Finally, by using Δ NFAT-GFP as a fluorescent marker of T cell activation, it was shown that neither the crawling nor the rolling T cells translocate NFAT into their nucleus. It is noteworthy to mention here, that due to the limited microscope scanning speed, only a fraction of fast rolling T cells was detected. These findings suggest that, unexpectedly, the inflammatory status of the perivascular milieu has little effect on the locomotion behavior and activation status of T cells, as long as they are inside of the vascular tube.

However, the interactions of immigrant T cells with components of the extravascular leptomeningeal milieu differ depending on their pathogenic potential. It was noted that following diapedesis, the weakly encephalitogenic T_{LE-MOG} cells fail to detach from the perivascular area of the leptomeningeal blood vessels, while highly encephalitogenic T_{LE-MBP} and T_{DA-MOG} cells left the perivascular area to evenly distribute throughout the leptomeninges. The key events underlying this discrepancy involved the interactions of T cells with local APCs, and the subsequent T cell activation.

Real-time imaging demonstrated that EAE^{hi} T cells show a lower motility and make longer contacts with local APCs, compared to the highly motile EAE^{lo} counterparts (average contact duration of EAE^{hi} T cells was around 6 min, and of EAE^{lo} T cells 3 min). Experiments using the Δ NFAT-GFP marker confirmed, that this discrepancy is directly correlated with the activation status of auto-reactive T cells. Namely, both

motility and APC contact duration of T cells that retained Δ NFAT-GFP in their cytosol (resting T cells) were indistinguishable (average contact duration is 3 min), regardless of their pathogenic potential. In contrast, T cells that translocated Δ NFAT-GFP into their nucleus exhibited a reduced motility and engaged in longer contacts with meningeal phagocytes. Δ NFAT-GFP as a fluorescent marker of T cell activation allowed here for the first time to visualize the *in situ* activation of auto-reactive T cells and even to correlate it directly with APC interactions. T cell/APC contacts leading to Δ NFAT-GFP translocation from the cytosol to the nucleus were also the longest interactions observed in leptomeninges (average duration of 20 min).

Formation of short and long lasting contacts with APCs is a general phenomenon, by no means unique to the CNS. Mempel et al. suggested a three phase model of antigen recognition in the peripheral LNs (Mempel et al., 2004). They found that antigen-specific T cells formed multiple short lasting contacts with APC at an early stage of antigen-recognition (within 8 hours). In the subsequent period, between 8 and 20 hours, T cells established longer lasting, stable contacts, which finally resulted in T cell activation. T cell/APC interactions that were observed here in the leptomeningeal area qualify as transient contacts and are similar to the interactions characteristic for the early stage of antigen recognition in the lymph node, while long lasting stable contact (duration of approximately 1 h) were rare.

Dustin et al. also distinguished stable contacts (“synapses”) from the transient interactions (“kinapses”), of T cells encountering exogenous antigens in secondary lymph organs (Dustin, 2008). According to this scheme, most of the APC contacts formed by the EAE^{hi} T cells in the leptomeningeal space qualify as kinapses (motility between 2.5 and 5.0 μ m/min), whereas synapses (motility slower than 2.5 μ m/min) were rarely observed. Both the kinapses and synapses might be sufficient to translocate NFAT to the nucleus and to induce the transcription of activation-dependent genes (Moreau et al., 2012). Elevation of intracellular calcium levels and following NFAT translocation are considered to be a stop-signal to T cells (Negulescu et al., 1996). However, this seems not to be the case in the leptomeningeal EAE^{hi} T cells, which continued to visit APCs successively even in the activated, Δ NFAT-GFP nucleus-localized state. This supports a previous suggestion (Bartholomäus et al., 2009), that contacts with leptomeningeal APCs serve to guide

immigrant autoimmune T cells into the CNS parenchyma rather than to arrest them for longer time periods.

Which factors determine the duration of T cell/APC contacts, and how are they related to the encephalitogenic potential of the T cell? The responsiveness of a T cell depends on the structure of the specific antigen receptor, and its surrounding co-activating and signal transducing machinery. Indeed, a slightly lower sensitivity of T_{LE-MOG} cells to low doses of antigen presented by professional APCs *in vitro* was noted, compared to other T cell lines. This might particularly account for antigen presentation by leptomeningeal APCs, which are not saturated with myelin antigens (Bartholomäus et al., 2009; Odoardi et al., 2007a).

However, the encephalitogenic potential of EAE^{lo} T_{LE-MOG} cells is demonstrable by supplying exogenous MOG. Intrathecal administration of MOG-loaded APCs lowered the motility, and extended contact duration of EAE^{lo} T cells with APCs, making their behavior similar to that observed in EAE^{hi} T cells. In addition, local infusion of MOG induced Δ NFAT-GFP translocation in EAE^{lo} T cells from the cytosol to the nucleus, and showed that, like in EAE^{hi} T cells, both motility as well as duration of T cell/APC interactions could be directly correlated with the activation status of the T cells. Increased antigen availability and following T cell reactivation in leptomeninges were associated with the development of clinical EAE.

This brings the attention to local meningeal APCs and their possibly insufficient ability to present auto-antigen to T cells. When isolated *ex vivo*, these phagocytes can indeed present locally produced myelin auto-antigens to specific T cells, but the antigenic strength *in vitro* is weak. The responding T cells are activated to release cytokines, but do not extensively proliferate unless supplemented with exogenous antigen (Bartholomäus et al., 2009). Meningeal APCs isolated from Lewis rats (LE) weakly present MOG to cognate T cells, but at the same time are efficient presenters of MBP, which excludes a strain-related defect in antigen presentation. Similarly, MOG is a weak encephalitogen in LE, but a strong in DA rats, ruling out a global reduction of auto-antigenic strength in rats. However, the level of locally produced MOG may be lower in LE than in DA rats (Pagany et al., 2003). To explore this possibility, we transferred T_{LE-MOG-GFP} or T_{DA-MOG-GFP} cells into F1 (LExDA) hosts. The

behavior of both cell types in F1 hosts mirrored the one in parental rats. T_{DA-MOG} cells showed lower motility and prolonged contacts with local APCs, compared to T_{LE-MOG} cells. T_{DA-MOG} cells also induced stronger EAE than T_{LE-MOG} cells in F1 host. Therefore, differences in clinical severity are not due to host properties. A further explanation might be different epitope presentation in context of MHC class II molecules. Weissert et al. demonstrated that Lewis rats and congenic rats sharing their MHC class II haplotype were largely protected from EAE induction by MOG/CFA immunization (Weissert et al., 1998). They found that the minimum amount of MOG required to induce EAE depended directly on the MHC haplotype. According to their hypothesis, the MHC haplotype dictates binding of MOG-peptides to the relevant MHC class II protein, which is in line with our finding.

Intravital two-photon microscopy revealed that EAE^{lo} T cells penetrated into the CNS leptomeninges similarly to EAE^{hi} T cells. However, they were engaged in only short contacts with local APCs, which failed to induce the translocation of Δ NFAT-GFP from cytosol to nucleus. As a result, they are not receiving the “go ahead” signal, allowing them to detach from the vessels and infiltrate the parenchyma. However, an increase of antigen availability on local APCs induced Δ NFAT-GFP translocation from the cytosol to the nucleus in EAE^{lo} T cells and recruited them into the CNS, leading to induction of clinical symptoms. The work by Hickey and Kimura indicated that bone-marrow derived perivascular cells are the essential elements interacting with encephalitogenic T cells to induce clinical EAE (Hickey and Kimura, 1988). In mice, these local meningeal APCs express markers of dendritic cells (Greter et al., 2005), while in rats their profile places them closer to macrophages (Bartholomäus et al., 2009). This discrepancy may be explained by species differences. Nevertheless, it was confirmed here and by others, that these APCs can *in vitro* present endogenous antigen to infiltrated T cells. Indeed, *in vivo* two-photon imaging showed that T cell reactivation by local APCs in leptomeninges is a major check-point for T cell infiltration into the parenchyma, and implicitly for induction of clinical EAE. This result might lead to novel therapeutic strategies for MS, which specifically block the infiltration of autoaggressive T cells into the CNS without modifying host immunity, and the method introduced here can be suitable for testing the same.

A truncated NFAT1 fused to GFP (Δ NFAT-GFP), used here as fluorescent reporter of *in vivo* T cell activation, represents an important technical advance. Δ NFAT-GFP displays qualities rendering it more suitable for two-photon imaging of T cell activation, than the various previously suggested activation indicators. Among these, TCR complex related genetic markers, such as a CD3zeta-GFP fusion protein (Huppa et al., 2003; Richie et al., 2002; Yudushkin and Vale, 2010), or Linker for Activation of T-Cells (LAT)-GFP fusion protein (Tanimura et al., 2003), showed T cell activation by clustering at the immunological synapses. However, due to the poor z-resolution (typically, 3-4 μ m spacing) of two-photon microscopy, detection of small clusters within three-dimensional volume is not reliably possible. In contrast, Δ NFAT-GFP subcellular localization was detectable in more than 90% of the T cells during intravital two-photon imaging. Moran and colleagues used GFP expressed from the immediate early gene locus, NUR77, as activation indicator (Moran et al., 2011). This system can distinguish the strength of TCR stimulation according to GFP expression level. However the GFP protein needs to be transcribed and matured, a process that takes at least few hours, which is too long for real-time imaging of T cell activation. In sharp contrast, Δ NFAT-GFP nuclear translocation occurs within only few minutes after stimulation. Finally, calcium indicators can be used to monitor T cell activation *in vivo* (Wei et al., 2007). Small molecular calcium indicator dyes are rapidly pumped out from T cells and thus fail to label them over extended periods of time. Recently, a genetically encoded Ca^{2+} indicator, Twitch-1, has also been developed as a marker of *in vivo* T cell activation (Mues et al., 2013). However, Δ NFAT-GFP is a robust downstream indicator, as elevated calcium might not always result in full T cell activation. Considering all this, the Δ NFAT-GFP fusion-protein qualifies as a marker to rapidly and reliably detect T cell activation induced by antigen recognition *in vivo*.

In CD4^+ T cells, NFAT family proteins act as key factors of Ca^{2+} controlled gene transcription. Following TCR engagement and increased intracellular calcium levels, calcineurin dephosphorylates NFAT, which then translocates from the cytoplasm to the nucleus where, in cooperation with other transcription factors, it binds to the DNA in order to initiate gene expression. However, although Δ NFAT-GFP is a reliable indicator of TCR/calcium-dependent cell activation, it is not absolutely specific. Apart from TCR activation, the pathway may also be triggered via signaling through

cytokine receptors such as IL-2R and IL-15R (Barlic et al., 2004) or IL-6R (Diehl et al., 2002). Conversely, T cells may be stimulated via alternative pathways, which would not be indicated by Δ NFAT-GFP (Macian, 2005). In addition, a truncated version of the NFAT1 protein, which is only one out of three variants expressed in CD4⁺ T cells (NFAT2 and NFAT4), was used here. This must be considered in the case of the intraluminal T cell migration modes for which no Δ NFAT-GFP translocation was observed. The negative finding of NFAT transition may exclude the classic TCR-mediated, NFAT1-driven activation, but not necessarily distinct stimulatory pathways with or without TCR participation. For instance, dephosphorylated NFAT2 translocation might also drive transcription of activation genes, and integrin-dependent stimulation can elevate Ca²⁺ levels but may not induce NFAT translocation. For this purpose, the recently developed Twitch-1 would be more suitable (Mues et al., 2013).

At the end it was attempted to test two existing hypotheses on T cell activation, using the motility data obtained from two-photon imaging in combination with a theoretical, physicist approach. The first hypothesis assumes, that after finding an APC with the right antigen, the T cell will interact with it, until becoming fully activated, while the second one suggests that a T cell will collect its activation signal on the way, without establishing long contacts with APCs. Our basic assumption is that T cells would prefer the energetically cheaper concept.

It is proposed that, in order to become activated, a T cell must spend energy first on finding an activating APC, and then on the activation itself during antigen recognition and signal transduction. We show that the total energy a T cell needs to spend on finding the right APC, depends on T cell velocity, and the probability that an APC/T cell contact is an activating one. Using experimental data, based on fluorescent T cell activation sensor, it could be calculated that a T cell needs to contact on average 16 APCs to find a right one. For this, considering the experimentally calculated velocity of 10 μ m/min, the T cell requires around 2 h. From the kinetics of T cell activation, that have been previously reported (Shaw et al., 1995; Toldi et al., 2011; Tomida et al., 2003), showing that the levels of influxed Ca²⁺ ions drop to basal values in approximately 20 min, it would be very unlikely that T cells can accumulate the calcium signal with 2 h difference between receiving the

triggers. Therefore, the first hypothesis would be more likely for the leptomeningeal reactivation of autoimmune T cells by local APCs.

Furthermore, conditions under which the second hypothesis would be preferable, were explored. It was calculated that for the second scenario to be possible, a T cell must have much higher probability of finding the right APC (0.4). Concentration of the specific antigen can have a major impact on this. As already mentioned, meningeal APCs are not saturated with myelin antigen, and external addition of antigen can improve their activating potential (Odoardi et al., 2007a). From this, it can be concluded that there is low probability of meningeal APC being the right one. However, in draining lymphoid organs the concentration of pathogenic antigen can reach very high levels, to ensure a strong immune response against it. It should be also taken into consideration, that meningeal APCs could have lower density, compared to dendritic cells in lymph nodes. This factor can affect the APC search-time, rendering the second hypothesis more likely (Bousso and Robey, 2003).

Overall, both hypotheses could be possible, depending on specific conditions in which T cells are receiving their activation signal. It is likely that T cells can become activated in both ways and that depending on antigen concentration and APC density they will do that by following the first or the second hypothesis. Here, it is suggested that in the immunoprivileged organs such as the CNS, T cells are activated most likely according to the first hypothesis. This work also offers a new, physical approach for solving immunological questions.

REFERENCES

- Adelmann, M., J. Wood, I. Benzel, P. Fiori, H. Lassmann, J.M. Matthieu, M.V. Gardinier, K. Dornmair, and C. Lington. 1995. The N-terminal domain of the myelin oligodendrocyte glycoprotein (MOG) induces acute demyelinating experimental autoimmune encephalomyelitis in the Lewis rat. *Journal of Neuroimmunology* 63:17-27.
- Alter, M., E. Kahana, and R. Loewenson. 1978. Migration and risk of multiple sclerosis. *Neurology* 28:1089-1093.
- Alter, M., U. Leibowitz, and J. Speer. 1966. Risk of multiple sclerosis related to age at immigration to Israel. *Archives of Neurology* 15:234-237.
- Alter, M., M. Okihiro, W. Rowley, and T. Morris. 1970. Multiple sclerosis among Caucasians and Orientals in Hawaii. *Neurology* 20:399.
- Aramburu, J., F. Garcia-Cozar, A. Raghavan, H. Okamura, A. Rao, and P.G. Hogan. 1998. Selective inhibition of NFAT activation by a peptide spanning the calcineurin targeting site of NFAT. *Molecular Cell* 1:627-637.
- Asperti-Boursin, F., E. Real, G. Bismuth, A. Trautmann, and E. Donnadieu. 2007. CCR7 ligands control basal T cell motility within lymph node slices in a phosphoinositide 3-kinase independent manner. *Journal of Experimental Medicine* 204:1167-1179.
- Avni, O., D. Lee, F. Macian, S.J. Szabo, L.H. Glimcher, and A. Rao. 2002. T(H) cell differentiation is accompanied by dynamic changes in histone acetylation of cytokine genes. *Nature Immunology* 3:643-651.
- Barlic, J., D.H. McDermott, M.N. Merrell, J. Gonzales, L.E. Via, and P.M. Murphy. 2004. Interleukin (IL)-15 and IL-2 reciprocally regulate expression of the chemokine receptor CX3CR1 through selective NFAT1- and NFAT2-dependent mechanisms. *The Journal of Biological Chemistry* 279:48520-48534.

- Bartholomäus, I. 2011. Untersuchung des Verhaltens autoaggressiver T-Zellen während der experimentellen autoimmunen Enzephalomyelitis der Ratte mittels intravitale 2-Photonen-Mikroskopie. In Ludwig-Maximilians-Universität München, Munich. 113.
- Bartholomäus, I., N. Kawakami, F. Odoardi, C. Schlager, D. Miljkovic, J.W. Ellwart, W.E.F. Klinkert, C. Flugel-Koch, T.B. Issekutz, H. Wekerle, and A. Flugel. 2009. Effector T cell interactions with meningeal vascular structures in nascent autoimmune CNS lesions. *Nature* 462:94-U104.
- Beltman, J.B., A.F.M. Marel, and R.J. de Boer. 2009. Analysing immune cell migration. *Nature Reviews Immunology* 9:789-798.
- Ben-Nun, A., H. Wekerle, and I.R. Cohen. 1981. The rapid isolation of clonable antigen-specific T lymphocyte lines capable of mediating autoimmune encephalomyelitis. *European Journal of Immunology* 11:195-199.
- Bettelli, E., D. Baeten, A. Jäger, R.A. Sobel, and V.K. Kuchroo. 2006. Myelin oligodendrocyte glycoprotein-specific T and B cells cooperate to induce a Devic-like disease in mice. *Journal of Clinical Investigation* 116:2393-2402.
- Bouso, P. 2008. T-cell activation by dendritic cells in the lymph node: lessons from the movies. *Nature Reviews Immunology* 8:675-684.
- Bouso, P., N.R. Bhakta, R.S. Lewis, and E. Robey. 2002. Dynamics of thymocyte-stromal cell interactions visualized by two-photon microscopy. *Science* 296:1876-1880.
- Bouso, P., and E. Robey. 2003. Dynamics of CD8+ T cell priming by dendritic cells in intact lymph nodes. *Nature Immunology* 4:579-585.
- Campbell, B., P.J. Vogel, and E. Fisher. 1973. Myelin basic protein administration in multiple sclerosis. *Archives of Neurology* 29:10-15.
- Castro, M. 2011. A Physicist's approach to Immunology. In *Mathematical Models and Immune Cell Biology* 339-350.

- Celli, S., F. Lemaitre, and P. Bousso. 2007. Real-time manipulation of T cell-dendritic cell interactions in vivo reveals the importance of prolonged contacts for CD4(+) T cell activation. *Immunity* 27:625-634.
- Compston, A., and A. Coles. 2008. Multiple sclerosis. *Lancet* 372:1502-1517.
- De Jager, P.L., K.C. Simon, K.L. Munger, J.D. Rioux, D.A. Hafler, and A. Ascherio. 2008. Integrating risk factors: HLA-DRB1*1501 and Epstein-Barr virus in multiple sclerosis. *Neurology* 70:1113-1118.
- Dean, G., and M. Elian. 1997. Age at immigration to England of Asian and Caribbean immigrants and the risk of developing multiple sclerosis. *Journal of Neurology, neurosurgery, and psychiatry* 63:565-568.
- Detels, R., B.R. Visscher, R.W. Haile, R.M. Malmgren, J.P. Dudley, and A.H. Coulson. 1978. Multiple sclerosis and age at migration. *American Journal of Epidemiology* 108:386-393.
- Diehl, S., C.W. Chow, L. Weiss, A. Palmetshofer, T. Twardzik, L. Rounds, E. Serfling, R.J. Davis, J. Anguita, and M. Rincon. 2002. Induction of NFATc2 expression by interleukin 6 promotes T helper type 2 differentiation. *Journal of Experimental Medicine* 196:39-49.
- Donnadieu, E., C. Bismuth, and A. Trautmann. 1994. Antigen Recognition by Helper T-Cells Elicits a Sequence of Distinct Changes of Their Shape and Intracellular Calcium. *Current Biology* 4:584-595.
- Dustin, M.L. 2008. T-cell activation through immunological synapses and kinapses. *Immunological Reviews* 221:77-89.
- Dustin, M.L., S.K. Bromley, Z.Y. Kan, D.A. Peterson, and E.R. Unanue. 1997. Antigen receptor engagement delivers a stop signal to migrating T lymphocytes. *Proceedings of the National Academy of Sciences of the United States of America* 94:3909-3913.

- Dustin, M.L., and D. Depoil. 2011. New insights into the T cell synapse from single molecule techniques. *Nature Reviews Immunology* 11:672-684.
- Dyment, D.A., A.D. Sadovnick, and G.C. Ebers. 1997. Genetics of multiple sclerosis (vol 6, pg 1693, 1997). *Human Molecular Genetics* 6:2189-2189.
- Engelhardt, B. 2006. Molecular mechanisms involved in T cell migration across the blood-brain barrier. *Journal of Neural Transmission* 113:477-485.
- Engelhardt, B., and C. Coisne. 2011. Fluids and barriers of the CNS establish immune privilege by confining immune surveillance to a two-walled castle moat surrounding the CNS castle. *Fluids and barriers of the CNS* 8:4.
- Feske, S. 2007. Calcium signalling in lymphocyte activation and disease. *Nature Reviews Immunology* 7:690-702.
- Feske, S., R. Draeger, H.H. Peter, and A. Rao. 2000. Impaired NFAT regulation and its role in a severe combined immunodeficiency. *Immunobiology* 202:134-150.
- Feske, S., J. Giltnane, R. Dolmetsch, L.M. Staudt, and A. Rao. 2001. Gene regulation mediated by calcium signals in T lymphocytes. *Nature Immunology* 2:316-324.
- Fischer, U.B., E.L. Jacovetty, R.B. Medeiros, B.D. Goudy, T. Zell, J.B. Swanson, E. Lorenz, Y. Shimizu, M.J. Miller, A. Khoruts, and E. Ingulli. 2007. MHC class II deprivation impairs CD4 T cell motility and responsiveness to antigen-bearing dendritic cells in vivo. *Proceedings of the National Academy of Sciences of the United States of America* 104:7181-7186.
- Flachenecker, P., and K. Stuke. 2008. National MS registries. *Journal of Neurology* 255 Suppl 6:102-108.
- Flügel, A., T. Berkowicz, T. Ritter, M. Labeur, D. Jenne, Z. Li, J. Ellwart, M. Willem, H. Lassmann, and H. Wekerle. 2001. Migratory activity and functional changes of green fluorescent effector T cells before and during experimental autoimmune encephalomyelitis. *Immunity* 14:547-560.

- Flügel, A., F. Odoardi, M. Nosov, and N. Kawakami. 2007. Autoaggressive effector T cells in the course of experimental autoimmune encephalomyelitis visualized in the light of two-photon microscopy. *Journal of Neuroimmunology* 191:86-97.
- Flügel, A., M. Willem, T. Berkowicz, and H. Wekerle. 1999. Gene transfer into CD4 + T lymphocytes: Green fluorescent protein engineered, encephalitogenic T cells used to illuminate immune responses in the brain. *Nature Medicine* 5:843-847.
- Fogdell-Hahn, A., A. Ligiers, M. Grønning, J. Hillert, and O. Olerup. 2000. Multiple sclerosis: a modifying influence of HLA class I genes in an HLA class II associated autoimmune disease. *Tissue Antigens* 55:140-148.
- Gale, C.R., and C.N. Martyn. 1995. Migrant studies in multiple sclerosis. *Progress in neurobiology* 47:425-448.
- Gold, R., C. Linington, and H. Lassmann. 2006. Understanding pathogenesis and therapy of multiple sclerosis via animal models: 70 years of merits and culprits in experimental autoimmune encephalomyelitis research. *Brain : a journal of neurology* 129:1953-1971.
- Goverman, J., A. Woods, L. Larson, L.P. Weiner, L. Hood, and D.M. Zaller. 1993. Transgenic mice that express a myelin basic protein-specific T cell receptor develop spontaneous autoimmunity. *Cell* 72:551-560.
- Greter, M., F.L. Heppner, M.P. Lemos, B.M. Odermatt, N. Goebels, T. Laufer, R.J. Noelle, and B. Becher. 2005. Dendritic cells permit immune invasion of the CNS in an animal model of multiple sclerosis. *Nature Medicine* 11:328-334.
- Gunzer, M., A. Schafer, S. Borgmann, S. Grabbe, K.S. Zanker, E.B. Brocker, E. Kampgen, and P. Friedl. 2000. Antigen presentation in extracellular matrix: Interactions of T cells with dendritic cells are dynamic, short lived, and sequential. *Immunity* 13:323-332.
- Hammond, S.R., D.R. English, and J.G. McLeod. 2000. The age-range of risk of developing multiple sclerosis: evidence from a migrant population in Australia. *Brain : a journal of neurology* 123 (Pt 5):968-974.

- Hickey, W.F., B.L. Hsu, and H. Kimura. 1991. T lymphocyte entry into the central nervous system. *Journal of Neuroscience Research* 28:254-260.
- Hickey, W.F., and H. Kimura. 1988. Perivascular microglial cells of the CNS are bone-marrow derived and present antigen in vivo. *Science* 239:290-293.
- Hogan, P.G., L. Chen, J. Nardone, and A. Rao. 2003. Transcriptional regulation by calcium, calcineurin, and NFAT. *Genes and Development* 17:2205-2232.
- Hogan, P.G., R.S. Lewis, and A. Rao. 2010. Molecular Basis of Calcium Signaling in Lymphocytes: STIM and ORAI. *Annual Review of Immunology* 28:491-533.
- Hohlfeld, R. 2009. Multiple sclerosis: Human model for EAE? *European Journal of Immunology* 39:2036-2039.
- Huitinga, I., N. Vanrooijen, C.J.A. Degroot, B.M.J. Uitdehaag, and C.D. Dijkstra. 1990. Suppression of Experimental Allergic Encephalomyelitis in Lewis Rats after Elimination of Macrophages. *Journal of Experimental Medicine* 172:1025-1033.
- Huppa, J.B., M. Gleimer, C. Sumen, and M.M. Davis. 2003. Continuous T cell receptor signaling required for synapse maintenance and full effector potential. *Nature Immunology* 4 749-755.
- Johns, T.G., and C.C.A. Bernard. 1999. The structure and function of myelin oligodendrocyte glycoprotein. *Journal of Neurochemistry* 72:1-9.
- Kawakami, N., S. Lassmann, Z. Li, F. Odoardi, T. Ritter, T. Ziemssen, W.E.F. Klinkert, J. Ellwart, M. Bradl, K. Krivacic, H. Lassmann, R.M. Ransohoff, H.D. Volk, H. Wekerle, C. Linington, and A. Flügel. 2004. The activation status of neuroantigen-specific T cells in the target organ determines the clinical outcome of autoimmune encephalomyelitis. *Journal of Experimental Medicine* 199:185-197.
- Kawakami, N., U.V. Nägerl, F. Odoardi, T. Bonhoeffer, H. Wekerle, and A. Flügel. 2005. Live imaging of effector cell trafficking and autoantigen recognition within the unfolding autoimmune encephalomyelitis lesion. *Journal of Experimental Medicine* 201:1805-1814.

- Kieseier, B.C., and H.P. Hartung. 2003. Current disease-modifying therapies in multiple sclerosis. *Seminars in neurology* 23:133-146.
- Kivisäkk, P., J. Imitola, S. Rasmussen, W. Elyaman, B. Zhu, R.M. Ransohoff, and S.J. Khoury. 2009. Localizing central nervous system immune surveillance: Meningeal antigen-presenting cells activate T cells during experimental autoimmune encephalomyelitis. *Annals of Neurology* 65:457-469.
- Kojima, K., T. Berger, H. Lassmann, D. Hinze-Selch, Y. Zhang, J. Gehrman, H. Wekerle, and C. Linington. 1994. Experimental autoimmune panencephalitis and uveoretinitis in the Lewis rat transferred by T lymphocytes specific for the S100 β molecule, a calcium binding protein of astroglia. *Journal of Experimental Medicine* 180:817-829.
- Koritschoner, R., and F. Schweinburg. 1925. Klinische und experimentelle Beobachtungen über Lähmungen nach Wutschutzimpfung. *Zeitschrift für Immunitätsforschung* 42:217-283.
- Krishnamoorthy, G., H. Lassmann, H. Wekerle, and A. Holz. 2006. Spontaneous opticospinal encephalomyelitis in a double-transgenic mouse model of autoimmune T cell/B cell cooperation. *Journal of Clinical Investigation* 116:2385-2392.
- Krishnamoorthy, G., and H. Wekerle. 2009. EAE: An immunologist's magic eye. *European Journal of Immunology* 39:2031-2035.
- Lafaille, J.J., K. Nagashima, M. Katsuki, and S. Tonegawa. 1994. High incidence of spontaneous autoimmune encephalomyelitis in immunodeficient anti-myelin basic protein T cell receptor transgenic mice. *Cell* 78:399-408.
- Lanzillo, R., M. Quarantelli, S. Bonavita, G. Ventrella, G. Lus, G. Vacca, A. Prinster, G. Orefice, G. Tedeschi, and V. Brescia Morra. 2012. Natalizumab vs interferon beta 1a in relapsing-remitting multiple sclerosis: a head-to-head retrospective study. *Acta neurologica Scandinavica* 126:306-314.
- Lassmann, H., W. Brück, and C.F. Lucchinetti. 2007. The immunopathology of multiple sclerosis: An overview. *Brain Pathology* 17 210-218.

- Lewis, C.J., and B.A. Cobb. 2010. Carbohydrate Oxidation Acidifies Endosomes, Regulating Antigen Processing and TLR9 Signaling. *Journal of Immunology* 184:3789-3800.
- Lioudyno, M.I., J.A. Kozak, A. Penna, O. Safrina, S.L. Zhang, D. Sen, J. Roos, K.A. Stauderman, and M.D. Cahalan. 2008. Orai1 and STIM1 move to the immunological synapse and are up-regulated during T cell activation. *Proceedings of the National Academy of Sciences of the United States of America* 105:2011-2016.
- Lünemann, J.D., T. Kamradt, R. Martin, and C. Münz. 2007. Epstein-Barr virus: Environmental trigger of multiple sclerosis? *Journal of Virology* 81:6777-6784.
- Lythe, M.D.u.G. 2011. Timescales of the Adaptive Immune Response. In *Mathematical Models and Immune Cell Biology*
- Macian, F. 2005. NFAT proteins: Key regulators of T-cell development and function. *Nature Reviews Immunology* 5:472-484.
- Macian, F., F. Garcia-Cozar, S.H. Im, H.F. Horton, M.C. Byrne, and A. Rao. 2002. Transcriptional mechanisms underlying lymphocyte tolerance. *Cell* 109:719-731.
- McAlpine, D. 1956. Multiple sclerosis. *The Practitioner* 176:123-129.
- Mempel, T.R., S.E. Henrickson, and U.H. von Andrian. 2004. T-cell priming by dendritic cells in lymph nodes occurs in three distinct phases. *Nature* 427:154-159.
- Moran, A.E., K.L. Holzapfel, Y. Xing, N.R. Cunningham, J.S. Maltzman, J. Punt, and K.A. Hogquist. 2011. T cell receptor signal strength in Treg and iNKT cell development demonstrated by a novel fluorescent reporter mouse. *The Journal of Experimental Medicine* 208:1279-1289.
- Moreau, H.D., F. Lemaitre, E. Terriac, G. Azar, M. Piel, A.M. Lennon-Dumenil, and P. Bousso. 2012. Dynamic In Situ Cytometry Uncovers T Cell Receptor Signaling during Immunological Synapses and Kinapses In Vivo. *Immunity* 37:351-363.

- Mues, M., I. Bartholomäus, T. Thestrup, O. Griesbeck, H. Wekerle, N. Kawakami, and G. Krishnamoorthy. 2013. Real-time in vivo analysis of activation in the central nervous system using a genetically encoded calcium indicator. *Nature Medicine*
- Negulescu, P.A., T.B. Krasieva, A. Khan, H.H. Kerschbaum, and M.D. Cahalan. 1996. Polarity of T cell shape, motility, and sensitivity to antigen. *Immunity* 4:421-430.
- Nourshargh, S., P.L. Hordijk, and M. Sixt. 2010. Breaching multiple barriers: leukocyte motility through venular walls and the interstitium. *Nature Reviews Molecular Cell Biology* 11:366-378.
- Odoardi, F., N. Kawakami, W.E.F. Klinkert, H. Wekerle, and A. Flügel. 2007a. Blood-borne soluble protein antigen intensifies T cell activation in autoimmune CNS lesions and exacerbates clinical disease. *Proceedings of the National Academy of Sciences (USA)* 104:18625-18630.
- Odoardi, F., N. Kawakami, Z.X. Li, C. Cordiglieri, K. Rune, W.E.F. Klinkert, J.W. Ellwart, J. Bauer, H. Lassmann, H. Wekerle, and A. Flügel. 2007b. Instant effect of soluble antigen on effector T cells in peripheral immune organs during immunotherapy of autoimmune encephalomyelitis. *Proceedings of the National Academy of Sciences (USA)* 104:920-925.
- Odoardi, F., C. Sie, K. Strey, V.K. Ulaganathan, C. Schlager, D. Lodygin, K. Heckelsmiller, W. Nietfeld, J. Ellwart, W.E. Klinkert, C. Lottaz, M. Nosov, V. Brinkmann, R. Spang, H. Lehrach, M. Vingron, H. Wekerle, C. Flügel-Koch, and A. Flügel. 2012. T cells become licensed in the lung to enter the central nervous system. *Nature* 488:675-679.
- Okamura, H., J. Aramburu, C. Garcia-Rodriguez, J.P.B. Viola, A. Raghavan, M. Tahiliani, X.L. Zhan, J. Qin, P.G. Hogan, and A. Rao. 2000. Concerted dephosphorylation of the transcription factor NFAT1 induces a conformational switch that regulates transcriptional activity. *Molecular Cell* 6:539-550.

- Oukka, M., I.C. Ho, F.C. de la Brousse, T. Hoey, M.J. Grusby, and L.H. Glimcher. 1998. The transcription factor NFAT4 is involved in the generation and survival of T cells. *Immunity* 9:295-304.
- Pagany, M., M. Jagodic, C. Bourquin, T. Olsson, and C. Linington. 2003. Genetic variation in myelin oligodendrocyte glycoprotein expression and susceptibility to experimental autoimmune encephalomyelitis. *Journal of Neuroimmunology* 139:1-8.
- Peng, S.L., A.J. Gerth, A.M. Ranger, and L.H. Glimcher. 2001. NFATc1 and NFATc2 together control both T and B cell activation and differentiation. *Immunity* 14:13-20.
- Piccio, L., B. Rossi, E. Scarpini, C. Laudanna, C. Giagulli, A.C. Issekutz, D. Vestweber, E.C. Butcher, and G. Constantin. 2002. Molecular mechanisms involved in lymphocyte recruitment in inflamed brain microvessels: Critical roles for P-selectin glycoprotein ligand-1 and heterotrimeric G(i)-linked receptors. *Journal of Immunology* 168 1940-1949.
- Pöllinger, B., G. Krishnamoorthy, K. Berer, H. Lassmann, M. Bösl, R. Dunn, H.S. Domingues, A. Holz, F.C. Kurschus, and H. Wekerle. 2009. Spontaneous relapsing-remitting EAE in the SJL/J mouse: MOG-reactive transgenic T cells recruit endogenous MOG-specific B cells. *Journal of Experimental Medicine* 206:1303-1316.
- Richie, L.I., P.J.R. Ebert, L.C. Wu, M.F. Krummel, J.J.T. Owen, and M.M. Davis. 2002. Imaging synapse formation during thymocyte selection: Inability of CD3 to form a stable central accumulation during negative selection. *Immunity* 16:595-606.
- Sawcer, S. 2008. The complex genetics of multiple sclerosis: pitfalls and prospects. *Brain : a journal of neurology* 131:3118-3131.
- Schwarz, S., and H. Leweling. 2005. Multiple sclerosis and nutrition. *Multiple Sclerosis* 11:24-32.
- Serafini, B., B. Rosicarelli, D. Franciotta, R. Magliozzi, R. Reynolds, P. Cinque, L. Andreoni, P. Trivedi, M. Salvetti, A. Faggioni, and F. Aloisi. 2007. Dysregulated

- Epstein-Barr virus infection in the multiple sclerosis brain. *Journal of Experimental Medicine* 204:2899-2912.
- Shaw, K.T.Y., A.M. Ho, A. Raghavan, J. Kim, J.N. Jain, J.C. Park, S. Sharma, A. Rao, and P.G. Hogan. 1995. Immunosuppressive Drugs Prevent a Rapid Dephosphorylation of Transcription Factor Nfat1 in Stimulated Immune Cells. *Proceedings of the National Academy of Sciences of the United States of America* 92:11205-11209.
- Skokos, D., G. Shakhar, R. Varma, J.C. Waite, T.O. Cameron, R.L. Lindquist, T. Schwickert, M.C. Nussenzweig, and M.L. Dustin. 2007. Peptide-MHC potency governs dynamic interactions between T cells and dendritic cells in lymph nodes. *Nature Immunology* 8:835-844.
- Smolders, J., J. Damoiseaux, P. Menheere, and R. Hupperts. 2008. Vitamin D as an immune modulator in multiple sclerosis, a review. *Journal of Neuroimmunology* 194:7-17.
- Sorokin, L. 2010. The impact of the extracellular matrix on inflammation *Nature Reviews Immunology* 10:712-723.
- Tanimura, N., M. Nagafuku, Y. Minaki, Y. Umeda, F. Hayashi, J. Sakakura, A. Kato, D.R. Liddicoat, M. Ogata, T. Hamaoka, and A. Kosugi. 2003. Dynamic changes in the mobility of LAT in aggregated lipid rafts upon T cell activation. *The Journal of Cell Biology* 160:125-135.
- Toldi, G., A. Folyovich, Z. Simon, K. Zsiga, A. Kaposi, G. Meszaros, T. Tulassay, and B. Vasarhelyi. 2011. Lymphocyte calcium influx kinetics in multiple sclerosis treated without or with interferon beta. *Journal of Neuroimmunology* 237:80-86.
- Tomida, T., K. Hirose, A. Takizawa, F. Shibasaki, and M. Iino. 2003. NFAT functions as a working memory of Ca²⁺ signals in decoding Ca²⁺ oscillation. *Embo Journal* 22:3825-3832.

Wei, S.H., O. Safrina, Y. Yu, K.R. Garrod, M.D. Cahalan, and I. Parker. 2007. Ca²⁺ signals in CD4(+) T cells during early contacts with antigen-bearing dendritic cells in lymph node. *Journal of Immunology* 179:1586-1594.

Weissert, R., E. Wallström, M.K. Storch, A. Stefferl, J. Lorentzen, H. Lassmann, C. Linington, and T. Olsson. 1998. MHC haplotype dependent regulation of MOG induced EAE in rats. *Journal of Clinical Investigation* 102:1265-1273.

Wekerle, H., K. Kojima, J. Lannes-Vieira, H. Lassmann, and C. Linington. 1994. Animal models. *Annals of Neurology* 36:S47-S53.

Wekerle, H., C. Linington, H. Lassmann, and R. Meyermann. 1986. Cellular immune reactivity within the CNS. *Trends in Neuroscience* 9:271-277.

Yudushkin, I.A., and R.D. Vale. 2010. Imaging T-cell receptor activation reveals accumulation of tyrosine-phosphorylated CD3zeta in the endosomal compartment. *Proceedings of the National Academy of Sciences of the United States of America* 107:22128-22133

ABBREVIATIONS

Δ NFAT	truncated NFAT
aa	amino acid
aEAE	active EAE
APC	Antigen Presenting Cell
AUC	Area under the curve
BBB	Blood-Brain-Barrier
BN	Brown Norvergicus
c	cytosolic
CaM	Calmodulin
CD	Cluster of differentiation
CFA	Complete Freund's Adjuvant
CK	Casein kinase
CNS	Central Nervous System
ConA	Concanavalin A
CRAC	Calcium release activated calcium
CsA	Cyclosporine A
CTLA	Cytotoxic T Lymphocyte Antigen
DA	Dark Agouti
DC	Dendritic cells
DMEM	Dulbecco's Modified Eagle's Medium
DMSO	Dimethyl Sulfoxide
EAE	Experimental Autoimmune Encephalomyelitis
EAE ^{hi}	High encephalytogenic
EAE ^{lo}	Low ancephalytogenic
EBV	Epstein bar virus

ECG	Electrocardiogram
EDTA	Ethylenediaminetetraacetic acid
EH	Eagle's HEPES
ER	Endoplasmic Reticulum
F1	First generation
FACS	Fluorescence-activated cell sorting
FCS	Fetal calf serum
GFP	Green Fluorescent Protein
GSK	Glycogen-synthase kinase
HEPES	4-(2-hydroxyethyl)-1-piperazineethanesulfonic acid
HLA	Human leukocyte antigen
ICAM	Inter-Cellular Adhesion Molecule
IFN γ	Interferon gamma
Ig	Immunoglobulin
IL	Interleukin
IS	Immunological Synapse
ITAM	Immunoreceptor tyrosine-based activation motif
ITK	IL-2 inducible T cell kinase
LAT	Linker for the activation of T cells
LCK	Lymphocyte-specific protein tyrosine kinase
LE	Lewis
LFA	Lymphocyte function-associated antigen
LPS	Lipopolysaccharide
MBP	Myelin basic protein
MCP-1	Monocyte chemoattractant protein-1
MHC	Major Histocompatibility Complex
MIP-1	Macrophage inflammatory protein-1

MOG	Myelin oligodendrocyte glycoprotein
MS	Multiple Sclerosis
MSD	Mean square displacement
n	nuclear
N.D	Not detected
nc	nuclear/cytosolic
NFAT	Nuclear Factor of Activated T cells
NHR	NFAT homology region
NLS	Nuclear localization signal
ns	Not significant
OCB	Oligoclonal bands
OSE	Opticospinal EAE
OVA	Ovalbumin
PBS	Phosphate buffer saline
PCR	Polymerase chain reaction
PFA	Paraformaldehyde
PLC	Phospholipase C
PLP	Proteolipid protein
PMA	Phorbol 12-Myristate 13-Acetate
PPMS	Primary Progressive MS
PRMS	Progressive Relapsing MS
RHR	REL-homology domain
RRMS	Relapsing Remitting MS
RT1	Major Histocompatibility Complex of the Rat
RV	Robin Virchow space
p.t.	post transfer
S.D	Standard deviation

SLP	SH2 domain containing leukocyte protein
SMAC	Supramolecular activation complexes
SNARF	Seminaphthorhodafluor
SOCE	Store operated calcium entry
SP	SPXX-repeat motifs
SPMS	Secondary Progressive MS
SRC	Sarcoma tyrosine kinase
SRR	Serine-rich regions
TAD	Transactivation domain
TCGF	T cell grow factor
TCM	T cell medium
TCR	T cell receptor
tEAE	transfer EAE
TNF	Tumor necrosis factor
VLA-4	Very late antigen-4
ZAP	Zeta-chain-associated protein kinase

RESOURCES

Δ NFAT-GFP coding retroviral construct was provided by Prof. Vigo Heissmeyer.

Δ NFAT-GFP expressing auto-antigen specific T cell lines were established by PD Dr. Naoto Kawakami with technical assistance of Sabine Kosin.

Programs for the automated export of two-photon imaging data and the analysis of T cell motility and APC contacts were provided by Dr. Ingo Bartholomäus.

Experiments regarding the Δ NFAT-GFP localization in intraluminal T cells were partially performed and analyzed by Nikolaos I. Kyratsous.

Theoretical physicist approach of the thesis was done as a project for the course “Energy, brain and you” under supervision of Dr. Alex Loebel and Dr. Martin Stemmler.

PUBLICATIONS

Parts of this work have already been published.

Pesic, M., I. Bartholomäus, N.I. Kyratsous, V. Heissmeyer, H. Wekerle, and N. Kawakami. 2013. 2-photon imaging of phagocyte-mediated T cell activation in the CNS. *Journal of Clinical Investigation* 123:1192-1201.

Kawakami, N., I. Bartholomäus, **M. Pesic**, and N.I. Kyratsous. 2013. Intravital imaging of autoreactive T cells in living animals. *Methods in Cell Biology* 113:149-168.

Kawakami, N., I. Bartholomäus, **M. Pesic**, and M. Mues. 2012. An autoimmunity odyssey: how autoreactive T cells infiltrate into the CNS. *Immunological Reviews* 248:140-155.

CURRICULUM VITAE

Personal data

Marija Pesic
Josef Schlicht Str. 23
81245 Munich
Germany
Tel: +49-89-7095-8392
Email: pesic@neuro.mpg.de

Date and place of birth:
26.08.1984, Krusevac, Serbia

Education

- 09/2008 - present PhD
Project: Visualizing T cell activation around the blood-brain barrier
Max Planck Institute of Neurobiology, Department of Neuroimmunology
International Max Planck Research School (IMPRS)
- 06/2003 - 07/2008 Graduated
University of Belgrade, Faculty of Biology, Serbia
Major - Molecular biology and physiology
Minor - Genetic engineering and biotechnology
Average mark 9.89 (max. 10)
Diploma thesis: Analysis of proteolytic activity and determination of proteinase gene type in selected *Lactobacillus* species

Congresses

- 01/2012 IFRc-SIgN Winter school on Advanced Immunology, Awaji, Japan (oral and poster presentation)
- 07/2011 FASEB Summer Conference on Autoimmunity, Saxtons River, Vermont, USA (poster presentation)
- 10/2010 10th International Congress of Neuroimmunology, Sitges, Barcelona, Spain (poster presentation)

ACKNOWLEDGEMENTS

I would first like to thank Prof. Hartmut Wekerle for giving me the opportunity to work on exciting projects in his department, and for his support and constant scientific advises throughout my thesis. Additionally, I express my deepest gratitude to my direct supervisor Dr. Naoto Kawakami, for his invaluable guidance during my PhD. I am especially grateful for providing me with perfectly balanced motivating atmosphere, resulting in doing high quality research.

I also wish to thank Prof. Mark Hübener for acting as my principal supervisor at the Faculty of Biology. Along with Prof. Hübener, I also kindly thank the members of my thesis examination board from the Ludwig Maximilians University. In addition, I would like to acknowledge the members of my thesis advisory committee, Prof. Edgar Meinl and Prof. Martin Kerschensteiner, for their helpful input during my thesis, as well as Dr. Alex Loebel and Dr. Martin Stemmler for their help with theoretical part of the thesis.

My special gratitude goes to International Max Planck Research School for Life Science, for both its scientific and financial support. I thank Hans-Joerg Schaeffer, and Maximiliane Reif for all their efforts in trying to solve any difficulties I encountered.

This could also not be done without the help of former and present members of the lab, Michalis, Nikos, Sabine, Marsilius, Sarah, and many others that not only offered direct help in my work but made the lab a fun place to be in, and I thank them for that. I am especially thankful to Ingo Bartholomäus who introduced me to intravital imaging, and programed all those software that enabled fast and automated analysis of my data. None of this would have been possible without you.

Many thanks go to my family and Marko for their unconditional support and understanding.